INTERACTIONS OF MESENCHYMAL STROMAL CELLS WITH THEIR MICROENVIRONMENT

by

LEWIS STUART COREY WARD

A thesis submitted to the University of Birmingham for the degree of

DOCTOR OF PHILOSOPHY

Institute of Inflammation and Ageing

College of Medical and Dental Sciences

University of Birmingham

October 2017

ABSTRACT

Mesenchymal stromal cells (MSC) suppress the inflammatory infiltrate through crosstalk with neighbouring endothelium. However, this response is lost at chronic inflammatory sites where stromal cells instead support leukocyte recruitment and upregulate expression of podoplanin. The mechanism and function by which this inflammatory phenotype is established is unknown. We hypothesise that MSC modulation of endothelium is also altered by exposure to inflammatory cytokines, and that expression of podoplanin confers an invasive phenotype, enabling the interaction of these perivascular MSC with circulating platelets.

MSC resisted functional transformation during acute or prolonged exposure to tumour necrosis factor alpha, instead maintaining their ability to suppress neutrophil recruitment in a flow-based assay. Expression of podoplanin promoted MSC migration through Ras-related C3 botulinum toxin substrate dependent signalling, enabling perivascular MSC to interact with cells confined to the circulation. Indeed, podoplanin induced the activation of platelets from flow through MSC protrusions in the endothelial lining.

The retention of MSC suppressive function under inflammatory conditions supports their use in equivalent environments for therapy. However, the implications of platelet CLEC-2 activation by its ligand, podoplanin on inflamed stroma have yet to be elucidated and warrant further investigation, with specific focus drawn to the pathophysiology of thromboinflammation and associated disorders.

ACKNOWLEDGEMENTS

The work described in this thesis was carried out in the Institute of Inflammation & Ageing at The University of Birmingham and was funded by the Medical Research Council.

First and foremost, I would like to thank my supervisors, Dr Helen McGettrick and Professor Gerard Nash for their continued support throughout this project. Both of whom have provided direction and scientific grounding on what were at times an eclectic range of ideas and experiments!

Secondly, I would like to acknowledge past and present members of the Leukocyte Trafficking, Rheumatology Research, and Vascular Tetraspanin Groups for their assistance in sourcing reagents and developing some of the experimental techniques used in this thesis. In particular, I would like to give thanks to Bonita, Hafsa, Aigli, and Arjun for their 'lab humour' and advice.

Finally, my warm thanks go to my close friends and family for all their encouragement. The past three years have been eventful, seeing many new friendships grow, my engagement and marriage to my wonderful wife Becky, as well as the start of our own home together in Cambridgeshire.

This thesis is dedicated to the memories of Anthony Smail, Eileen Clarke, Roland Ward, and Susan Ward.

Table of Contents

TABLE OF FIGURES

LIST OF TABLES

ABBREVIATIONS

ANOVA	Analysis of variance
BEC	Human dermal blood endothelial cells
BECGM	Blood endothelial cell growth medium
BMMSC	Bone marrow-derived mesenchymal stromal cells
BSA	Bovine serum albumin
cDNA	Complementary deoxyribonucleic acid
CCL	C-C chemokine ligand
CCR	C-C chemokine receptor
CD	Cluster of differentiation
CHO	Chinese hamster ovary cells
CXCL	C-X-C chemokine ligand
CXCR	C-X-C chemokine receptor
C_T	Threshold cycle
DC	Dendritic cell
DAS	Disease activity score
DMEM	Dulbecco's modified Eagle's medium
DMSC	Dental pulp-derived mesenchymal stromal cells
EDTA	Ethylenediaminetetraacetic acid
EGF	Epidermal growth factor
ERM	Ezrin, radixin, moesin proteins
ELISA	Enzyme linked immunosorbent assay
EMT	Epithelial to mesenchymal transition
FBM	Fibroblast medium
FBS	Foetal bovine serum
FGF	Fibroblast growth factor
FITC	Fluorescein isothiocyanate
GM-CSF	Granulocyte macrophage colony-stimulating factor
gRNA	Guide ribonucleic acid
GTP	Guanine triphosphate
HEV	High endothelial venules
HGF	Hepatocyte growth factor
HIF	Hypoxia-inducible factor
HLA	Human leukocyte antigen
HUVEC	Human umbilical vein endothelial cells
IDO	Indolamine 2,3-dioxygenase
IFN	Interferon
IgG	Immunoglobulin
IL	Interleukin
ISCT	International Society for Cell Therapy
ITP	Immune thrombocytopenic purpura
JAMs	Junctional adhesion molecules
LPS	Lipopolysaccharide
M199	Medium 199
MDCK	Madin-Darby canine kidney cells

MFI	Median fluorescence intensity
M-MLV	Moloney murine leukaemia virus
mRNA	Messenger ribonucleic acid
MSC	Mesenchymal stromal cells
MSCGM	Mesenchymal stromal cell growth medium
MSCLG	Mesenchymal stromal cell growth medium – low glucose
LB	Luria-Bertani
NF-κB	Nuclear factor - kappa B
NK	Natural killer
NO	Nitric oxide
PBS	Phosphate buffered saline without Ca^{2+} and Mg^{2+}
PBS^{+}	Phosphate buffered saline with Ca^{2+} and Mg^{2+}
PD-L	Programmed death-ligand
PE	Phycoerythrin
PE-Cy7	Phycoerythrin-cyanine7
PGE_2	Prostaglandin E_2
Prox1	Prospero homeobox protein 1
Poly(I:C)	Polyinosinic-polycytidylic acid
qPCR	Real-time polymerase chain reaction
RA	Rheumatoid arthritis
Rac1	Ras-related C3 botulium toxin substrate 1
RASF	Rheumatoid arthritis synovial fibroblasts
REU	Relative expression units
Rho	Ras homolog gene family
RPMI	Roswell park memorial institute
ROCK	Rho-associated protein kinase
RT	Reverse transcriptase
SEM	Standard error of the mean
SC	Serum control
SCC	Squamous cell carcinoma
SD	Standard deviation
sgRNA	Single-guide ribonucleic acid
TBMSC	Trabecular bone-derived mesenchymal stromal cells
SLE	Systemic lupus erythematosus
SOCS3	Suppressor of cytokine signalling 3
TGF	Transforming growth factor
TNF	Tumour necrosis factor
UCMSC	Umbilical cord-derived mesenchymal stromal cells
VE	Vascular endothelial
VEGF	Vascular endothelial growth factor
γ_W	Wall shear rate
τ_W	Wall shear stress

Chapter 1. General introduction

1.1. OVERVIEW

This thesis explores the interactions that occur between mesenchymal stromal cells (MSC) and their microenvironment, and how these interactions are modified by inflammation. The following introductory chapter will encompass the biology of MSC, detailing their immunosuppressive crosstalk with endothelium and how the inflammatory microenvironment transforms the phenotype of stroma in general. It will further describe the role of the mucin-like protein podoplanin (PDPN) in this transformation, and the functional properties it confers.

1.2. MSC BIOLOGY

1.2.1. International Society for Cell Therapy criteria for defining MSC

MSC are endogenous multipotent precursor cells, localised to the perivascular niche of many tissues (Crisan et al. 2008). Due to their pleiotropic nature, guidelines were written in 2006 by the ‘International Society for Cell Therapy’ (ISCT) (Dominici et al. 2006), stating the minimal criteria for MSC characterisation requires they;

- Are plastic-adherent under standard culture conditions.
- Differentiate into adipocytes, chondroblasts, and osteoblasts.
- Express a panel of surface markers: ‘human leukocyte antigen’ (HLA)-DR$^-$, CD14$^-$, CD19$^-$, CD34$^-$, CD45$^-$, CD73$^+$, CD90$^+$, and CD105$^+$.

However, the criteria set out by the ISCT also defines other stromal cells such as fibroblasts, hence these markers describe a heterogenous population of cells that are likely to have equally varied functions (Halfon et al. 2011; Kundrotas 2012).

Furthermore, even standardised nomenclature cannot address the differences observed between tissue-specific sources of MSC, suggesting that cell function is influenced by their individual microenvironments (see Chapter 4) (Kern et al. 2006). In addition to their homeostatic function of replacing cell turnover via self-renewal and differentiation, MSC are also potent modulators of the immune system and are likely to play a key role in the regulation and resolution of inflammation [reviewed by (Ma et al. 2013)]. As such, these properties along with their low immunogenicity, make them a popular choice for cell-based therapies [reviewed by (Squillaro et al. 2016)].

1.2.2. MSC REPARATIVE FUNCTION

MSC self-renewal and multipotent differentiation enables these cells to maintain, replenish, and repair the stromal environment in response to apoptosis, senescence, and tissue damage [reviewed by (Huang & S. Li 2008)]. Endogenous perivascular MSC have been shown to migrate toward sites of tissue damage in teeth, whereupon they aid in the repair process through differentiation into odontoblasts (Feng et al. 2011). Indeed, ‘bone marrow derived MSC’ (BMMSC) repaired and replaced senescent myocardium in 18 month old mice (Khan et al. 2011). Interestingly, the age of donor BMMSC negatively correlated with their reparative capacity (Khan et al. 2011), suggesting their reparative function may diminish with age. Whereas, intradermal injection of BMMSC in a murine model of wound repair saw BMMSC-mediated recruitment of macrophages and endothelial progenitor cells at the site of damage, resulting in enhanced repair (Chen et al. 2008). Furthermore, only conditioned medium from BMMSC, but not dermal fibroblasts, was found to promote endothelial angiogenesis at the wound site and aid tissue repair (Chen et al. 2008;

Wu et al. 2007). However, this supportive role of MSC is not always beneficial. For instance, at locations where BMMSC have integrated into the intercellular junctions of ‘human umbilical vein endothelial cells’ (HUVEC) *in vitro*, HUVEC apoptosis and loss of neocapillary network structure has been observed, along with the release of reactive oxygen species (Otsu et al. 2009). Furthermore, BMMSC promoted tumour growth when co-injected with B16 melanoma cells in C57BL/6 mice (K. Suzuki et al. 2011). ‘Umbilical cord derived MSC’ (UCMSC) were also found to contribute to the maintenance of vascular integrity in HUVEC by increasing the endothelial expression of cell-cell adhesion proteins; ‘vascular endothelial’ (VE)-cadherin and β-catenin (Pati, Khakoo, et al. 2011). These studies indicate that MSC can respond and migrate toward sites of damage where they utilise their multipotent differentiation capacity to replace cells, and paracrine signalling to support tissue proliferation and angiogenesis.

1.2.3. MSC MIGRATION: LINKS WITH REPAIR

Endogenous MSC are enriched within the perivascular niche (Crisan et al. 2008), where they are aptly positioned to communicate with the endothelium and influence angiogenesis, tissue repair/turnover, vascular permeability, and regulation of leukocyte recruitment during inflammation. MSC preferentially migrate toward sites of injury and inflammation to exert their reparative and immunomodulatory effector functions [reviewed by (Spaeth et al. 2008), also see Section 1.2.4 below]. Stromal cells can migrate either as single cells or as a collective group with coordinated movements, where both types of migration require a dynamic interaction with the substratum on which the cells are attached [reviewed by (Friedl & K. Wolf 2010)].

Collective migration differs in that it requires the retention of cell-cell junctions and mostly relies on the coordinated cycles of cellular protrusions at the leading edge, as the trailing edge remains adherent to other cells or extracellular matrix components (Farooqui & Fenteany 2005). Mesenchymal migration is defined by a multistep cycle that involves a synchronised redistribution of the actin cytoskeleton from a continuously extending and anchoring cellular protrusion, to stabilisation of the actin cytoskeleton at leading edge and eventual detachment of the trailing edge, which results in the cell body being pulled forward (Grinnell 2008). Cellular protrusions are formed of podosomes, invadopodia, filopodia and lamellipodia [reviewed by (Alblazi & Siar 2015)]. Lamellipodia are responsible for driving cell migration through broad flat protrusions at the leading edge, whilst filopodia are utilised in cell direction by probing the space around the leading edge through thin tubular projections (Suraneni et al. 2012). Podosomes and invadopodia are F-actin rich protrusions on the basal surface of the cell which contribute to the invasive properties of the cell through degradation of the extracellular matrix [reviewed by (Sibony-Benyamini & Gil-Henn 2012)]. Podosomes are numerous and small at approximately 0.4μm in length and 1μm in diameter, whilst invadopodia are smaller in diameter and can extend over 2μm [reviewed by (Alblazi & Siar 2015)]. These cellular protrusions adhere to the substratum through regulation of the Rho family of ‘small guanine triphosphate’ (GTP)ases, RhoA, Rac1, and Cdc42 (Nobes & Hall 1999). MSC utilise a combination of these processes during single cell mesenchymal migration, however the mechanisms of the migration-related signalling pathways in MSC specifically are poorly defined.

In general, ‘Rho-associated protein kinase’ (ROCK) signalling controls retraction of the trailing edge through actomyosin-mediated signalling and together with Rac1-mediated protrusions they form the basis of the migration cycle [reviewed by (Ridley 2003)]. Rac1 drives mesenchymal-type migration by stabilising lamellipodia formation, indeed overexpression of Rac1 in Rat2 fibroblasts resulted in membrane ruffling and localisation of Rac1 to the leading edge of the cell (Ridley et al. 1992). Rac1 also interacts with RhoA, and RhoA with ROCK in promoting the formation of the actin stress fibres required for inducing actomyosin contraction of the cell through myosin light chain (MLC) (Ridley et al. 1992; Amano et al. 1997). Blockade of Rac1 in melanoma cells either with the Rac1 inhibitor (NSC23766) or siRNA targeting Rac1 impaired mesenchymal migration was shown to confer a rounded ‘amoeboid-like’ morphology (Sanz-Moreno et al. 2008). Furthermore, Rac1 formed part of a larger signalling cascade with the melanoma metastasis gene ‘neural precursor cell expressed developmentally downregulated protein’ (NEDD)9 signalling through ‘dedicator of cytokinesis’ (DOCK)3, Rac1, and lastly ‘Wiskott-Aldrich syndrome protein family member’ (WASF)2, which regulates the ‘actin-related protein’ (Arp)2/3 complex to promote actin filament reorganisation (Sanz-Moreno et al. 2008). This Rac1-involved signalling pathway had the overall effect of promoting mesenchymal migration and hindering amoeboid-like migration (Sanz-Moreno et al. 2008). Indeed, amoeboid-like migration of cells such as leukocytes has been shown to be separately regulated by Rho/ROCK signalling in tumour cells, as shown by the use of inhibitors (Rho, TAT-C3; ROCK, Y27632) (Lämmermann & Sixt 2009; Sahai & Marshall 2003). These studies demonstrate the generic mechanisms involved in mesenchymal migration and how these might be perturbed.

1.2.4. MSC TRANSMIGRATION THROUGH ENDOTHELIUM

MSC-specific migration has mostly been explored in their therapeutic context, with a focus on their extravasation into tissue from the circulation [reviewed by (Nitzsche et al. 2017)]. This is of importance as few cells reach the target tissue after systemic infusion, with most becoming trapped within the lungs (Fischer et al. 2009). Indeed, BMMSC have been shown to adhere to HUVEC stimulated with ‘interleukin’ (IL)-1 or ‘tumour necrosis factor’ (TNF)-α in a dose-dependent manner (Luu et al. 2013). However, this only occurred at extremely low flow rates indicating that BMMSC are not recruited from flow in the same fashion as leukocytes (see Section 1.2.5 below) and are likely to become trapped in smaller vessels given their size. *In vitro* culture of BMMSC on endothelial monolayers have shown them to spread over the surface and integrate with the endothelium, the addition of platelets enhanced both BMMSC migration in a model of scratch-induced wounds (scratch-wound assay) and endothelial integration in a basic fibroblast growth factor (FGF)-dependent manner (Langer et al. 2009). Indeed, BMMSC have been shown to transmigrate through TNF-α stimulated lung and cardiac microvascular endothelium using CD106 (VCAM1)-rich gaps in the endothelial monolayer, termed ‘transmigratory cups’, whereby BMMSC undergo non-apoptotic membrane blebbing and take on a rounded morphology (Teo et al. 2012). Regarding the mechanisms of BMMSC transmigration, inhibition of ROCK (Y27632) was shown to promote BMMSC migration through brain microvascular endothelium, whilst a phosphoinositide 3-kinase (PI3K) inhibitor (LY294002) prevented this process (Lin et al. 2013). Indeed, treatment of prostate cancer cells with LY294002 was shown to significantly inhibit cell migration and reduce Rac1 activity, suggesting PI3K interacts with Rac1 to promote cell migration

(Henderson et al. 2015). MSC were also shown to transmigrate in response to external stimuli. Indeed, BMMSC migrated through HUVEC monolayers seeded on collagen gels in a ‘C-X-C motif chemokine receptor’ (CXCR)4 dependent manner in response to a ‘C-X-C motif chemokine ligand’ (CXCL)12 gradient established in a custom microfluidic device (Park et al. 2017). Furthermore, the addition of inhibitors against ROCK (Y27632) or Rac1 (NSC23766) significantly impaired CXCL12-induced migration of BMMSC (Park et al. 2017). All the above studies investigated MSC migration through the apical surface of endothelium in an extravasation model, whether alternative mechanisms are employed for endogenous MSC migration through the basal surface in an intravasation model have yet to be determined. It would appear that exogenous factors are capable of influencing the migration of MSC toward sites of tissue damage or inflammation whereby they can exert their reparative functions.

1.2.5. MSC IMMUNOMODULATORY FUNCTION

MSC have well-documented immunomodulatory abilities capable of regulating both the innate and adaptive immune response through both direct cell contact and a range of paracrine factors, such as ‘transforming growth factor’ (TGF)-β, IL-6, ‘programmed death 1’ (PD-1) ligand, ‘indoleamine 2,3-dioxygenase’ (IDO), and ‘prostaglandin E_2’ (PGE_2) (Trivanović et al. 2013). MSC modulation of leukocytes is well described within the literature, with most studies focussing on their ability to suppress T-cell proliferation [reviewed by (Haddad & Saldanha-Araujo 2014; Lotfinegad et al. 2014; Munir & McGettrick 2015)]. Briefly, MSC from different sources have been shown to inhibit activated T-cells through IDO-mediated catabolism of tryptophan (Meesuk et al. 2016; François et al. 2012; Meisel et al. 2004; Ling et al. 2014). Moreover, direct coculture of BMMSC with ‘natural killer’ (NK) cells inhibited their proliferation, ‘interferon’ (IFN)-γ secretion, and cytotoxic activity (Spaggiari et al. 2008). In addition, soluble mediators released by the crosstalk of BMMSC with monocytes was sufficient to impair the differentiation into ‘dendritic cells’ (DC) and bias differentiation of monocytes towards an anti-inflammatory ‘M2’ macrophage phenotype (Jiang et al. 2005; François et al. 2012). Selmani *et al.*, (2008) showed that IL-10 induction of HLA-G was capable of attenuating IFN-γ secretion and cytotoxicity of NK cells, as well as promoting the expansion of regulatory T-cells (Selmani et al. 2008). Whilst MSC are clearly capable of directly suppressing leukocyte function in inflamed tissue, we will focus on their ability to regulate endothelium and hence hinder entry of the inflammatory infiltrate into underlying tissue.

Adhesion assays represent a robust means of investigating the mechanism by which MSC modulate endothelium and the resulting effect on leukocyte recruitment. Static adhesion assays enable high-throughput analysis of leukocyte adhesion to endothelial monolayers. Leukocytes can be labelled to roughly determine adhesion to endothelium by measuring the fluorescent signal for each well with a microplate reader. Conditioned medium can also be collected from MSC and used to pre-treat the endothelium in these assays to determine the impact of soluble immunomodulatory factors. Indeed, conditioned medium generated from BMMSC coculture with pulmonary endothelium (PEC), but not monoculture controls, was shown to decrease the surface expression of CD54 (ICAM1) and VCAM1 on TNF-α stimulated PEC (Pati, Gerber, et al. 2011). This was associated with a reduction in the adhesion of a calcein-labelled monocytic leukaemia cell line (U937) to PEC, as measured by a microplate reader (Pati, Gerber, et al. 2011). Phase-contrast microscopy of adherent leukocytes will permit further analysis in their ability to transmigrate through the endothelial monolayer where they take on a phase-dark morphology. In-depth analysis of migration is better suited to a 3D multicellular collagen gel construct where leukocytes can be tracked as they migrate through the endothelium and penetrate through the gel in the presence of stromal cells (Jeffery et al. 2013). However, these static assays are primarily limited in that the cells aren't exposed to flow-derived shear stress, overlooking rolling capture mechanics and instead biasing adhesion through the sedimentation of leukocytes. Alternatively, flow-based adhesion assays have enabled us to better our understanding of the different stages of leukocyte recruitment by mimicking *in vivo* conditions. This methodology has also demonstrated stromal cells to be potent regulators of the inflammatory infiltrate through their ability to regulate endothelium, though the response differs with the source of stroma [reviewed by (McGettrick et al. 2012)]. Indeed, both neutrophil and lymphocyte adhesion to inflamed HUVEC are reduced in MSC coculture compared to controls (Munir et al. 2016; Luu et al. 2013). However, UCMSC and 'trabecular bone-derived MSC' (TBMSC) required proximity to the endothelium (i.e. neighbouring on opposite sides of a filter) to exert these effects, whereas, BMMSC could exert suppressive actions distally (Munir et al. 2016). This indicated tissue specific differences in the degree of cell contact or utility of soluble mediators was required for the communication of MSC with endothelium. Further interrogation revealed the mechanism of suppression to occur through the release of soluble mediators, namely IL-6, in coculture, which signalled via the ‘suppressor of cytokine signalling’ (SOCS)3 to regulate endothelial responses to TNF-α stimulation (Figure 1-1) (Luu et al. 2013). Collectively, these studies demonstrate that MSC suppress the endothelial response to inflammation, through crosstalk with soluble mediators. Fully understanding the mechanisms by which this occurs in different tissues will allow the development of therapeutic targets capable of reducing leukocyte-mediated tissue damage in chronic inflammatory diseases. However, further work is required to understand whether these cross-talk pathways are modified at sites of acute and chronic inflammation.

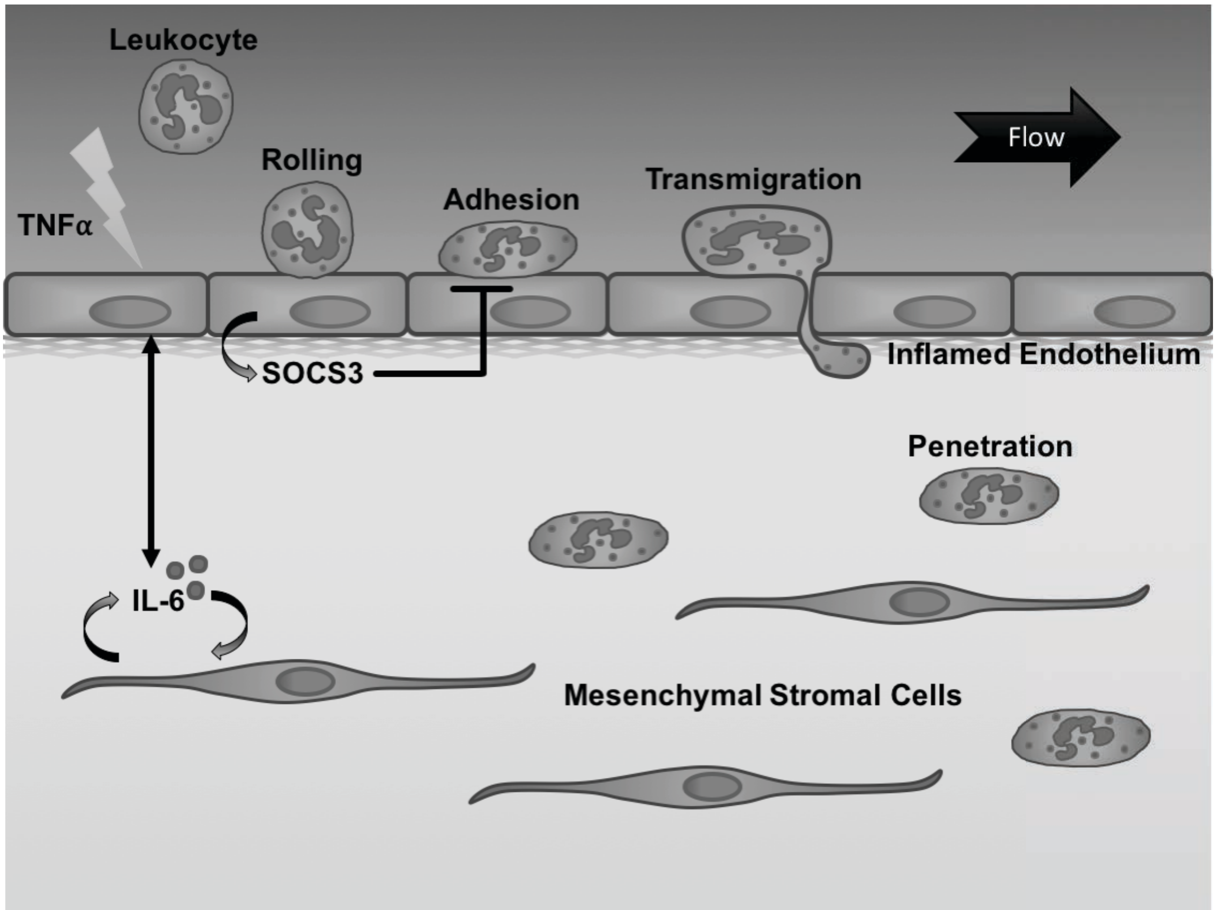

Figure 1-1 Diagram of MSC suppression of leukocyte recruitment

TNFα stimulation upregulates adhesion molecules on endothelium that assist in the recruitment of leukocytes from flow. Under these inflammatory conditions MSC increase secretion of IL-6 through crosstalk with endothelium. IL-6 stimulation upregulates endothelial expression of SOCS3 which in turn suppresses the response of endothelium to pro-inflammatory cytokines, hence reducing leukocyte adhesion and further tissue infiltration. Information from Luu et al. 2013.

1.2.6. Neutrophil recruitment cascade

This thesis will partly focus on MSC immunomodulation of endothelium, using neutrophil recruitment as a readout and thus necessitating a brief overview of this process [reviewed by (Kolaczkowska & Kubes 2013)]. The recruitment of neutrophils into tissue typically occurs in the post-capillary venules in response to endothelial activation by pro-inflammatory mediators and upregulation of adhesion molecules (Sadik et al. 2011). The post-capillary venules are subject to low haemodynamic shear, under which conditions erythrocytes stack together into larger aggregates known as rouleaux in the centre of blood vessels (Goldsmith & Spain 1984). The increased density of erythrocytes in the centre of the vessel forces leukocytes and platelets to the circumference of the vessel, proximal to the endothelial lining in a process known as margination (Goldsmith & Spain 1984).

Initial capture is mediated through tethering and rolling of neutrophils along the apical surface of the endothelium via transient interactions with selectin molecules (CD62) (McEver 2002). During rolling, neutrophils are exposed to CXCL-2, -5, and -8 presented on the endothelium by heparin sulfate, which induce an activating conformational change in the ligand-binding domains of β2-integrins (CD11a/CD18 and CD11b/CD18) heterodimers [reviewed by (Mould & Humphries 2004)]. This change enables prolonged interactions with rolling neutrophils, causing them to come to a complete arrest through CD11a/CD18 complex binding to ICAM1 (Smith et al. 1989). Arrest is followed by cytoskeletal reorganisation and intraluminal crawling of neutrophils toward endothelial junctions (Phillipson et al. 2006).

Transendothelial migration of neutrophils into the tissue can occur either by paracellular or transcellular means, through interactions with cell adhesion molecules, CD31 (PECAM1), CD99, and ‘junctional adhesion molecules’ (JAMs) [reviewed by (Hyun & Hong 2017)]. After migrating through the endothelial lining, neutrophils must then navigate the basement membrane and pericytes in a process known as abluminal crawling, with pericytes shown to enhance neutrophil transmigration *in vivo* by intravital microscopy in mice (Proebstl et al. 2012). In some instances, neutrophils are capable of ‘reverse migration’, whereby they intravasate from the abluminal space in a stimulus specific manner (Colom et al. 2015). Otherwise, neutrophils continue to infiltrate into the inflamed tissue in response to CXCR2 ligand gradients, whereupon they exert their effector functions [reviewed by (Sadik et al. 2011)].

As indicated above, endothelial cells act as reporters of their local environment with their responses either facilitating or hindering the recruitment cascade. Indeed, endothelial monocultures may not accurately reflect the physiological situation, thus highlighting the importance of establishing stromal coculture for the inflammatory site of interest. Conversely, chronically inflamed endothelium may also modify MSC function and thus leukocyte recruitment.

1.3. MSC RESPOND TO ENVIRONMENTAL CUES

1.3.1. Regulation of MSC differentiation

MSC differentiation can be regulated through a variety of means as illustrated below: Stimulation of BMMSC with TGF-β over 6 days was sufficient to induce differentiation into a smooth muscle cell (SMC) phenotype based on expression of SMC markers such as alpha smooth muscle actin when compared to untreated controls (Ross et al. 2006). Alternatively, BMMSC differentiation into osteoblasts (as determined by MSC mineralisation and expression of osteogenic genes such as *BMP2* and *RUNX2*) was induced through vibrations of a nanoscale amplitude in the absence of soluble osteogenic differentiation factors (Tsimbouri et al. 2017). The same effect was observed through changes in the tension of BMMSC extracellular matrix, with rigid gels (34 kPa) also biasing toward an osteogenic transcriptional profile, whereas intermediate (11 kPa) or soft gels (1 kPa) were associated with myogenic and neurogenic markers respectively (Engler et al. 2006). These responses were often dependent on the tissue specific microenvironment, with soluble factors, mechanical strain, and the extracellular matrix all applying various outcomes on MSC reparative function and the lineage MSC differentiate down. These aspects of MSC biology are of importance to the regenerative medicine field.

1.3.2. Environmental regulation of MSC migration

With regard to the role of the microenvironment on MSC migration, overexpression of hypoxia-inducible factor (HIF)-1α resulted in significantly increased ‘dental pulp-derived MSC’ (DMSC) migration in the closure of scratch-wound assay and in a model of single cell migration across a porous filter (transwell assay) (Ciria et al. 2017). The addition of a gamma-secretase ‘RO4929097’ inhibitor that impairs Notch receptor processing abrogated this response, thus implicating the Notch signalling pathway in HIF-1α induced DMSC migration (Ciria et al. 2017). Indeed, HIF-1α has been shown to regulate BMMSC migration in a transwell assay through increased expression of the signalling proteins ROCK1 and Rac1/2/3 which are involved in regulating cell motility through the actin cytoskeleton (Choi et al. 2016). These studies indicate that MSC migration is enhanced by hypoxic environments.

The presence of certain cytokines and chemokines within the stromal microenvironment are also capable of promoting MSC migration. The MSC tissue source (bone marrow, adipose, or gingival) was shown to have no effect on collective migration in scratch-wound assays, however stimulation with IL-3 significantly increased wound closure compared to untreated controls (Barhanpurkar-Naik et al. 2017). IL-3 treatment was also found to upregulate (bone marrow, adipose, or gingival) MSC expression of CXCR4, to a similar extent as pro-inflammatory cytokines TNF-α and IL-17A, and enhanced MSC chemotaxis toward CXCL12 in transwell assays (Barhanpurkar-Naik et al. 2017). Indeed, BMMSC migration/chemotaxis through transwells has been shown to be enhanced by a number of factors including IL-6, CXCL12, ‘vascular endothelial growth factor’ (VEGF), or FGF (Schmidt et al. 2006). TGF-β1 has also been shown to act as an TBMSC chemoattractant *in vivo* when it is released from the trabecular surface during osteoclast bone remodelling (Yi Tang et al. 2009). Indeed, BMMSC migration was significantly impaired in *Tgfb1*$^{-/-}$*Rag2*$^{-/-}$ mice (Yi Tang et al. 2009). In contrast, TGF-β-mediated MSC migration has been reported to detrimental contributing to the progression of arterial calcification in mice (W. Wang et al. 2014). TGF-β release from injured endothelium was found to increase numbers of circulating MSC and their subsequent recruitment to arteriolar lesions, whereupon vascular calcification was driven through osteogenic differentiation (W. Wang et al. 2014). Thus, MSC migration is dependent on the context of their microenvironment. However, the exact mechanisms and circumstances by which MSC enter the circulation in response to environmental factors is unknown.

The expression of certain surface markers are also associated with enhanced migratory function. Indeed, the ‘pseudo tyrosine kinase receptor’ (PTK)-7 is found to be overexpressed in colorectal cancers where it confers increased motility when tracked *in vitro* and increased metastatic potential in a mouse xenograft model (Lhoumeau et al. 2015). The ‘collagen triple helix repeat containing’ (CTHRC)-1 is a similar marker found to promote the migration of ‘synovial fibroblasts isolated from ‘rheumatoid arthritis’ (RA) patients’ (RASF) (Shekhani et al. 2016). Furthermore, CTHRC-1 was induced by the inflammatory environment with expression significantly increased compared to normal synovium (Shekhani et al. 2016). Another pro-migratory marker that is upregulated by the inflammatory environment is the glycoprotein PDPN (Del Rey et al. 2014; Payne et al. 2017; Inoue et al. 2015), which colocalises with CD44 at plasma membrane protrusions to promote directional cell migration (Martin-Villar et al. 2010). Thus, expression of cell surface markers confer prolonged changes to stromal cell function in response to their environment, here we will focus on the role of PDPN in this response as discussed below.

1.3.3. Role of podoplanin in regulating stromal cell migration

PDPN is a 43-kD, heavily glycosylated, mucin-type, transmembrane protein (Breiteneder-Geleff et al. 1997). It is enriched at cellular protrusions where its short cytoplasmic tail directly interacts through the ezrin, radixin, moesin (ERM) family of proteins to connect with the actin cytoskeleton (Martín-Villar et al. 2006). PDPN is typically expressed by kidney podocytes, lymphatic endothelial cells, lymphoid stromal cells, thymic epithelial cells, and inflammatory macrophages (Breiteneder-Geleff et al. 1997; Farr et al. 1992; Schacht et al. 2003; Kerrigan et al. 2012).

PDPN function is linked with cell migration, as well as cancer invasiveness and metastasis (Yuan et al. 2006; Kunita et al. 2007; Y.-Y. Li et al. 2015; Takemoto et al. 2017; Takagi et al. 2014; Yurugi et al. 2017; Wicki et al. 2006; Martin-Villar et al. 2010; Martín-Villar et al. 2006). Incidentally, PDPN is induced in cancer-associated fibroblasts (CAF) in response to hypoxia, with its expression promoting migration and invasion (Wicki et al. 2006; Tejchman et al. 2017; Neri et al. 2015). PDPN is also upregulated on stroma in hypoxic tissues, such as cancer and RA (Schacht et al. 2005; Croft et al. 2016; Del Rey et al. 2014), though its role on stromal cell migration is still under debate. However, hypoxia was previously shown to promote MSC migration (Ciria et al. 2017; Choi et al. 2016). Importantly, we have recently demonstrated that UCMSC differentially express PDPN (Dr L Sheriff, University of

Birmingham, 2017, personal communication), indicating that it may have a role in MSC function, in particular their migration.

The mechanisms by which MSC intravasate into the circulation, particularly with regard to the endogenous MSC ‘homing’ literature have not been described. A popular source of these circulating MSC-like cells are derived from the process of epithelial-mesenchymal transition (EMT), whereby epithelial cells lose apical-basal polarity and reorganise their cytoskeleton to take on a motile and invasive phenotype [reviewed by (Lamouille et al. 2014)]. Indeed, Martín-Villar *et al*., (2006) showed that PDPN induces EMT in ‘Madin-Darby canine kidney‘ (MDCK) cells through interactions with ‘ezrin, radixin, and moesin’ (ERM) proteins at the cytoplasmic tail of PDPN and subsequent activation of RhoA GTPase (Martín-Villar et al. 2006). However, the exact role of EMT in tumour pathogenesis is under debate. Transfection of PDPN into CHO cells was shown to promote pulmonary metastasis formation compared to PDPN-negative controls through formation of platelet aggregates when injected intravenously into mice (Kunita et al. 2007). Indeed, Takemoto *et al*., (2017) recently demonstrated that PDPN-mediated activation of platelets aids invasion through the endothelial lining via the release of platelet TGF-β inducing EMT of tumour cells (Takemoto et al. 2017). Furthermore, FGF derived from activated platelets was also shown to promote BMMSC migration and their integration with the endothelial monolayer (Langer et al. 2009). The role of PDPN and the intravasation capacity of MSC requires much work, even though the process of MSC luminal to abluminal transmigration has been studied in detail.

With regard to protein interactions, PDPN is the only known ligand for CLEC-2, with expression of CLEC-2 in platelets, neutrophils, B-cells, and dendritic cells (Lowe et al. 2015). PDPN mediates the migration of lymphatic endothelium (LEC), with crosslinking of PDPN inhibiting vascular endothelial growth factor (VEGF)-induced migration of lymphatic endothelium in a transwell assay (Langan et al. 2017). Furthermore, the presence of the PDPN receptor, CLEC-2 on platelets also impaired VEGF-induced LEC migration (Langan et al. 2017). This suggests that activation of PDPN inhibits its associated functions. Indeed, recombinant CLEC-2 was found to inhibit PDPN-mediated contraction of fibroblastic reticular cells (Astarita et al. 2015). We have recently described the first instance of PDPN expression in UCMSC, however its role and mechanism of action in the migration of UCMSC has yet to be determined (Dr L Sheriff, University of Birmingham, 2017, personal communication).

Discrepancies have been observed in downstream signalling of PDPN. Overexpression of PDPN in several adenocarcinoma cell lines (MSU1.1, Hs578, MDCK, and MCF7) resulted in increased RhoA, but no effect on Cdc42 or Rac1 (Martín-Villar et al. 2006; Suchanski et al. 2017), whilst another study saw decreases in all three GTPases (Wicki et al. 2006). Furthermore, knockdown of PDPN in lymphatic endothelium resulted in reduced RhoA expression, but increased Cdc42 expression (Navarro et al. 2011). It appears that downstream signalling for PDPN varies between different cell types, though all studies demonstrated that expression of PDPN conferred a pro-migratory phenotype on these cells. The significance of this and the GTPase linked to PDPN in MSC remains unclear. However, it could be dependent on the preferred form of migration by these cell types, whether that be amoeboid- or mesenchymal-like migration.

PDPN is thought to interact with other surface proteins on the parent cell to modify its signal transduction and functional consequences [reviewed by (Astarita et al. 2012)]. Colocalisation of the tetraspanin CD9 with PDPN, inhibited PDPN-mediated pulmonary metastasis and platelet aggregation when PDPN-positive ‘Chinese hamster ovary cells’ (CHO) were intravenously administered (Nakazawa et al. 2008). CD44 also colocalises with PDPN at cellular protrusions in HN5 oral carcinoma and transfected MDCK cells, both PDPN and CD44 were required for directional cell migration, as shown by siRNA knockdown of CD44 (Martin-Villar et al. 2010). It is possible that changes in the co-receptors linked with PDPN may influence the downstream signalling elicited and ultimately the functional output from PDPN engagement.

1.3.4. Effect of acute inflammation on MSC function

MSC appear to be primed by inflammatory cytokines with augmented functions conferred (Table 1-1, Table 1-2). Some of which are beneficial: as observed with inflammation-induced secretion of TGF-β3 by BMMSC reducing tissue fibrosis through the impaired proliferation and extracellular matrix deposition of myofibroblasts (Wu et al. 2015). Indeed, resolution of fibrosis through secretion of TGF-β3 could hold true for similar studies, where the administration of MSC in rat models of chemically or surgically induced tissue damage was associated with a reduction of fibrosis at the site of injury (Abdel Aziz et al. 2007; Semedo et al. 2009; L. Li et al. 2008). Attempts to model acute inflammation *in vitro* using cytokine priming models have enabled a cause and effect study of MSC responses to specific stimuli, but with conflicting results (Table 1-1). Treatment of UCMSC with TNF-α or lipopolysaccharide (LPS) over 48 hours increased the expression and secretion of both TGF-β1 and TGF-β3 when compared to unstimulated controls (Wu et al. 2015). However, 6-hour priming of murine BMMSC with IFN-γ or TNF-α increased PGE_2 secretion and HGF expression, but decreased TGF-β1 secretion (English et al. 2007). Furthermore, 72-hour IFN-γ pre-treatment increased PGE_2 secretion and IDO activity in both BMMSC and UCMSC, but 72-hour TNF-α treatment decreased hepatocyte growth factor (HGF) secretion in UCMSC (Prasanna et al. 2010). Differences in TGF-β1 secretion and HGF expression might be accounted for by species-specific responses, or that prolonged priming may induce refractory HGF expression.

Stimulation of MSC toll-like receptors (TLR) appears to induce differential inflammatory responses. TLR-3 activation of MSC promotes neutrophil survival *in vitro* through MSC secretion of IL-6, IFN-β, and granulocyte macrophage colony-stimulating factor (Cassatella et al. 2011; Raicevic et al. 2011; Liotta et al. 2008). The same survival response is observed with TLR-4 stimulation, but with the additional secretion of the neutrophil chemoattractants, CXCL8 and CXCL10 by MSC (Brandau et al. 2010; Raicevic et al. 2011; Liotta et al. 2008). However, Waterman *et al.*, (2010) reported that BMMSC are ‘polarised’ to an anti-inflammatory or pro-inflammatory phenotype with TLR-3 or TLR-4 stimulation respectively (Waterman et al. 2010). Specifically, PGE_2 secretion increased, TGF-β1/3 expression decreased, and IDO expression increased in response to TLR-3 stimulation with poly(I:C), whereas TLR-4 priming with LPS caused BMMSC to deposit more collagen (associated with fibrosis) and no longer suppress T-cell proliferation (Waterman et al. 2010). These studies would suggest that ISCT criteria used to define MSC do not describe a homogenous population of cells, indeed numerous factors such as; donor age and species, isolation methodology, culture conditions, tissue-source, and experimental parameters can all modify the experimental outcome.

Table 1-1 Effect of cytokine priming on MSC function

Stimulus	**Effect**	**MSC source**	**Species**	**References**
IFN-γ	↑ PD-L1, HGF, and PGE_2 expression ↑ IDO activity	BM	Human/Mouse	(Prasanna et al. 2010; English et al. 2007)
	↓ TGF-β1 secretion	BM	Mouse	(English et al. 2007)
TNF-α	↓ TGF-β1 and HGF secretion	BM/UC	Human/Mouse	(Prasanna et al. 2010; English et al. 2007)
	↑ TGF-β1 expression	UC	Human	(Wu et al. 2015)
	↑ HGF, PGE_2 secretion	BM/UC	Human/Mouse	(Prasanna et al. 2010; English et al. 2007)
Poly(I:C)	↑ IDO, PGE_2, and SMAD7 expression ↓ TGF-β1, IL-6, IL-8, and CCL10 secretion ↑ fibronectin deposition ↓ differentiation capacity	BM	Human	(Waterman et al. 2010)
LPS	↓ TGF-β1 and HGF expression ↑ osteogenesis and collagen deposition	BM/AD	Human	(Wu et al. 2015; Waterman et al. 2010)
	↓ adipogenesis ↑ IL-1Ra, IL-4, IL-6, and IL-8 secretion	AD		(Raicevic et al. 2011; Waterman et al. 2010)
TGF-β1	↑ migration	BM	Mouse	(Yi Tang et al. 2009)

This table describes the effect of individual cytokines on direct MSC function. AD = adipose; BM = bone marrow; CCL= C-C chemokine ligand; HGF = hepatocyte growth factor; IDO = indolamine 2,3-dioxygenase; IFN = interferon; IL = interleukin; LPS = lipopolysaccharide; PD-L = programmed death-ligand; PG = prostaglandin; Poly(I:C) = polyinosinic:polycytidylic acid; SMAD = mothers against decapentaplegic homolog; TGF = transforming growth factor; TNF = tumour necrosis factor; UC = umbilical cord.

In other instances, cytokine priming directly modifies the immunomodulatory function of MSC on other cells (Table 1-2) [reviewed by (Najar et al. 2017; Lee et al. 2015)]. Briefly, IL-10 stimulation potentiates BMMSC function through the release of another soluble factor, HLA-G5 (Selmani et al. 2008). HLA-G5 attenuated natural killer cell IFN-γ secretion and cytotoxicity, as well as promoting BMMSC suppression of T-cell proliferation and the expansion of regulatory T-cells, though the mechanisms of action were unknown (Selmani et al. 2008). Thus, MSC are likely to respond to changes in their microenvironment that may have beneficial or adverse effects on their function – aiding resolution or contributing to pathology. Whether prolonged priming with cytokines or environmental changes influences the ability of MSC to regulate leukocyte recruitment is unclear. Further work to delineate the mechanisms involved and any tissue specific, disease specific responses is required.

Table 1-2 Effect of cytokine priming on MSC immunomodulation

Stimulus	Effect	Mediator(s)	MSC source	Species	References
IFN-γ	↓ T- and B-cells proliferation	IDO, PD-1	Placental/BM	Human/Mouse	(Schena et al. 2010; Jones et al. 2007)
	↓ B-cell differentiation into plasma cells	PD-1	BM	Mouse	(Schena et al. 2010)
	↓ T-cell IFN-γ and TNF-α secretion	-	BM	Human	(Prasanna et al. 2010)
IL-10	↑ T-regulatory cell proliferation ↓ NK cytotoxicity ↓ T-cell proliferation	HLA-G5	BM	Human	(Selmani et al. 2008)
LPS	↑ neutrophil recruitment and survival	IL-8, IL-6	Parotid gland/BM	Human	(Brandau et al. 2010; Cassatella et al. 2011)
Poly(I:C)	↑ neutrophil survival	IL-6, IL-8, IFN-β, GM-CSF	BM	Human	(Cassatella et al. 2011)
TNF-α	↓ DC maturation ↓ DC CCR7 expression ↓ DC CCL19 migration	-	BM	Mouse	(English et al. 2008)

This table describes how individual cytokines alter MSC immunomodulation of other cells and the secreted mediators by which these functions occur. BM = bone marrow; CCL= C-C chemokine ligand; CCR = C-C chemokine receptor; DC = dendritic cell; GM-CSF = granulocyte macrophage colony-stimulating factor; HLA = human leukocyte antigen; IDO = indolamine 2,3-dioxygenase; IL = interleukin; IFN = interferon; LPS = lipopolysaccharide; NK = natural killer; Poly(I:C) = polyinosinic:polycytidylic acid; PD = programmed cell death; TNF = tumour necrosis factor.

1.4. Transformation of stroma in disease

MSC immunomodulation can be either pro-inflammatory or anti-inflammatory depending on the context of their microenvironment [reviewed by (Bernardo & Fibbe 2013)]. Other stromal cells from sites of chronic inflammation acquire a transformed phenotype. As is the case with RA, whereby RASF lose their ability to suppress recruitment of lymphocytes to cytokine-stimulated HUVEC compared with fibroblasts from non-inflamed sites (Filer et al. 2017). Even to the extent that RASF were capable of promoting lymphocyte recruitment in the absence of cytokine treatment (Filer et al. 2017). However, the effect of the chronic inflammatory environment on MSC function is unclear.

Ex vivo studies have shown that BMMSC isolated from RA patients displayed an altered transcriptional profile, with reduced proliferative capacity, senescent morphology, and impaired support of haematopoiesis compared to healthy controls (Kastrinaki et al. 2008; Papadaki et al. 2002). Furthermore, Kastrinaki *et al*., (2008) also noted a reduction in gene expression of cyclin-D and upregulation of its inhibitors in RA BMMSC compared to healthy controls, which was suggested to be attributable to exhaustive replicative senescence in response to chronic inflammation (Kastrinaki et al. 2008) (Table 1-3).

These functional abnormalities were also observed in BMMSC isolated from patients with ‘immune thrombocytopenic purpura’ (ITP), whereby their proliferative capacity and ability to suppress activated T-cell proliferation was impaired compared to healthy controls (Pérez-Simón et al. 2009) (Table 1-3). Indeed, several studies have also reported that BMMSC from systemic lupus erythematosus (SLE) exhibit a low proliferative rate (L. Sun et al. 2007; Nie et al. 2010). SLE-derived BMMSC also showed a significant reduction in IL-6 and IL-7 gene expression (L. Sun et al. 2007), impaired osteogenesis (Yu Tang et al. 2013), and a senescent morphology (Nie et al. 2010) (Table 1-3). A caveat of these studies is that they were all performed using BMMSC, where only systemic inflammatory factors would reach this compartment. As of yet, no work has investigated differences in MSC functional capacity when isolated from the chronically inflammatory microenvironment compared to healthy tissue.

Table 1-3 Effect of inflammatory diseases on MSC function

Stimulus	Effect	MSC source	Species	References
ITP	↓ proliferation ↓ suppression of T-cell proliferation	BM	Human	(Pérez-Simón et al. 2009)
RA	↓ proliferation Impaired haematopoiesis support ↓ cyclin-D expression ↑ cyclin-D inhibitor	BM	Human	(Papadaki et al. 2002; Kastrinaki et al. 2008)
SLE	↓ proliferation ↓ osteogenesis	BM/UC	Human/Mouse	(L. Sun et al. 2010; Nie et al. 2010; El-Badri et al. 2007; Yu Tang et al. 2013)

This table describes the effect of inflammatory diseases on the function of MSC derived from these patients. BM = bone marrow; ITP = immune thrombocytopenic purpura; RA = rheumatoid arthritis; SLE = systemic lupus erythematosus; UC = umbilical cord.

Interestingly, MSC that have undergone a high number of passages in culture lose their capacity to suppress neutrophil adhesion to endothelium (Munir et al. 2016). However, tissue-specific differences appear to occur with UCMSC retaining their immunosuppressive capacity at higher passages than their BMMSC counterparts (Munir et al. 2016). This may hint that inflammation-induced replicative senescence of MSC impairs their immunomodulatory function. Conversely, oncogenic transformation of BMMSC in several sarcoma models showed significantly increased proliferative capacity of BMMSC compared to healthy or non-immortalised controls, but an inability to suppress activated T-cell proliferation (Rodriguez et al. 2014). Moreover, healthy BMMSC have been shown to upregulate gene expression of the immunomodulatory components, IL-6 and IDO in response to culture in 20% synovial fluid from osteoarthritis patients (van Osch 2012). Whilst MSC differentiation usually repairs damaged tissue, it can also be detrimental and sometimes an undesirable by-product of disease. Indeed, ectopic fat deposits have been reported in inflammatory arthritis (Arend et al. 2013), type II diabetes (Goodpaster & D. Wolf 2004), and Duchenne muscular dystrophy (Uezumi et al. 2010). In addition, BMMSC-derived adipocytes have been shown to lose their ability to suppress neutrophil recruitment to TNF-α stimulated endothelium (Munir et al. 2017). However, mature adipocytes or MSC-derived from adipose tissue retain this suppressive function (Munir et al. 2017). These few examples demonstrate the ways in which MSC may experience change of phenotype and function as a result of their microenvironment. However, there isn't sufficient evidence within the literature to state whether MSC are modified at sites of chronic inflammation.

1.5. Role of PDPN in vascular biology and thromboinflammation

The physiological function of PDPN is mostly unknown, but appears to have roles in cell migration (see Section 1.3.3), platelet aggregation, and epithelial-mesenchymal transition (Kato et al. 2003; Wicki & Christofori 2007; Wicki et al. 2006). Overexpression of 'prospero homeobox protein' (Prox)1 in blood vascular endothelial cells induces PDPN expression and differentiation into lymphatic endothelium, as evidenced through adoption of a lymphatic transcription profile (Petrova 2002). However, deletion of Prox1 in mice prevents formation of the lymphatics (Wigle & Oliver 1999), suggesting that PDPN is required lymphatic development. Indeed, PDPN knockout mice die at birth from lymphedema and respiratory failure (Schacht et al. 2003). Whilst, an inducible deletion of T-synthase, which regulates O-glycosylation in the extracellular domain of PDPN causes leakage of blood into the lymphatics, suggesting that o-glycosylation is required for PDPN function (Fu et al. 2008). Deletion of the PDPN receptor in *Clec2*$^{-/-}$ bone marrow chimaera mice resulted in similar bleeding at mucosal lymph nodes to that observed in PDPN knockouts. Finally, post-natal deletion of PDPN in lymphatic endothelium resulted in impaired dendritic cell migration toward the lymph nodes and blood-filled lymphatics (Bianchi et al. 2017). These data highlight an important role for PDPN/CLEC-2 interactions in the embryonic development of the blood and lymphatic vasculature, as well as in the maintenance of vascular integrity in adult tissue.

Platelets are now recognised as active participants in the inflammatory response, with overarching roles in leukocyte recruitment [reviewed by (Ed Rainger et al. 2015)], maintenance of inflamed vascular integrity [reviewed by (Ho-Tin-Noé et al.

2011)], liver regeneration and fibrosis [reviewed by (Chauhan et al. 2016)], as well as metastasis and thromboinflammation [reviewed by (Franco et al. 2015)]. Under normal conditions platelet CLEC-2 cannot interact with PDPN due to separation of the stromal and circulatory compartments by the endothelial lining. However, PDPN is upregulated in the perivascular space in response to hypoxia-induced sterile inflammation (Payne et al. 2017). Surprisingly, Payne *et al*., (2017) demonstrated that blocking PDPN-CLEC2 interactions regulates the size of thrombi (Payne et al. 2017). However, the mechanisms by which these PDPN/CLEC-2 interactions occur are unknown.

During inflammation platelet CLEC-2 has been shown to be an essential component in maintaining vascular integrity, with thrombocytopenic CLEC-2 knockout mice having inflammation-induced haemorrhage (Boulaftali et al. 2013). Boulaftali *et al*., (2013) suggested that CLEC-2 activation by PDPN inhibits the leakage of platelets from hyperpermeable vessels during inflammation, though the mechanisms regulating this were not deciphered (Boulaftali et al. 2013). Herzog *et al*., (2013) reported that the integrity of ‘high endothelial venules’ (HEV) is maintained by sphingosine-1-phosphate (S1P) release from platelets in response to CLEC-2 activation by PDPN-expressing fibroblastic reticular cells (Herzog et al. 2013). S1P upregulates HEV cadherin expression and thus was suggested to prevent the blood-filled lymph nodes observed in CLEC-2 knockout mice (Herzog et al. 2013). These data indicate the importance of PDPN/CLEC-2 interactions (i.e. stromal-platelet interactions) in the maintenance of vascular integrity and prevention of haemorrhage during inflammatory responses. This raises the question as to whether perivascular

PDPN expressing MSC may interact with CLEC-2 on circulating platelets during inflammation to elicit a protective vascular response.

PDPN expression is elevated in pathological conditions (Kawase et al. 2008; Shields et al. 2010; Inoue et al. 2015; Payne et al. 2017). Indeed, fibroblasts from a pro-inflammatory environment, such as those in the synovial lining of RA, constitutively express PDPN and can further upregulate expression in response to IL-1β or TNF-α stimulation (Del Rey et al. 2014; Ekwall et al. 2011; Croft et al. 2016). In contrast, TGF-β has been shown to upregulate PDPN in fibrosarcoma (H. Suzuki et al. 2008), but not RASF (Croft et al. 2016). Whilst upregulated PDPN expression is associated with pathology, it may not be directly contributing to pathogenesis. For example, interactions between PDPN and CLEC-2 have been shown to suppress inflammation and tissue damage in an inducible Clec1b deleting mouse model of inflammatory arthritis (Desanti et al. 2017). However, the mechanism of this protective outcome is unknown.

Many systemic inflammatory disorders predispose to thrombosis in a process known as thromboinflammation, though its pathogenesis varies widely and includes disorders such as Behçet disease, RA, SLE, and inflammatory bowel disease [reviewed by (Aksu et al. 2012)]. Hyperglycemia is strongly associated with acute ischaemic stroke (Muir et al. 2011). Rat models of hyperglycemia also observe thrombosis of the post-capillary venules at sites of neutrophil and platelet adhesion (Desilles et al. 2017). Indeed, scanning electron micrographs of TNF-α stimulated inferior vena cava in mice saw localisation of thrombi to sites of increased leukocyte transmigration (Eriksson et al. 2005). Platelet counts were also shown to be significantly reduced in patients with PDPN-positive brain tumours, and were associated with a high incidence of venous thromboembolism (Riedl et al. 2017). Finally, thrombosis can observed at disrupted atherosclerotic lesions, with these plaques typically harbouring PDPN-positive stroma and macrophages, particularly where necrotic cores are present (Hatakeyama et al. 2012; Inoue et al. 2015). Overall, these studies show a possible link between areas of increased leukocyte transmigration and the subsequent formation of thrombi, with PDPN being a possible culprit for inducing platelet activation in thromboinflammation.

In an *S*. Typhimurium mouse model of systemic non-sterile inflammation, PDPN-mediated platelet coagulation induces localised thrombosis which serves to contain bacteria and contribute toward its clearance (Hitchcock et al. 2015). Infection resulted in extensive liver thrombosis at sites of perivascular inflammation, typically within branches of the portal vein (Hitchcock et al. 2015). Confocal microscopy of liver vasculature identified an upregulated expression of PDPN in the perivascular space with thrombus formation at openings within the endothelial lining. Clodronate-loaded liposome treatment saw depletion of both phagocytic macrophages and thrombi within the liver, but little effect on liver PDPN staining at inflammatory lesions (Hitchcock et al. 2015). This suggests that in non-sterile inflammation, thrombosis is driven by platelet CLEC-2 interactions with PDPN-expressing inflammatory macrophages. However, PDPN-expressing inflammatory macrophages were localised deeper within the stroma, with another population of CD105^{+} PDPN^{+} cells proximal to the endothelium (Hitchcock et al. 2015). In RA, CD105$^+$ PDPN$^+$ cells describe RASF whose interactions with resident macrophages are essential for the resulting inflammatory response [reviewed by (Kinne et al. 2007)]. These data suggest an underlying role for perivascular PDPN expression by stromal cells in inflammation-induced thrombosis, however it is unclear what the outcome of these stromal-myeloid interactions are as well as the mechanism by which PDPN is presented to platelet CLEC-2. We hypothesise that perivascular MSC express PDPN, utilising its invasive properties to present PDPN to circulating platelets and induce their activation.

1.6. Hypothesis and aims

Depending on the context of their microenvironment perivascular stromal cells such as MSC are capable of suppressing leukocyte recruitment to inflamed endothelium (Luu et al. 2013; Munir et al. 2016; Filer et al. 2017; Munir et al. 2017). However, chronic inflammatory disorders are associated with excessive immune infiltrates. Therefore, the inflammatory microenvironment may transform MSC in such a way that they are rendered ineffective or take on a stimulatory role in promoting pathogenesis. Expression of the protein PDPN is also associated with the inflammatory microenvironment, with contact of its receptor, CLEC-2 inducing platelet activation (Ekwall et al. 2011; Inoue et al. 2015; Payne et al. 2017; Hitchcock et al. 2015). However, the mechanism by which these proteins interact at inflammatory sites and the function of such an interaction is unclear. Therefore, we hypothesise that (i) MSC modulation of endothelium is transformed in chronic inflammation; (ii) that perivascular MSC expression of PDPN has implications in thromboinflammation or maintenance of vascular integrity. With this in mind, the aims of this project were:

1. To assess *in vitro* models of neutrophil recruitment.
2. To determine the effect of exogenous TNF-α priming on the transcription profile of MSC and their modulation of endothelium.
3. To characterise PDPN expression and function in MSC.
4. To assess signalling pathways downstream of PDPN.
5. To determine the mechanism by which perivascular PDPN interacts with CLEC-2 on circulating platelets.

Chapter 2. METHODS

2.1. ETHICS

The study was conducted in compliance with the Declaration of Helsinki. All samples were obtained with written, informed consent and approval. 'Umbilical cord-derived MSC' (UCMSC) and HUVEC were sourced with approval of the Human Biomaterial Resource Centre (Birmingham, UK; 12-073) and the North East – Tyne & Wear South Ethics Committee (Birmingham, UK; 15-NE-0285) from umbilical cords obtained from women undergoing elective caesarean section. Fibroblasts were sourced with approval of the West Midlands and Black Country Research Ethics Committee (07H1204191) from synovial tissue obtained from patients undergoing joint replacement therapy. Whole blood was sourced from healthy adult volunteers with approval of the University of Birmingham Local Ethical Review Committee (ERN-12-0079).

2.2. CELL ISOLATION AND CULTURE

2.2.1. HUMAN MESENCHYMAL STROMAL CELLS FROM UMBILICAL CORD

UCMSC were isolated by enzymatic digestion from umbilical cords as previously described (Munir et al. 2015). Briefly, a bilateral incision was made through the amnion. Vessels were resected and the remaining Wharton's jelly and amnion washed of residual blood with 'phosphate-buffered saline' (without calcium and magnesium; PBS; Sigma-Aldrich, Dorset, UK) before roughly cutting into $2mm^3$ pieces with a 10A scalpel (Swann-Morton, Sheffield, UK). The diced tissue was incubated with 1mg/mL clostridium histolyticum collagenase type II and 50U/mL bovine hyaluronidase (both Sigma-Aldrich) in 'phosphate-buffered saline' (with calcium and magnesium; PBS^+) at 37°C for 5 hours on a tube roller (Cole-Parmer, Staffordshire, UK). Remaining tissue fragments were removed by diluting in five volumes of PBS prior to filtration through a 100μm cell strainer (Greiner Bio-One, Stonehouse, UK). The filtered cell suspension was centrifuged at 400g for 10 minutes, before washing the pellet in PBS and centrifuging at 400g for 5 minutes at room temperature. The pellet was re-suspended and subsequently cultured in 'MSC low glucose medium' (MSCLG), which consists of 'Dulbecco's modified Eagle medium' (DMEM) - low glucose formulation (Biosera, Boussens, France) supplemented with 10% foetal bovine serum (FBS), 100U/ml penicillin, and 100μg/ml streptomycin (all from Sigma-Aldrich) and seeded into a '75cm^2 tissue culture treated flask' (T75; BD Falcon, Scientific Laboratory Supplies, Nottingham, UK) before incubating at 37°C and 5% CO_2. MSCLG was initially replaced after 24 hours, and then every 3 days. The cells were subcultured at a ratio of 1:3 (Section 2.3). The cells were used in experiments or cryopreserved (Section 2.4) at passage three unless stated otherwise. All donors were phenotyped according to ISCT guidelines (Section 1.2.1) (Dominici et al. 2006).

2.2.2. Human mesenchymal stromal cells from bone marrow

Cryopreserved bone marrow-derived MSC (BMMSC; Lonza, Basel, Switzerland) were purchased at passage two. Cells were thawed by warming in a 37°C water bath for 1 minute before sterilising the cryovial exterior with 70% ethanol (ThermoFisher Scientific, Paisley, UK). The cells were re-suspended in pre-warmed 'MSC growth medium' (MSCGM), as recommended by the manufacturer which consists of human MSC basal medium supplemented with hMSC SingleQuot Kit containing; 10% heat-inactivated FBS, 2% L-glutamine, 30mg/mL gentamicin, and 15μg/mL amphotericin (all from Lonza). The cell suspension was centrifuged at 400g for 5 minutes at room temperature. The pellet was re-suspended and subsequently cultured in T75 flasks with MSCGM replaced every 3 days. The cells were subcultured at a 1:3 ratio (Section 2.3). The cells were used in experiments or cryopreserved (Section 2.4) at passage five unless stated otherwise. All donors were phenotyped according to ISCT guidelines (Section 1.2.1) (Dominici et al. 2006).

2.2.3. HUMAN WHOLE BLOOD AND ISOLATED NEUTROPHILS

Whole venous blood was collected in tubes containing citrate-phosphate-dextrose with adenine solution at a 10:1 ratio (Sigma-Aldrich) and used in whole blood platelet adhesion and aggregation assays as described (Sections 2.8.3 and 2.15). In some experiments platelets were labelled by incubating whole blood with mouse anti-human CD41a-PE antibody (Dako, Cheshire, UK) for 10 minutes.

Alternatively, neutrophils were isolated as previously described (Munir et al. 2015). Briefly, venous blood was collected in K_3EDTA-coated (1.6mg/mL) tubes (Sarstedt, Leicester, UK). A histopaque density gradient was setup by adding 2.5mL histopaque 1119 to a round-bottom tube followed by 2.5mL histopaque 1077 (both Sigma-Aldrich), 5mL of whole blood per tube was layered on the histopaque gradient and centrifuged at 1200g for 30 minutes at room temperature. The neutrophils sediment 2cm above the haematocrit, this band was collected and washed twice in 'basal medium 199' (M199) with 0.15% bovine serum albumin (BSA) (MBSA; both Gibco, ThermoFisher) by centrifugation at 400g for 5 minutes at room temperature. The neutrophil pellet was re-suspended in MBSA and the cell concentration determined using a Z2-series Coulter Counter (Beckman Coulter, High Wycombe, UK), before further diluting to 1×10^6 cells/mL in MBSA.

2.2.4. Human umbilical vein endothelial cells

Endothelial cells were isolated using a collagenase digest of the veins as previously described (Munir et al. 2015). Briefly, the vein was cannulated and washed with PBS^+ to remove blood. The PBS^+ was aspirated, the vein filled with 1mg/mL collagenase type Ia (all Sigma-Aldrich) diluted in PBS^+ and incubated for 15 minutes at 37°C and 5% CO_2. The cord was massaged and the endothelial cell suspension collected by flushing the vein with PBS followed by air. The suspension was centrifuged at 400g for 5 minutes and the pellet resuspended in HUVEC medium, which consists of M199 supplemented with 20% FBS, 35μg/mL gentamicin, 1μg/mL hydrocortisone, 10ng/mL epidermal growth factor (all from Sigma-Aldrich), and 2.5μg/mL amphotericin B (ThermoFisher). The isolated endothelium were cultured to confluence (approximately 5 days) in a 25cm^2 tissue culture treated flask (T25; BD Falcon), with HUVEC medium replaced every other day. The cells were used for experiments at the first passage.

In some experiments, Ibidi microslides were prepared as previously described (Munir et al. 2015). Briefly, HUVEC (1.25×10^5 cells/channel) were seeded onto a 6-channel Ibidi microslide (μ-Slide $VI^{0.4}$; Ibidi, Thistle Scientific, Glasgow, UK) (Figure 2-6A) in MSCGM and incubated at 37°C and 5% CO_2 for 1 hour. The channels were washed three times with MSCGM to remove non-adherent cells and incubated at 37°C and 5% CO_2 for 24 hours. HUVEC was treated with 'recombinant human tumour necrosis factor alpha' (TNF-α; R&D Systems, Oxford, UK) at 0, 10, or 100U/mL diluted in MSCGM, then incubated for a further 4 hours at 37°C and 5% CO_2 prior to setup in the Ibidi microchannel flow-based adhesion assay (Section 2.8.10).

2.2.5. Human dermal blood endothelial cells

Cryopreserved human dermal blood endothelial cells (BEC; PromoCell, Heidelberg, Germany) were purchased at passage two and thawed. The cells were subsequently cultured in T75 flasks using BEC growth medium (BECGM), as recommended by the manufacturer which consists of endothelial cell basal medium MV supplemented with endothelial cell growth medium MV Supplement Mix containing; 5% FBS, 0.4% bovine hypothalamic extract, 10ng/mL human epidermal growth factor (EGF), 90μg/mL heparin, and 1μg/mL hydrocortisone (all from PromoCell). BECGM was replaced every 3 days. The cells were subcultured at a 1:3 ratio (Section 2.3). The cells were used in experiments or cryopreserved (Section 2.4) at passage four unless stated otherwise.

2.2.6. Human fibroblasts

Synovial fibroblasts were obtained from patients with established, treated RA undergoing knee replacement surgery at the Royal Orthopaedic Hospital (Birmingham, UK). They were isolated as previously described (Salmon et al. 1997), and provided by Dr. A. Filer (Rheumatology Research Group, University of Birmingham, UK) in a cryopreserved state at passage four. All patients conformed to the 1987 American College of Rheumatology definition of RA (Arnett et al. 1988). All donors were female and positive for rheumatoid factor, age was 51±15 years, 'disease activity score' (DAS)28 baseline was 6.1±1.2, disease duration was 910±150 weeks (data expressed as median ± standard deviation). Fibroblasts were thawed and subsequently cultured in T75 flasks using fibroblast growth medium (FGM), which consists of 'Roswell park memorial institute' (RPMI) 1640 medium supplemented with 1x MEM non-essential amino acids, 2mM L-glutamine, 1mM sodium pyruvate, 100U/mL penicillin and 100μg/mL streptomycin (all from Sigma-Aldrich), and 10% FBS (Labtech, East Sussex, UK). Two-thirds of the medium was replaced every 7 days. The cells were subcultured at a 1:3 ratio (Section 2.3). The cells were used in experiments or cryopreserved (Section 2.4) at passage six to nine unless stated otherwise.

2.2.7. Human embryonic kidney 293T cells

An immortalised 'human embryonic kidney' (HEK293T) cell line was gifted by Dr. M. Tomlinson (Biosciences, University of Birmingham, UK) in a proliferating state (Reyat et al. 2017). The cells were cultured in T75 flasks with MSCLG replaced every 3 days. The cells were subcultured at a 1:5 ratio (Section 2.3). The cells were used in experiments or cryopreserved (Section 2.4).

2.3. Subculture

Briefly, plastic-adherent cells were subcultured at 80% confluence by washing with 2mM EDTA for 1 minute, before incubating with 2.5mg/mL trypsin (from porcine pancreas; both Sigma-Aldrich) at room temperature. A phase-contrast microscope was used to determine when the adherent cells had detached, at which point one volume of respective cell culture medium was added to quench the reaction. The cell suspension was centrifuged at 400g for 5 minutes at room temperature and the resulting pellet re-suspended in respective cell culture medium and either; seeded into tissue culture treated flasks for further expansion at 37°C and 5% CO_2, used in experiments, or cryopreserved (Section 2.4).

2.4. Cryopreservation

For cryopreservation, cells at 80% confluence were subcultured (Section 2.3) and the pellet re-suspended in cryo-SFM (PromoCell) and stored in 1.5mL cryovials (Greiner Bio-One, Stonehouse, UK). Cryovials were slowly cooled to -80°C before storing in liquid nitrogen.

2.5. ESTABLISHING COCULTURES ON TRANSWELL FILTERS

Seeding cells onto filters and establishing cocultures were performed as previously described (Munir et al. 2015). The cells were subcultured (Section 2.3) and re-suspended in their respective culture medium.

For cocultures, BMMSC or UCMSC were seeded at 1.0×10^4 cells/mm^2 or 2.4×10^3 cells/mm^2 respectively onto the basal surface of an inverted 6-well transwell filter (BD Falcon) for 1 hour at 37°C and 5% CO_2. Following which, the filter was inverted again and suspended in a matched culture plate containing MSCGM for 24 hours at 37°C and 5% CO_2. RASF, HUVEC, or BEC, were subcultured, re-suspended in MSCGM, and seeded at 1.0×10^4 cells/mm^2 on the apical surface of the filter for 24 hours at 37°C and 5% CO_2 (Figure 2-7A, B). For comparison, BMMSC, UCMSC, RASF, HUVEC, or BEC monocultures were established as controls. In some experiments, BMMSC were stimulated with 100U/mL TNF-α in MSCGM for 24 or 72 hours at 37°C and 5% CO_2 prior to coculture with BEC. Conditioned medium from 24 hours of cell culture was collected from untreated or TNF-α pretreated monocultures and cocultures; cellular debris was pelleted by centrifugation at 1200g for 10 minutes and the supernatant collected and stored at -80°C until used for measuring the concentration of IL-6 by ‘enzyme-linked immunosorbent assay’ (ELISA) (Section 2.10). BMMSC-HUVEC/BEC cocultures and the respective endothelial monoculture control were stimulated with 100U/mL TNF-α for 4 hours at 37°C and 5% CO_2 prior to the flow assay (Section 2.8.2). In other experiments, BMMSC-RASF cocultures and the respective monoculture controls were analysed for gene expression (Section 2.7.5). In other experiments, UCMSC monocultures or UCMSC-BEC cocultures and the respective monoculture controls were setup and used in platelet adhesion and aggregation assays (Sections 2.8.2 and 2.15).

2.6. Migration of MSC through transwell filters

For migration assays, UCMSC were seeded at 2.4×10^3 cells/mm^2 on an 8.0μm pore 12-well transwell filter (BD Falcon) and cultured for 48 hours at 37°C and 5% CO_2. Migration was assessed by detaching cells from the upper and lower surfaces of the filter using 2.5mg/mL trypsin with 0.5mM EDTA. Cell suspensions were quantified using a Z2-series Coulter Counter (Beckman Coulter). Data are expressed as the number of cells that had migrated to the lower chamber as a percentage of the total number of cells counted in both chambers.

In some experiments, PDPN was crosslinked to induce receptor clustering and downstream signalling. At 1 hour post-seeding, PDPN-positive UCMSC were incubated with 2μg/mL anti-human podoplanin (NZ-1.3) for 30 minutes (ThermoFisher) at 37°C and 5% CO_2. An additional 30μg/mL of goat anti-rat IgG2a (ThermoFisher) was added to induce crosslinking for 47 hours at 37°C and 5% CO_2.

In other experiments, cells were treated with inhibitors against; Ras homolog gene family GTPases (Rho) at 1, 2, or 4μg/mL (CT04; Cytoskeleton Inc, Colorado, USA), Rho-associated protein kinase (ROCK) at 10 or 100μM (Y27632; Sigma Aldrich), or Ras-related C3 botulinum toxin substrate one (Rac1) at 1 or 10μM (NSC23766; Calbiochem, Merck Millipore, Nottingham, UK) for the experiment duration.

2.7. MSC CHARACTERISATION

2.7.1. FLOW CYTOMETRY

Expression of MSC ISCT surface markers was determined by flow cytometry; CD105, CD90, CD73, CD45, CD34, CD19, CD14, and HLA-DR (Dominici et al. 2006). In some experiments PDPN (gp38; NZ-1.3) expression was also determined. The cells were detached from culture plastic and the pellet re-suspended in ice-cold MACS buffer (PBS with 2mM EDTA and 1% BSA) at 3×10^4 cells/100μl/tube prior to staining with conjugated antibodies or respective isotype controls (Table 2-1). Samples were incubated for 20 minutes at 4°C in the dark. The cells were washed twice with MACS buffer at 400g for 5 minutes at 4°C. The cells were analysed on the CyAn ADP flow cytometer (Beckman Coulter) within an hour of staining. Data were analysed using FlowJo (FlowJo LLC, Ashland, Oregon) and expressed as ‘median fluorescence intensity’ (MFI) with the IgG isotype control subtracted, unless indicated otherwise. BMMSC and UCMSC were positive for CD73, CD90 and CD105 expression, and negative for CD45, CD34, CD19, CD14, and HLA-DR; thus, conforming to the criteria set out by the ISCT for defining MSC (Figure 2-1) (Dominici et al. 2006).

Table 2-1 Antibodies used for fluorescent labelling in flow cytometry:

Antigen	Clone	Host & isotype	Fluorophore	Concentration	Supplier	Catalogue number
Isotype Controls						
	MOPC-21	Mouse IgG_1, κ	FITC	50μg/mL	Becton Dickinson, Oxford, UK	551954
	MOPC-21	Mouse IgG_1, κ	BV421	50μg/mL	Biolegend, London, UK	400158
	P3.6.2.8.1	Mouse IgG_1, κ	eFluor 450	50μg/mL	ThermoFisher	48-4714-82
	eBR2a	Rat IgG_{2a}, κ	PE	50μg/mL	ThermoFisher	12-4321-42
Negative MSC Markers						
CD14	M5E2	Mouse IgG_{2a}, κ	PE	50μg/mL	Biolegend	301806
CD19	HIB19	Mouse IgG_1, κ	PE-Cy7	50μg/mL	Biolegend	302216
CD34	563	Mouse IgG_1, κ	PE	50μg/mL	Becton Dickinson	301806
CD45	UCHL1	Mouse IgG_{2a}, κ	PE	50μg/mL	Becton Dickinson	347967
HLA-DR	LN3	Mouse IgG_{2b}, κ	eFluor450	50μg/mL	ThermoFisher	48-9956-42
Positive MSC Markers						
CD73	AD2	Mouse IgG_1, κ	FITC	50μg/mL	ThermoFisher	11-0739-42
CD90	5E10	Mouse IgG_1, κ	BV421	50μg/mL	Biolegend	328122
CD105	SN6	Mouse IgG_1, κ	eFluor 450	50μg/mL	ThermoFisher	48-1057-42
Others						
gp38	NZ-1.3	Rat IgG_{2a}, κ	PE	50μg/mL	ThermoFisher	12-9381-42

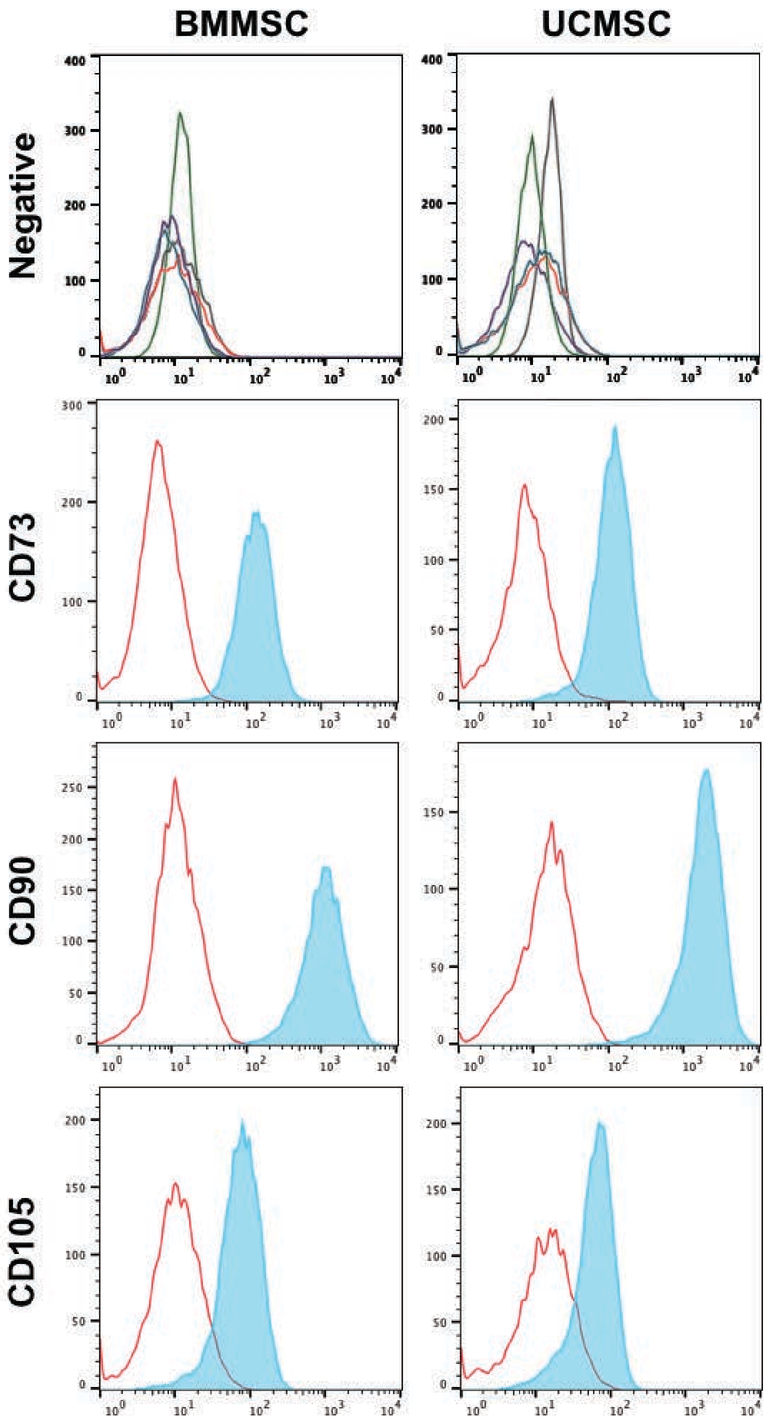

Figure 2-1 MSC ISCT Flow Cytometric Phenotyping
BMMSC at passage five and UCMSC at passage three were stained with antibodies against MSC specific markers (filled); CD73, CD90, CD105, and respective isotype controls (outline). Overlaid negative-MSC markers **(Negative)**; HLA-DR (red), CD14 (black), CD19 (green), CD34 (blue), and CD45 (purple). Images are representative of n=7-9 different donors for each cell type.

2.7.2. *Adipogenesis*

MSC adipogenic differentiation was induced using human MSC Adipogenic Differentiation BulletKit (adipogenic medium; Lonza), which consists of human MSC adipogenic induction basal medium supplemented with human MSC SingleQuot Kit containing human recombinant insulin, L-glutamine, MCGS, dexamethasone, indomethacin, 3-isobutyl-1-methyl-xanthine, 30mg/mL gentamicin, and 15μg/mL amphotericin (all from Lonza). MSC were seeded onto 6-well culture plastic at 2×10^4 cells/cm^2 in MSCGM till 80% confluent. Differentiation was induced using adipogenic medium, which was replaced every 5 days for a total of 21 days. Differentiated MSC were washed in PBS and subsequently fixed in 10% neutral-buffered formalin (4% formaldehyde, 40mg/mL sodium phosphate monobasic, 65mg/mL sodium phosphate dibasic anhydrous [all from Sigma-Aldrich] diluted in distilled water) overnight before washing again in distilled water. Adipogenic MSC were stained with 60% isopropanol for 5 minutes followed by filtered 0.1% Oil Red O (Sigma-Aldrich) in 60% isopropanol for 15 minutes at room temperature. Stained cells were imaged with an EOS 450D digital SLR camera (Canon, Surrey, UK). Adipogenesis was confirmed by the presence of Oil Red O stained lipid droplets within the cell cytoplasm (Figure 2-2C, D).

2.7.3. *Osteogenesis*

MSC osteogenic differentiation was induced using MesenCult Osteogenic Stimulatory Kit (osteogenic medium; STEMCELL Technologies, Cambridge, UK), Human MesenCult MSC Basal Medium supplemented with: 15% osteogenic stimulatory supplement, 10nM dexamethasone, 50μg/ml ascorbic acid (all STEMCELL Technologies). MSC were seeded onto 6-well culture plastic at 6×10^3 cells/cm^2 in MSCGM till 80% confluent. Differentiation was induced using osteogenic medium which was replaced every three days until multi-layering of cells is observed, upon which 3.5mM β-glycerophosphate (STEMCELL Technologies) was added to osteogenic medium for a further 14 days. Osteogenic MSC were washed and fixed as above, before being stained with 20mg/mL Alizarin Red S solution (Sigma-Aldrich) diluted in distilled water, (adjust pH to 4.1-4.3 with 0.1% NH_4OH) for 45 minutes at room temperature in the dark. Stained cells were imaged with an EOS 450D digital SLR camera (Canon). Osteogenesis was confirmed by the presence of Alizarin Red S stained calcium deposits on mineralised cells (Figure 2-2E, F).

2.7.4. Chondrogenesis

MSC chondrogenic differentiation was induced using MesenCult-ACF Chondrogenic Differentiation Medium (chondrogenic medium, STEMCELL Technologies) which consists of MesenCult-ACF Chondrogenic Differentiation Basal Medium supplemented with: 5% MesenCult Chondrogenic Differentiation Supplement (all from STEMCELL Technologies). MSC were centrifuged at 400g for 10 minutes at 5×10^5 cells per polypropylene tube in chondrogenic medium. The pellets were cultured in said tubes at 37°C and 5% CO_2, with the caps loosened a quarter-turn to allow gas exchange. Chondrogenic medium was replaced every 3 days for a total of 21 days. Chondrogenic MSC spheroids were delivered to musculoskeletal pathology (NHS, Birmingham, UK) where they were embedded in paraffin, sectioned into 7μm slices, and melted onto glass slides. Upon receipt, the slides were deparaffinised in xylene, stepwise rehydrated and stained with 0.1mg/mL Alcian Blue 8GX (Alfa Aesar, Heysham, UK) dissolved in 40% acetic acid (ThermoFisher) and 60% ethanol for 30 minutes at room temperature in the dark. Spheroids were washed twice with destaining solution (40% acetic acid and 60% ethanol) for 20 minutes each, before counterstaining with nuclear fast red (Vector Laboratories, Peterborough, UK) for 10 minutes. Slides were washed under running tap water for 10 minutes prior to stepwise dehydration with ethanol and final xylene clearing. The slides were mounted with VectaMount (Vector Laboratories) and stored at room temperature in the dark. Stained cells were imaged with an EOS 450D digital SLR camera (Canon). Chondrogenesis was confirmed by the presence of sulfated proteoglycans stained with Alcian Blue (Figure 2-2G, H).

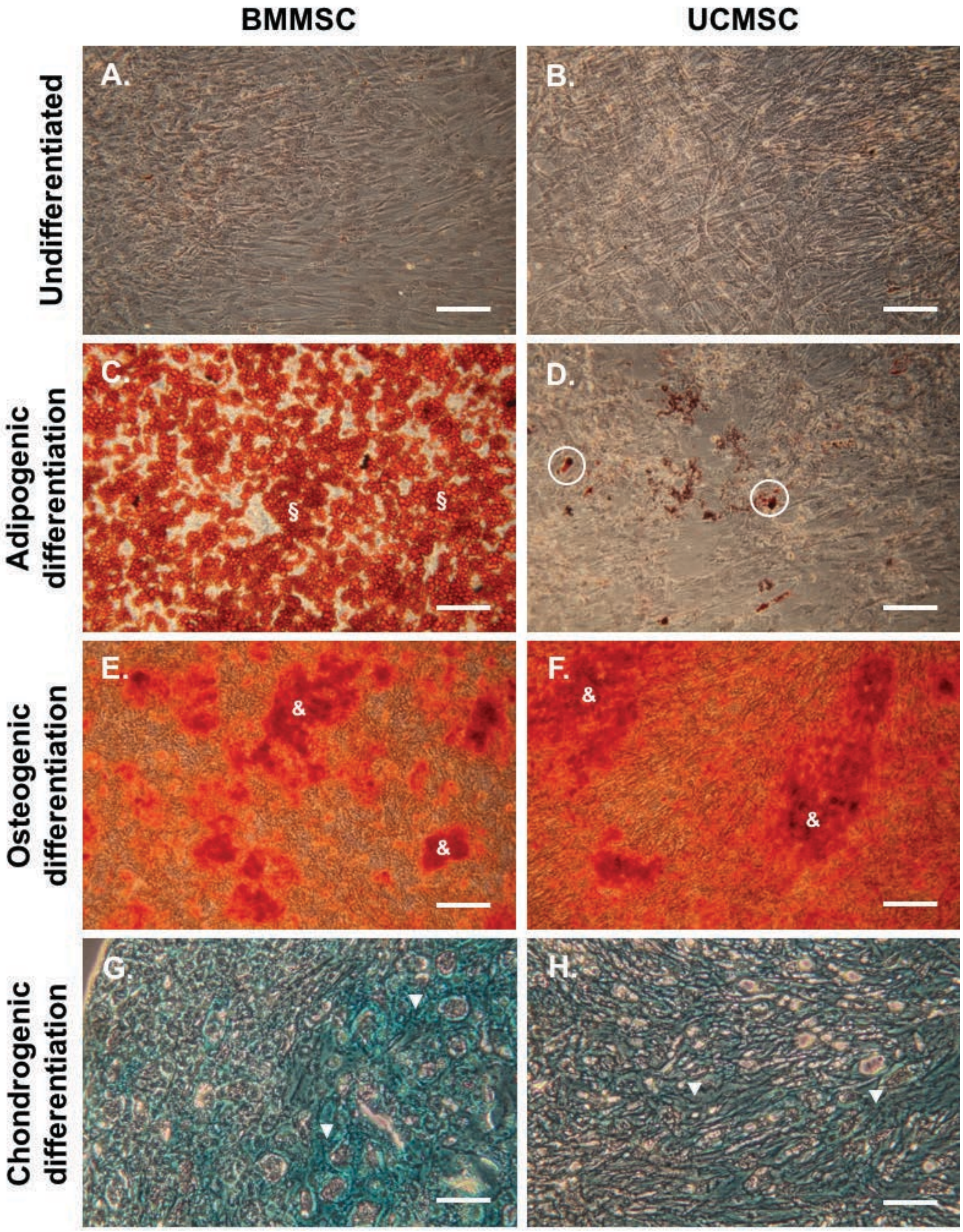

Figure 2-2 MSC tri-lineage differentiation histology
Human MSC were cultured in **(A)** MSCGM or **(B)** MSCLG, or **(C, D)** adipogenic medium, or **(E, F)** osteogenic medium, or **(G, H)** chondrogenic medium, then stained using oil red O, alizarin red S, or alcian blue respectively. Images are representative of n=4-6 different donors for each cell type. Scale bar represents 10μm. Circles and '§' denote areas of oil red O staining for lipids. '&' denotes areas of alizarin red S staining for calcium deposits. Arrows denote areas of alcian blue staining for sulfated proteoglycans.

2.7.5. MESSENGER RIBONUCLEIC ACID ISOLATION AND QUANTITATIVE POLYMERASE CHAIN REACTION

Messenger ribonucleic acid (mRNA) was isolated from BMMSC, UCMSC, adipocytes, osteoblasts, and chondroblasts using an RNeasy Mini kit (Qiagen, Manchester, UK) as per the manufacturer's instructions. The cells were subcultured and the resulting pellets vigorously re-suspended in 350μL of RLT lysis buffer (supplemented with 1:100 β-mercaptoethanol; Sigma-Aldrich) and stored at -80°C. Within 14 days of initial storage, the samples were vigorously mixed with 350μl of 70% ethanol and further vortexed for a minimum of 30 seconds. The mixture was transferred to RNeasy columns and centrifuged at 10000g for 1 minute. The column was washed once with RW1 buffer and twice with RPE by centrifugation at 10000g for 1 minute for each treatment. Any flow-through was discarded. The column was dry spun at 10000g for 2 minutes, prior to elution of RNA with RNase-free water (Qiagen) by centrifugation at 10000g for 1 minute. The elution step was repeated with the flow-through to maximise mRNA recovery, and the purity and concentration determined using a NanoDrop 1000 spectrophotometer (ThermoFisher). RNA purity was deemed acceptable when the 260/280nm and 260/230nm absorbance ratio were both within a range of 1.8-2.1.

Isolated mRNA was reverse transcribed into cDNA as described (Chimen et al. 2015). Briefly, 0.5μg mRNA was annealed with 1μg random primers (Promega, Southampton, UK) in 15μL of RNase-free water for 5 minutes at 70°C, followed by the addition of 11.63μL of master mix per sample comprising 5× M-MLV buffer, 10mM dNTP mix (dATP, dCTP, dGTP, dTTP), 200U M-MLV reverse transcriptase, and 40U RNasin Plus (all from Promega) diluted in RNase-free water. RT-PCR was performed at 37°C for 1 hour using Touchgene Gradient PCR thermal cycler (Techne, Staffordshire, UK). Quantitative PCR (qPCR) was performed using TaqMan Gene Expression Assays according to the manufacturer's instructions in a 384-well optical reaction plate (Applied Biosystems, ThermoFisher). Each sample was run in triplicate and reactions were composed of 0.5μL cDNA, 4μL TaqMan universal PCR master mix, 5μL RNase-free water, and 0.5μL FAM-labelled TaqMan gene expression assay primers and probes (all from Applied Biosystems) for each gene analysed (Table 2-2). Samples were run on a 7900HT Real Time PCR machine for 40 cycles and subsequently analysed using SDS 2.2 software (both from Applied Biosystems). Triplicates were averaged to obtain the threshold cycle (C_T) for each sample, and subtracted from the average C_T value for the housekeeping control; *18S* or *GAPDH* (ΔC_T). Technical repeats outside of 1 C_T were discarded. 'Relative expression units' (REU) for each gene were calculated with the following formula.

$$REU = 2^{-\Delta C_T}$$

MSC adipogenesis was determined by upregulation of *PPAR*γ, *C/EBP*α, and *FABP4* adipogenic genes compared to untreated MSC (Rosen et al. 2002; Garin-Shkolnik et al. 2014). BMMSC significantly upregulated *PPAR*γ in response to adipogenic medium (Figure 2-3A), however no effect was observed for UCMSC, or *C/EBP*α and *FABP4* in BMMSC (Figure 2-3). MSC osteogenesis was determined by upregulation of *RUNX2* and *BMP2* osteogenic genes compared to untreated MSC (Jang et al. 2012). No effect of osteogenic medium was observed on MSC expression of osteogenic genes (Figure 2-4). UCMSC chondrogenesis was determined by upregulation of *SOX5* and *SOX9* chondrogenic genes compared to untreated UCMSC (Liu & Lefebvre 2015). UCMSC significantly upregulated expression of *SOX5* but not *SOX9* in response to chondrogenic medium (Figure 2-5). In other experiments, BMMSC or RASF were stimulated with 100U/mL TNF-α in MSCGM for 24 or 72 hours at 37°C and 5% CO_2, or BMMSC-RASF cocultures and respective monocultures were also determined by qPCR.

Table 2-2 Primers used for human gene expression analysis:

Gene ID	Assay ID
BMP2	Hs00154192_m1
C/EBPα	Hs00269972_s1
CD248	Hs00535586_s1
FABP4	Hs01086177_m1
FAP	Hs00990806_m1
GAPDH	Hs02786624_g1
ICAM1	Hs00164932_m1
IDO1	Hs00984148_m1
PDPN	Hs00366766_m1
PPARγ	Hs00234592_m1
RNA18S5	Hs03928990_g1
RUNX2	Hs01047973_m1
SOX5	Hs00753050_s1
SOX9	Hs01001343_g1
VCAM1	Hs01003372_m1

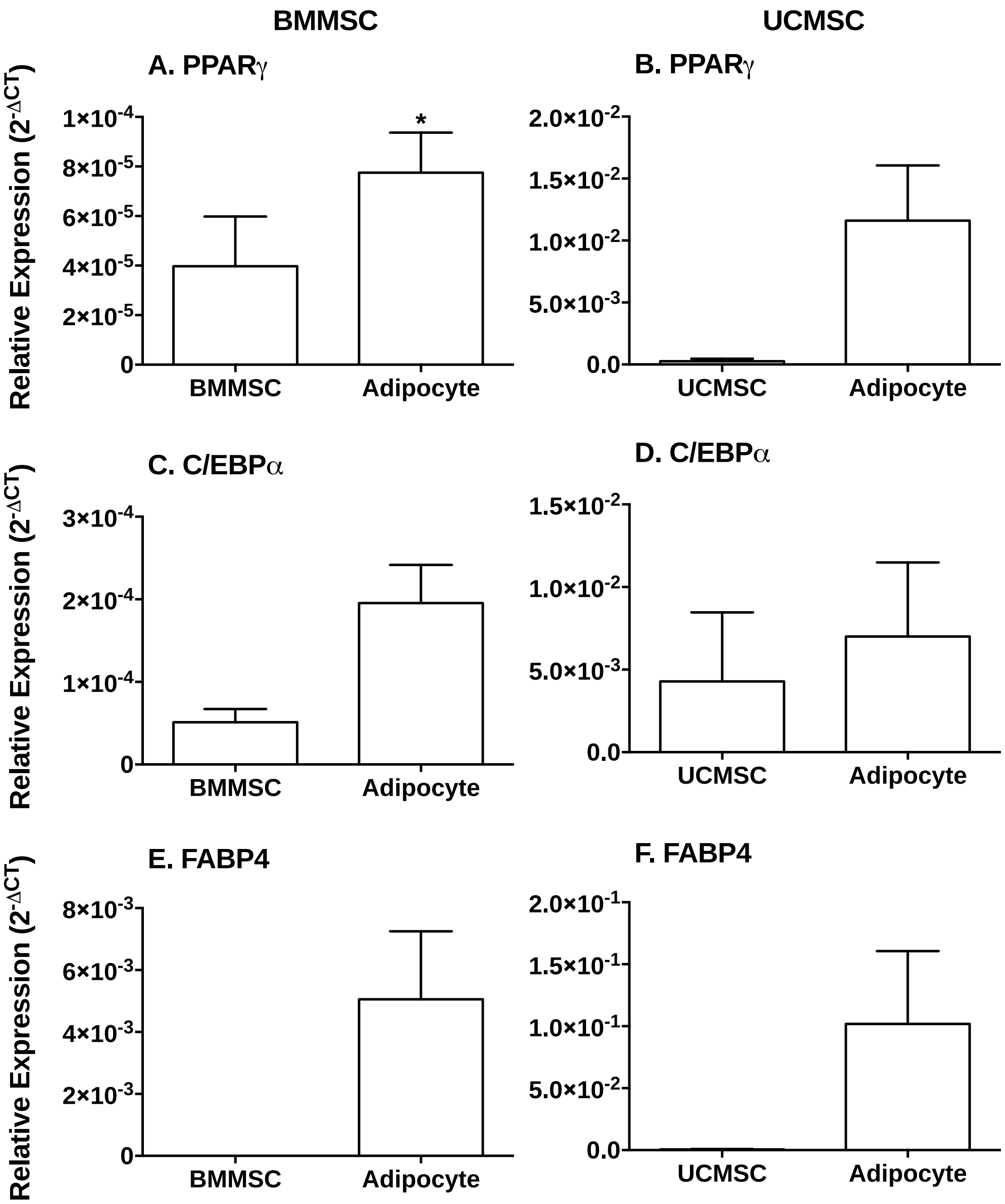

Figure 2-3 MSC adipogenic differentiation qPCR
(A, C, E) BMMSC or **(B, D, F)** UCMSC were cultured in the presence or absence of adipogenic medium for 21 days. Gene expression for adipocyte markers **(A, B)** *PPARγ*, **(C, D)** *C/EBPα*, and **(E, F)** *FABP4* were measured by qPCR. Data are mean ± SEM from n=4-6 independent experiments using four or six different donors for each cell type**.** * = $p<0.05$ by paired t-test.

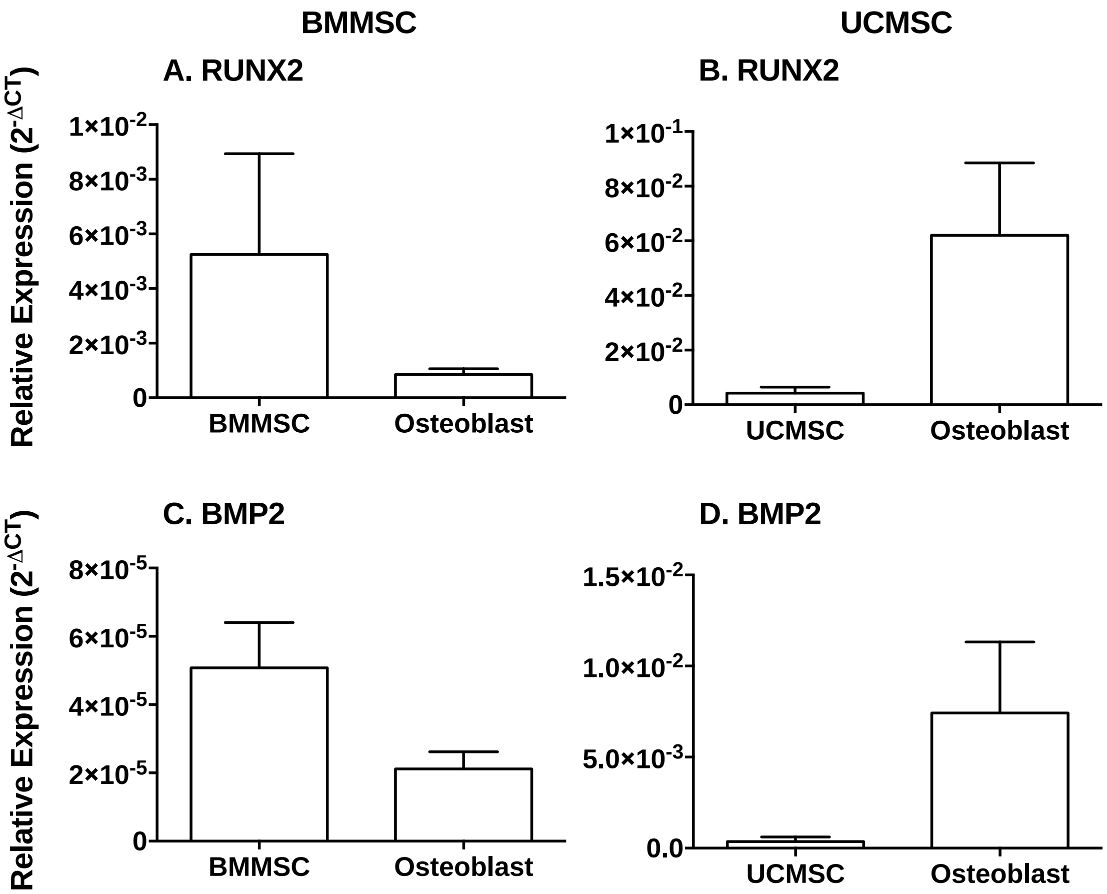

Figure 2-4 MSC osteogenic differentiation qPCR
(A, C) BMMSC or **(B, D)** UCMSC were cultured in the presence or absence of osteogenic medium for 14 days. Gene expression for osteoblast markers **(A, B)** *RUNX2* and **(C, D)** *BMP2* were measured by qPCR. Data are mean ± SEM from n=4 independent experiments using four different donors for each cell type.

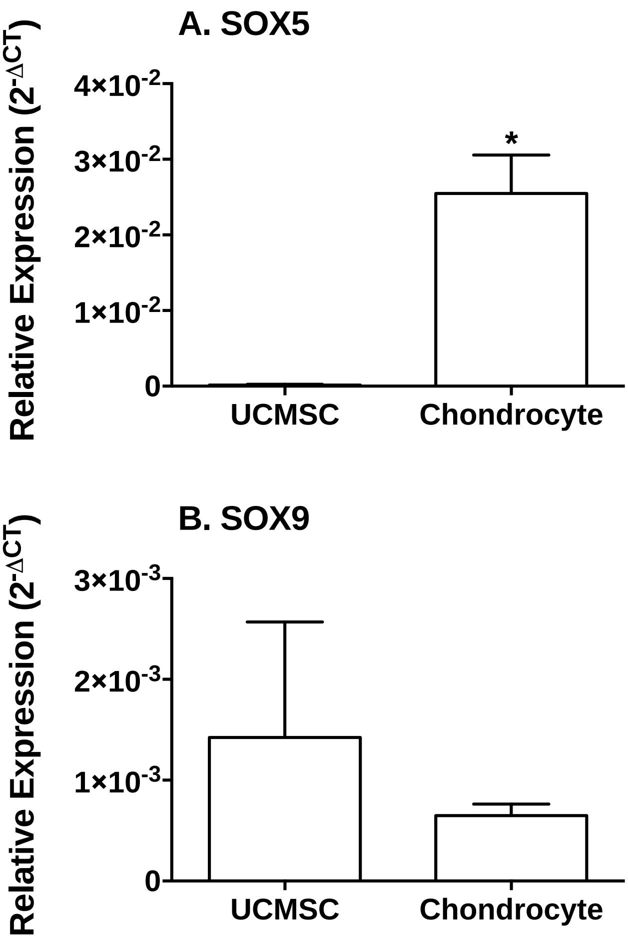

Figure 2-5 UCMSC chondrogenic differentiation qPCR

UCMSC were cultured in the presence or absence of chondrogenic medium for 21 days. Gene expression for chondroblast markers **(A)** *SOX5* and **(B)** *SOX9* were measured by qPCR. Data are mean ± SEM from n=4 independent experiments using four different donors**.** * = $p<0.05$ by paired t-test.

2.8. ADHESION ASSAYS

2.8.1. IBIDI MICROSLIDE FLOW-BASED ADHESION ASSAY SETUP

The flow system was setup as shown and described (Figure 2-6C). The Ibidi microslide channel inlet was connected by a female to male Luer elbow fitting (Labhut, Pennsylvania, USA) with a 10mm length piece of flexible silicon rubber 2/4mm tubing overlapping the end of 1/3mm tubing (both from ThermoFisher) which was in turn connected to the outlet port of an electronic switching valve (Lee Products, Gerards Cross, UK). The electronic switching valve selected flow from two fluid reservoirs. The ‘sample reservoir’ was directly connected to the valve inlet via 5mm length 1/3mm tubing with overlapping 5mm length 2/4mm tubing connected to an inverted 2mL syringe (without plunger, BD Falcon), filled with a neutrophil suspension (1×10^6 cells/mL in MBSA). The ‘wash reservoir’ was indirectly connected to the second valve inlet via 5mm length 1/3mm tubing with overlapping 2/4mm tubing connected to the three-way tap and an inverted 20mL syringe (without plunger, BD Falcon), filled with cell-free MBSA. A third 5mL syringe (with plunger) filled with cell-free MBSA was attached to the three-way tap to manually remove air bubbles. The Ibidi microslide channel outlet was connected by a female to male Luer elbow fitting with a 10mm length of 2/4mm tubing overlapping a 5mm length of 1/3mm tubing overlapping Portex blue line manometer tubing (Smiths-Medical, Luton, UK) connected to a 50mL Popper Micro-Mate glass syringe mounted on a withdrawal syringe pump (both from Harvard Apparatus, Cambridge, UK). The tubing was primed with cell-free MBSA and any bubbles were removed prior to performing the flow-based adhesion assay (Section 2.8.3).

2.8.2. Transwell coculture flow-based adhesion assay setup

The transwell coculture adhesion assays were setup as previously described (Munir et al. 2015). Pre-stimulated BMMSC-HUVEC/BEC or UCMSC-BEC cocultures, or respective monocultures were subsequently incorporated into a bespoke parallel plate chamber as described (Munir et al. 2015). Briefly, the filters were cut out with a 10A scalpel onto a glass coverslip (76×26mm – ThermoFisher) with the apical filter surface or endothelial monolayer facing up. The coverslip and filter were covered with a paraffin film gasket (Parafilm, Neenah, Wisconsin, USA) with a central 20×4mm slot cut into it to form the flow channel overlaying the filter (Figure 2-6B). The combination of the coverslip, filter, and gasket were placed into a custom flow chamber as shown and described (Figure 2-6C). The tubing for the parallel plate chamber was setup as described for the Ibidi microslide with the following exceptions. The channel inlet was connected by a 10mm length piece of Portex blue line manometer tubing underlapping 1/3mm tubing which was in turn connected to the outlet port of an electronic switching valve. The parallel plate chamber channel outlet was connected by Portex blue line manometer tubing to a 50mL Popper Micro-Mate glass syringe.

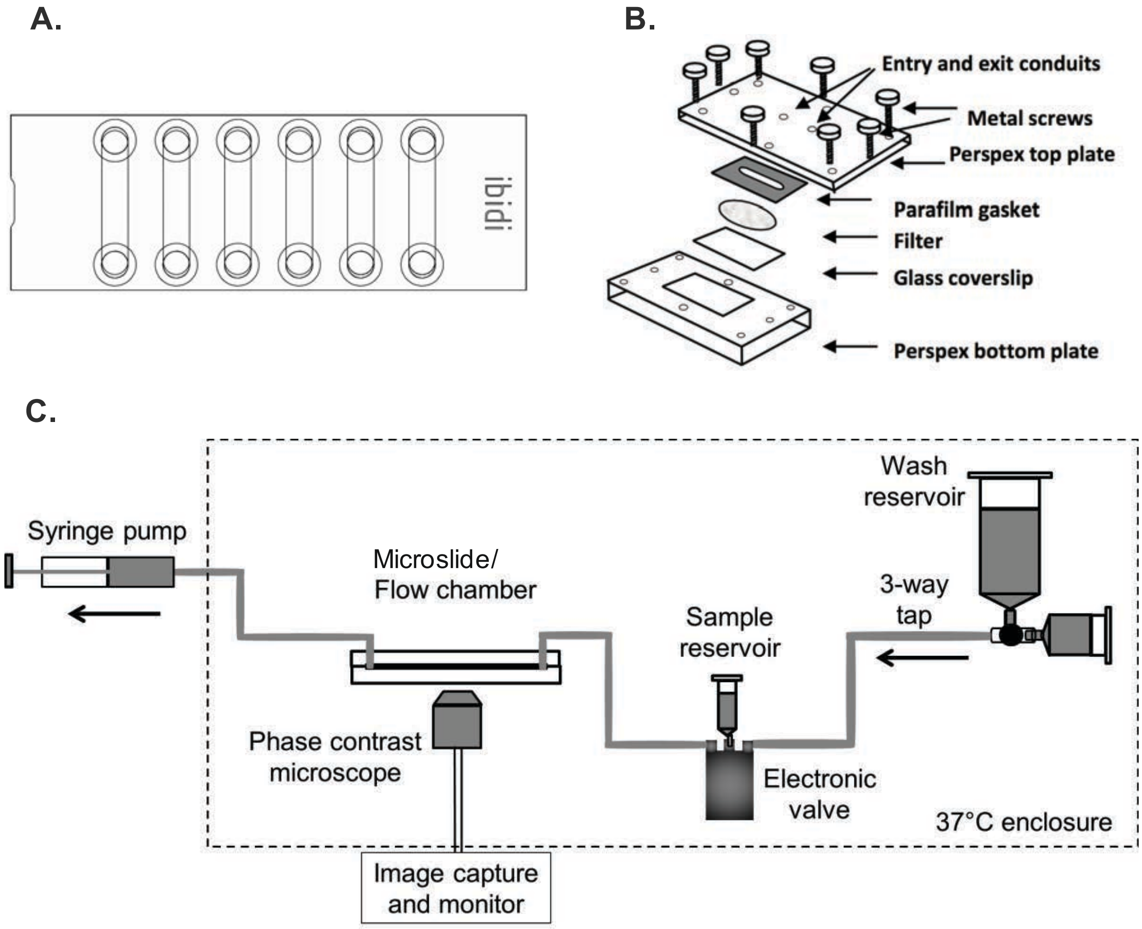

Figure 2-6 Representative schematic of the Ibidi microslide, custom parallel plate flow chamber and assembled flow system

(A) Schematic diagram of the 6-channel Ibidi microslide (μ-Slide VI$^{0.4}$), each channel was 17×3.8×0.4mm with female Luer adapters on each end whereby tubing could be connected (image from; Ibidi μ-Slide VI$^{0.4}$ product details., 2011). **(B)** Schematic diagram of the parallel plate chamber. Transwell filter-based monoculture or cocultures were sealed between a glass coverslip and paraffin film gasket with a 20×4mm slot cut for the flow channel; these were secured between two parallel Perspex plates. The lower plate had a viewing slot for the inverted microscope, and a shallow recess milled into the upper side to hold the coverslip, filter, and gasket. The upper plate had inlet and outlet holes that when assembled overlaid each end of the flow channel (image from; (Munir et al. 2015)). **(C)** Schematic diagram of the assembled flow system. The Ibidi microslide or parallel plate flow chamber was placed in a 37°C maintained Perspex chamber wherein they were attached to a perfusion system mounted on an inverted phase-contrast video microscope. Perfusion was controlled from the outlet by a glass syringe mounted on a withdrawal syringe pump. The inlet was connected to an electronic valve that switches flow between the sample and wash reservoirs (image from; (Munir et al. 2015)).

2.8.3. Flow-based adhesion assay

The Ibidi microslide or parallel plate chamber was placed inside a Perspex chamber that was maintained at 37°C, then attached to a perfusion system mounted on an IX71 inverted phase-contrast video microscope (Olympus, Southend-on-Sea, UK) with a Hitachi KP-M1AP digital camera (Hitachi, Maidenhead, UK) attached (Figure 2-6C). Perfusion was controlled from the outlet tubing with a withdrawal syringe pump (Harvard Apparatus) to maintain a constant shear rate of $150s^{-1}$ for CD41a-labelled whole blood (Navarro-Nunez et al. 2015), or a wall shear stress (τ_w) of 0.05Pa for Ibidi microslide or 0.1Pa for filter flow chambers. The necessary flow rate (Q) to achieve a wall shear stress of 0.05Pa or 0.1Pa for the Ibidi microslide or parallel plate flow chamber respectively, was calculated using the below formula where: η = viscosity of perfused medium ($\cong 0.7\times10^{-3}$Pa for aqueous buffer at 37°C); w = width (3.8mm for Ibidi; 4mm for the chamber); h = height (0.4mm for Ibidi; 0.133mm for the chamber).

$$\tau_w = \frac{6\eta Q}{wh^2}$$

The Ibidi microchannel or parallel plate chamber were initially perfused with MBSA or PBS with 0.15% BSA and 5U/mL heparin (PBSAH; Sagent Pharmaceuticals, Schaumburg, Illinois, USA) for 2 minutes to either wash out residual TNF-α and or acclimatise the endothelium. A 4-minute bolus of purified neutrophils or 5- or 10-minute bolus of CD41a-labelled whole blood, was subsequently perfused over the apical surface of the filter or endothelium before returning to cell-free MBSA for 2 minutes or PBSAH for 5 minutes. For purified neutrophils, phase-contrast images of five random fields along the centre line were recorded every second for 30 seconds, at 2 and 9 minutes' post-perfusion (Figure 2-7A). For CD41a-labelled whole blood, fluorescent images of 5 random fields were taken along the centre line of the channel after washout with PBSAH. The total number of neutrophils per field and their behaviour was analysed offline using Image-Pro Plus 7.0 software (Media Cybernetics, Rockville, USA). Total adhesion was assessed at 2 minutes' post-perfusion and expressed as the number of adherent neutrophils per mm^2 of endothelium per $1x10^6$ neutrophils perfused ($cells/mm^2/10^6$). It was calculated using the below formula: where: μ = mean adherent neutrophils per field, A = field area (mm^2), C = leukocyte concentration (10^6/mL), Q = flow rate (mL/minute), t = bolus duration (minutes).

$$Total\ adhesion = \frac{\mu}{ACQt}$$

Furthermore, rolling, stationary, and migratory behaviour was assessed at both 2 and 9 minutes' post-perfusion and expressed as a percentage of the total adherent neutrophils. These classes were defined as: (i) rolling adherent neutrophils that were phase-bright, spherical and rolled across the apical endothelial surface; (ii) firmly adherent neutrophils that were phase-bright and migrated across the surface of the endothelium; or (iii) transmigrated neutrophils that were phase-dark, flattened and migrated underneath the endothelial monolayer; as previously characterised (Luu et al. 1999).

Platelet adhesion and aggregation was expressed as average size using ImageJ software (NIH) particle analysis of fluorescence. In some experiments, UCMSC were treated with 30μg/mL of human recombinant CLEC-2 protein (R&D systems) for 10 minutes prior to perfusion (Suzuki-Inoue et al. 2007). In others, CD41a-labelled whole blood was perfused in the presence of 9μM integrilin (Sigma-Aldrich), an inhibitor of αIIbβ3-integrin that mediates activated platelet-platelet binding (Thomas et al. 2011).

2.8.4. Seeding cells into collagen gels

Collagen gel adhesion assays were setup and performed as previously described (Jeffery et al. 2013). Rat tail type I collagen (2.15mg/ml; First Link Ltd, West Midlands, UK) was mixed with 10× M199 and neutralised with 1N NaOH. MSC (2.5×10^4 cells in FBS) were added to the gel solution (500μl/well of a 12-well plate), before setting at 37°C and 5% CO_2 for 30 minutes. Once set, the gel was equilibrated in MSCGM for 24 hours at 37°C and 5% CO_2. To form the coculture, HUVEC (4×10^5 cells in MSCGM) were seeded onto the gel and incubated at 37°C and 5% CO_2 for 24 hours (Figure 2-7C, D). These collagen gels were subsequently used in collagen gel migration assays (Section 2.8.5). For spheroid migration assays, the gel was set in the absence of any cells (Section 2.9).

2.8.5. Collagen gel migration assay

HUVEC monocultures and MSC:HUVEC cocultures were treated with 100U/mL TNF-α for 4 hours. After stimulation, neutrophils (1×10^6 cells/mL, at 1mL/well) were incubated with the endothelium for 20 minutes at 37°C and 5% CO_2. Non-adherent neutrophils were washed off the endothelium with MBSA, the plate was placed on the stage of an IX71 inverted phase-contrast microscope within a Perspex chamber maintained at 37°C. The stage was connected via a computer-operated motorised focus. Four random z-stacks were imaged with a digital camera at 2μm intervals through the gel. After 2-hours at 37°C and 5% CO_2, the endothelium was washed and another four z-stacks imaged (Figure 2-7C, D). The data were analysed offline using Image-Pro Plus 7.0 software, whereby the number of cells within each stack of the gel were analysed and assigned to a designated depth based on their distance from the apical surface of the gel. Adhesion was expressed as the average number of phase-bright adherent neutrophils as a percentage of those initially added. Gel penetration is expressed as the number of migrated neutrophils that had entered the gel as a percentage of adherent between 50μm intervals. Gel depth is expressed as the distance between the apical and basal surface of the gel.

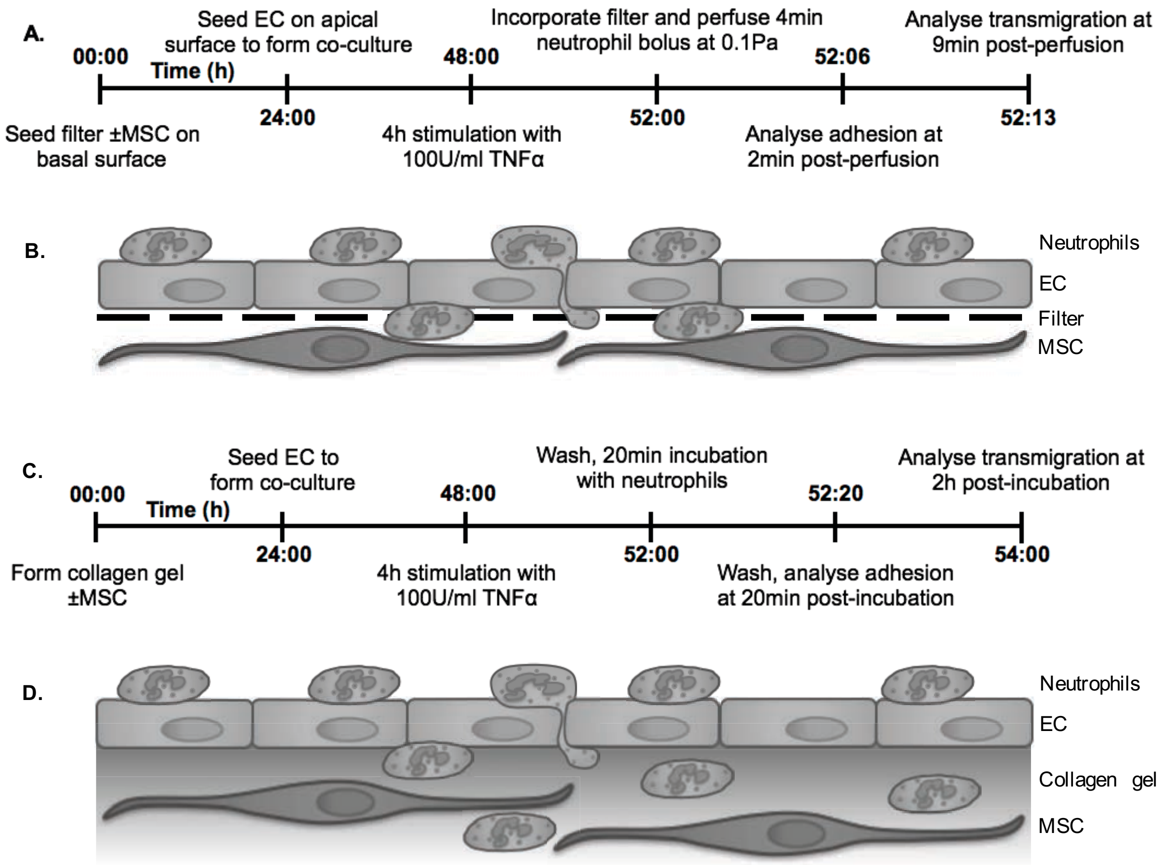

Figure 2-7 Timeline schematic of coculture neutrophil adhesion assays
(A) The transwell filter was inverted and stromal cells were seeded onto the basal surface at a density of 1.0×10^4 cells/mm^2 for 1 hour at 37°C and 5% CO_2. The filter was inserted into a matching plate containing MSCGM. After 24 hours, endothelial cells were seeded onto the apical surface at a 1:1 ratio to the stromal cells and cultured at 37°C and 5% CO_2 for 1-3 days. The coculture was stimulated with TNF-α for 4 hours prior to leukocyte adhesion and migration assays. **(B)** Diagram of transwell adhesion assay. **(C)** Stromal cells were suspended in a collagen gelling solution for 24 hours prior to establishing an endothelial coculture on the apical surface for a further 24 hours. The coculture was stimulated with TNF-α for 4 hours prior to neutrophil adhesion and migration assays. **(D)** Diagram of collagen gel adhesion assay. MSC, mesenchymal stromal cells; EC, endothelial cells; TNF-α, tumour necrosis factor alpha.

2.9. COLLAGEN GEL SPHEROID MIGRATION ASSAY

UCMSC were re-suspended at 2.5×10^4 cells in 35μL MSCLG droplets onto the inner surface of a Petri dish lid (BD Falcon). Distilled water was added to the Petri dish base to humidify the dish. The lid was inverted to suspend the cells as a hanging droplet over 48 hours, and allow the cells to form spheroids under gravity. Spheroids were subsequently placed on the surface of the collagen gel and MSC migration onto the gel imaged after 24 and 48 hours. Marginal cells were determined as the number of ‘tubules’ using AngioSys2.0 software (Cellworks, Buckingham, UK) semi-automated analysis (Figure 2-8). Data were expressed as the number of marginal cells migrating into the collagen matrix as a percentage of the total number initially seeded within the spheroid.

2.10. IL-6 ENZYME-LINKED IMMUNOSORBENT ASSAY

Human IL-6 concentration was measured in conditioned media collected from untreated or TNF-α stimulated BMMSC-BEC coculture and respective monoculture controls, using Quantikine ELISA (D6050; R&D Systems). Data were expressed as pg/mL as determined by subtracting the absorbance readings at 450nm from 550nm then cross-referencing against a standard curve, according to the manufacturer’s instructions (Figure 2-9).

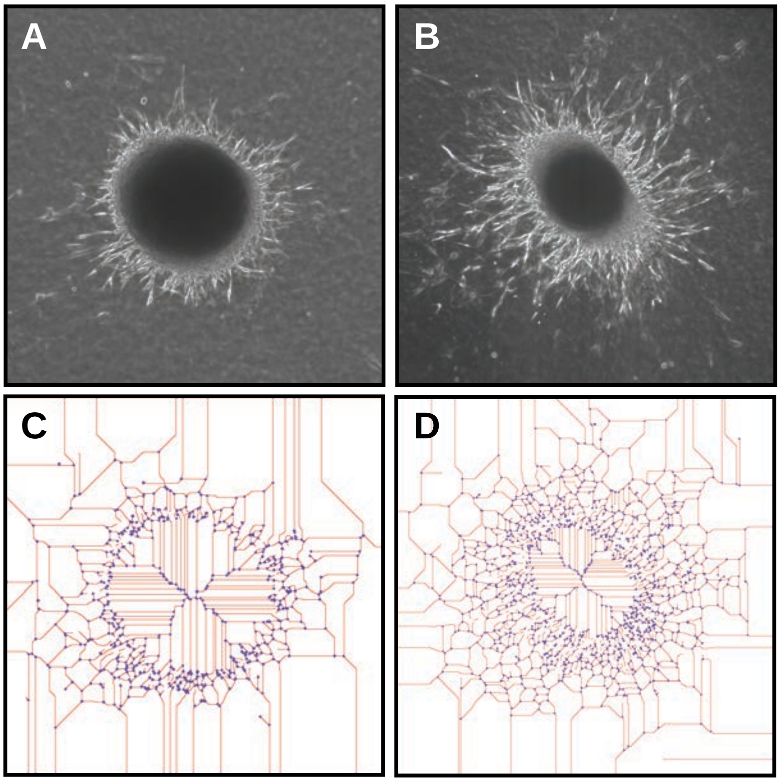

Figure 2-8 AngioSys2.0 spheroid migration assay semi-automated analysis

The invasive capabilities of MSC to migrate from a spheroid and over a collagen gel matrix were analysed. Phase-contrast images of the spheroid were taken at **(A)** 24 and **(B)** 48 hours post-incubation with the collagen gel. AngioSys2.0 software was utilised to determine the extent of invasion by automatically smoothing the image and manually setting the threshold to select marginal cells. The binary overlay image was automatically skeletonised and cleaned until each cell was rendered as a single line of pixels. The software was then able to locate and count the branching points between cells and the length and number of cells between these points at **(C)** 24 and **(D)** 48 hours post-incubation.

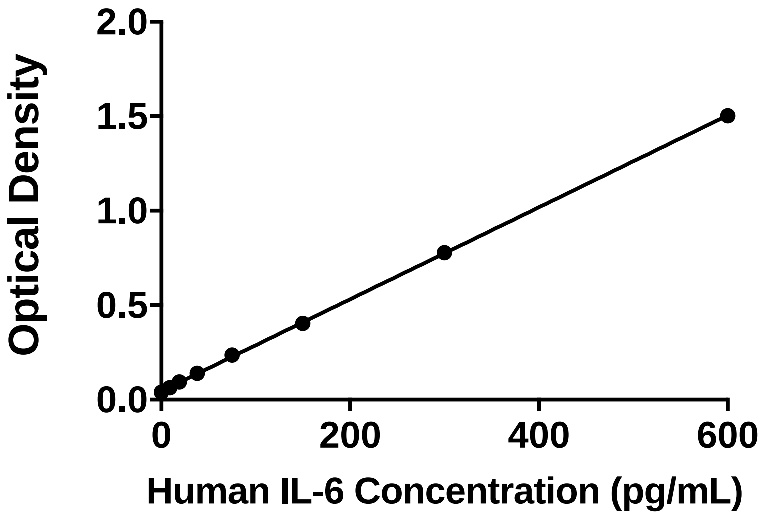

Figure 2-9 IL-6 ELISA standard curve
A serial dilution of human recombinant IL-6 was analysed using Quantikine ELISA kit and spectrometry. Mean optical density for technical replicates were plotted against IL-6 concentration and linear regression analysis performed. The equation of the line was calculated as $y = 0.002x + 0.045$, and $R^2 = 0.99$.

2.11. Umbilical cord immunohistochemistry

Umbilical cord was cut into $2cm^2$ pieces before flash freezing in liquid nitrogen vapour and storage at -80°C. Frozen umbilical cord pieces were embedded in optimum cutting temperature compound (Sakura Finetek, Thatcham, UK) and loaded onto the cryostat (CM1950, Leica, Milton Keynes) for sectioning into 10μm slices at -30°C. Sections were mounted onto Superfrost Ultra Plus Adhesion Slides (ThermoFisher) and left to dry at room temperature. Tissue was rehydrated in PBS^+ for 5 minutes prior to blocking with Bloxall (Vector Laboratories) for 10 minutes. The slides were stained with an IgG2 rat anti-human isotype control (eBR2a) (ThermoFisher) or rat anti-human PDPN (NZ-1.3) at 5μg/mL for 1 hour at room temperature. The slides were washed in PBS^+ for 5 minutes before incubating with 5μg/mL secondary rabbit anti-rat horseradish peroxidase (P0450, Dako) for 45 minutes. The slides were washed in PBS^+ for 5 minutes before staining with haematoxylin and 3,3'-diaminebenzidine (both from Vector Laboratories). Slides were washed again in running tap water for 5 minutes prior to mounting with VectaMount (Vector Laboratories). Slides were imaged using the AxioScan.Z1 and Zen lite 2012 software (both from Carl Zeiss, Cambridge, UK). Data were quantified using ImageJ software, and expressed as the percentage area of PDPN staining for the entire umbilical cord cross-section.

2.12. siRNA knockdown of podoplanin and effect on UCMSC proliferation

PDPN-positive UCMSC were seeded in 12-well tissue culture plates (BD Falcon) at 4.2×10^3 cells/mm^2 in MSCLG. The cells were incubated at 37°C and 5% CO_2 till 80%

confluence, upon which the siRNA duplexes against PDPN or a single scrambled siRNA duplex control (all Sigma-Aldrich) (Table 2-3) were mixed with Lipofectamine RNAiMAX (ThermoFisher) and added to the cells at 50nM. The cells were incubated for a further 6 hours at 37°C and 5% CO_2 before replacing the medium with fresh MSCLG and analysing gene or protein expression 24, 48, and 72 hours post-transfection by qPCR (Section 2.7.5) or flow cytometry (Section 2.7.1).

In some experiments, cell proliferation was recorded over 72 hours in response to PDPN siRNA knockdown using a Cell-IQ Imagen and associated software (both Chipman Technologies, Tampere, Finland). Data were normalised as the average number of cells per field over time compared to 0 hours, with time representing the number of hours post-transfection.

2.13. CRISPR/CAS9 KNOCKOUT OF PODOPLANIN

2.13.1. CUSTOM CRISPR/CAS9 MOLECULAR CLONING

Three 'guide RNA' (gRNA) sequences were assigned using the CRISPR Finder online browser tool (WTSI Genome Editing) for PDPN with off-target counts in less than the tenth percentile (Table 2-4). Reverse sequences were generated and sticky ends complimentary to the 'pSpCas9n(BB)-2A-Puro (PX459) V2.0' plasmid BbsI restriction site were added (plasmid was gifted by Feng Zhang (Addgene plasmid # 62988). The custom 'single-gRNA' (sgRNA) sequences were ordered from Sigma-Aldrich, and the forward and reverse strands annealed to form three distinct

Table 2-3 siRNA duplexes

Name	Duplex sequence	Catalogue number
Podoplanin siRNA-1	GUCUAGUUUGGUCUAUCUU[dT][dT] AAGAUAGACCAAACUAGAC[dT][dT]	SASI_Hs01_00094891
Podoplanin siRNA-2	GUCUAGUUUGGUCUAUCUU[dT][dT] AAGAUAGACCAAACUAGAC[dT][dT]	SASI_Hs01_00192618
Universal negative control		SIC001

Table 2-4 CRISPR gRNA sequences

Name	Sequence	ID
gRNA1	GTTTGCTGTCCGGCTGCCTAGGG	902053749
gRNA2	CCTCCTCGGGAGAGATAAATGCT	902053743
gRNA3	CCTGTGGCCGCGGTGCTTTTTAA	902053786

Sequence details can be found online at 'http://www.sanger.ac.uk/htgt/wge/crispr/ID', where ID is the number in the table.

oligonucleotide duplexes, the following methodology was adapted from Ran *et al*., (2013) and repeated for each duplex (Ran et al. 2013). Briefly, 1μL 100μM forward sgRNA, 1μL 100μM reverse sgRNA, 1μL T4 DNA ligase buffer (10×), 1μL T4 polynucleotide kinase (both from ThermoFisher), and 6μL distilled water were incubated at 37°C for 30 minutes, then 95°C for 5 minutes, and slowly reduced to 25°C (by 5°C per minute). The resulting oligonucleotide duplex was diluted 1:200 with distilled water.

The plasmid vector was cut at the BbsI site by restriction enzyme digest. Briefly, 5μg plasmid DNA was incubated at 37°C for 3 hours with 2μL NEBuffer 2.1 (10×) and 1μL Bbs1 (both from New England Biolabs, Hitchin, UK) then made up to 20μL with distilled water. The restriction digest products were stained with 4μL DNA gel loading dye (6×) (ThermoFisher) and ran on a 1% agarose gel (Sigma-Aldrich) containing 1:10000 SYBR safe DNA gel stain (ThermoFisher) at 100V for 30 minutes.

The plasmid vector was extracted from the gel using QIAquick gel extraction kit (Qiagen) as per the manufacturer’s instructions. Briefly, the heavy band from the gel was excised using a sterile scalpel blade under ultraviolet light. QG buffer (Qiagen) was added at 3μL per mg of gel and incubated for 10 minutes at 50°C until dissolved. An equivalent volume of isopropanol (3μL per mg of initial gel; ThermoFisher) was added to the mixture and centrifuged at 10000g for 1 minute in the provided QIAquick spin columns (Qiagen). The flow-through was discarded and 750μL Buffer PE

(Qiagen) was left to stand within the column for 5 minutes at room temperature before centrifuging at 10000g for 1 minute. The flow-through was discarded and the column spun dry by centrifugation at 10000g for 1 minute. The column was placed in a sterile 1.5mL Eppendorf tube (Scientific Laboratory Supplies) and the plasmid vector eluted with 40μL of Buffer EB (Qiagen) then the flow-through passed through the column a second time, both were centrifuged at 10000g for 1 minute.

The plasmid vector (100ng) was ligated with 2μL of the diluted oligonucleotide duplex prepared earlier, with 2μL T4 DNA ligase buffer (10×), made up to 19μL with distilled water, and 1μL of T4 DNA ligase (both ThermoFisher) added last. The ligase mixture was incubated at room temperature for 30 minutes, then 5μL was transferred to a sterile Eppendorf tube with 50μL of competent bacteria (*E. coli* – DH5α; ThermoFisher) for 30 minutes on ice. The Eppendorf tube was subsequently placed in a water bath at 42°C for 30 seconds to induce heat shock, before returning to ice for 2 minutes. A plasmid vector only control was also prepared. Super optimal broth with catabolite repression (200μL; S.O.C.; ThermoFisher) was added to the Eppendorf tube and incubated at 37°C for 1 hour in an orbital shaker at 200rpm. Each mixture was inoculated by spreading on a pre-poured ‘Luria-Bertani’ (LB) agar plate with 100μg/mL ampicillin (Sigma-Aldrich) and incubating at 37°C overnight (None or few colonies should be visible on the plasmid vector control inoculated plate). Four colonies (and colony absent control; PCR mix without bacterial colony) were picked from the LB agar plate and mixed with 25μL REDTaq ReadyMix PCR reaction mix (Sigma-Aldrich), 23μL distilled water, 1μL plasmid forward primer

(MT5470; U6 promoter region; GAGGGCCTATTTCCCATGATTCC) (Sigma-Aldrich), and 1μL plasmid reverse primer (respective reverse sgRNA). The PCR mixture was cycled as follows:

1. 95°C for 5 minutes.
2. 95°C for 30 seconds.
3. 55°C for 15 seconds.
4. 72°C for 60 seconds.
5. Repeat steps 2-4 for 35 cycles.
6. 72°C for 5 minutes.

The PCR products and control were stained with 4μL DNA gel loading dye (6×) (New England Biolabs) and ran on a 1% agarose gel containing 1:10000 SYBR safe DNA gel stain at 100V for 30 minutes. A 100bp DNA ladder (New England Biolabs) was placed in the first lane to verify the size of the PCR products. A 268bp product indicated that the oligonucleotide duplex had been correctly inserted; all colonies except 'gRNA1, colony a' were successful (Figure 2-10). A successful colony for each gRNA was picked and used to inoculate 100mL of LB medium with 100μg/mL ampicillin (both Sigma-Aldrich) each, then incubated at 37°C overnight in an orbital shaker (Cole-Parmer) at 300rpm.

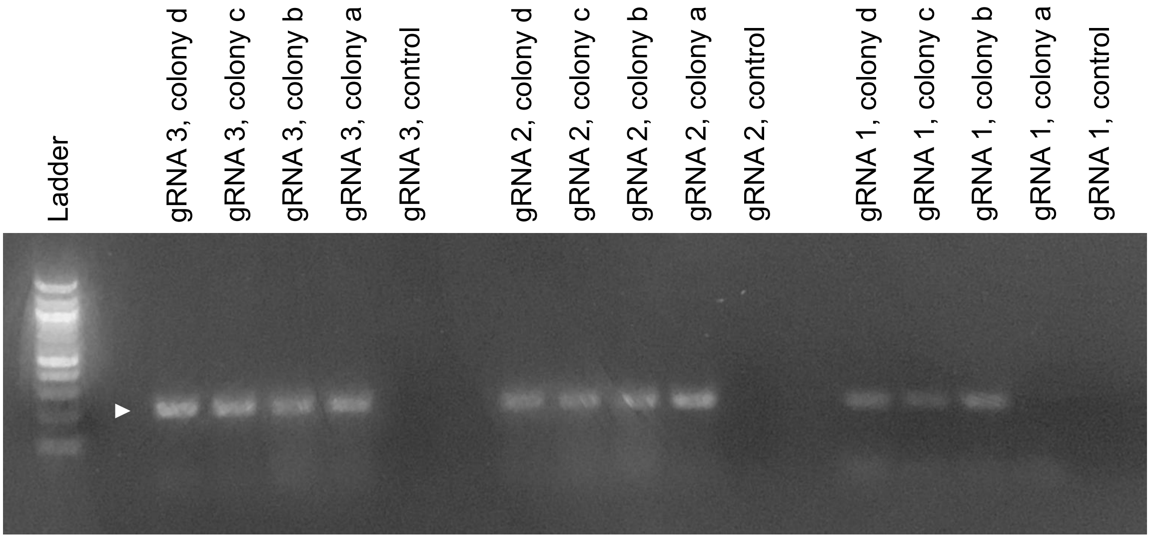

Figure 2-10 Custom PDPN CRISPR plasmid PCR validation
The products of the pSpCas9n(BB)-2A-Puro (PX459) V2.0 plasmid vector and oligonucleotide duplex ligation were amplified by competent cell transformation and the resulting colonies were validated using PCR for the correct orientation of the inserted oligonucleotide duplex, using a U6 promoter forward primer and the reserve sgRNA as a complimentary reverse primer. Colony absent PCR mixtures were used as a negative control. A 268bp product (white arrow) indicated correct orientation and integration of the oligonucleotide duplex with the plasmid vector.

The plasmids from the resulting culture were isolated using a plasmid maxi kit (Qiagen) as per the manufacturer's instructions. Briefly, the bacterial cells from 50mL of culture were harvested after 4°C centrifugation at 6000g for 15 minutes. The supernatant was discarded and the pellet vortexed in 10mL of Buffer P1 with RNase A and LyseBlue supplements (Qiagen) until no cell clumps remain. Buffer P2 (Qiagen) was added to the mixture and inverted until a homogenous blue suspension was achieved, then incubated at room temperature for 5 minutes. Chilled Buffer P3 (Qiagen) was added to the mixture and inverted until a homogenous clear suspension was achieved. The plasmid-containing supernatant was harvested after 4°C centrifugation at 20000g for 30 minutes, this step was repeated once. Meanwhile a QIAGEN-tip 500 was equilibrated with 10mL of Buffer QBT (both Qiagen) and allowed to empty by gravity flow. The plasmid-containing supernatant was loaded into the QIAGEN-tip and allowed to enter the resin by gravity flow, before washing twice with 30mL Buffer QC (Qiagen), any flow-through was discarded. The plasmid was eluted with 15mL of Buffer QF (Qiagen), then the plasmid precipitated by adding 10.5mL of isopropanol, and the plasmid pellet harvested after 4°C centrifugation at 15000g for 30 minutes. The plasmid pellet was washed with 70% ethanol and centrifuged at 15000g for 10 minutes. The supernatant was decanted, and allowed to air-dry for 10 minutes before dissolving in 1mL of distilled water. The purity and concentration of the yield was determined using a NanoDrop 1000 spectrophotometer. DNA purity was deemed acceptable when the 260nm absorbance was within a range of 0.1-1.0. The plasmids for each gRNA were sequenced by the University of Birmingham sequencing facility (Figure 2-11).

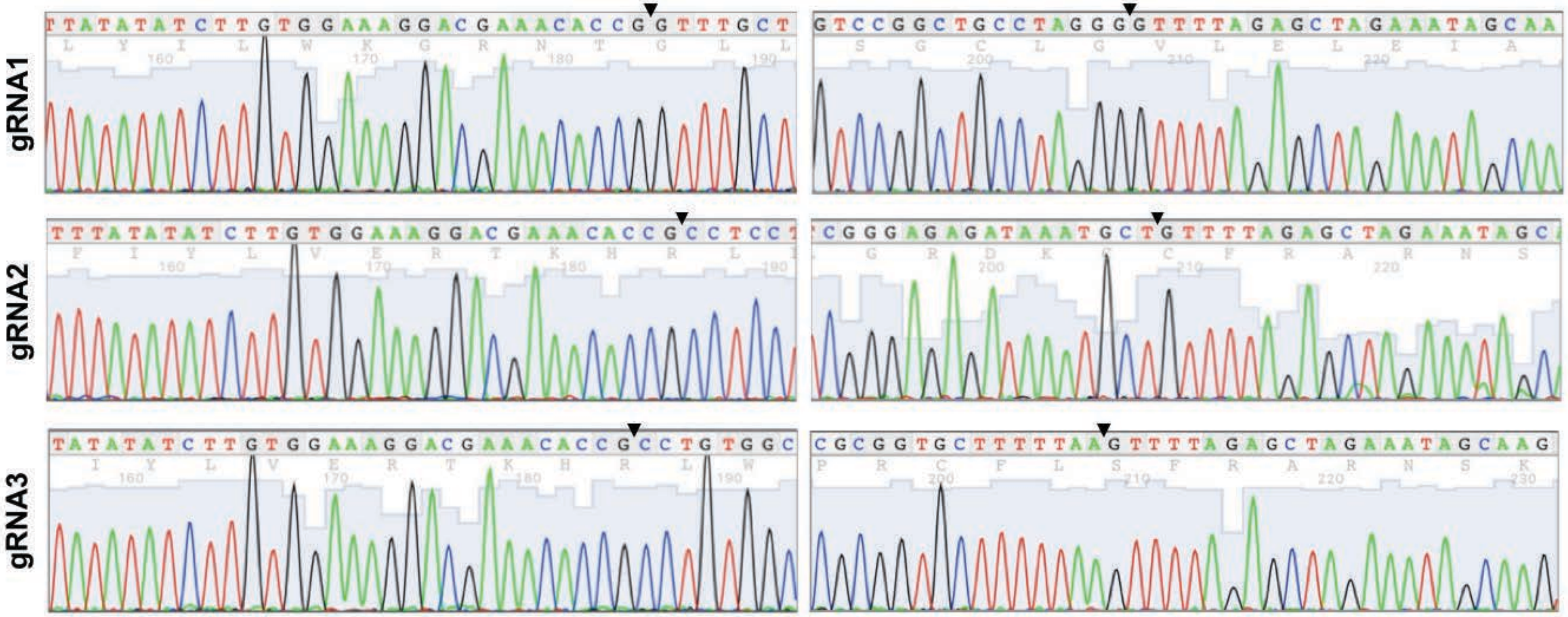

Figure 2-11 Custom PDPN CRISPR plasmid sequencing validation
The plasmids were sequenced from the U6 promoter to determine whether the correct gRNA sequence had been successfully incorporated without point mutations. Images depict the sequence and adjacent nucleotides for each gRNA. Arrows denote the start and end of each gRNA sequence.

2.13.2. Puromycin kill curve

The ‘pSpCas9n(BB)-2A-Puro (PX459) V2.0’ plasmid contained a puromycin resistance cassette to select cells that had successfully been transfected. The minimum concentration of puromycin required to kill 100% of cells had previously been determined for HEK293T cells (2.5μg/mL) but not UCMSC [An email (PJ Noy 2016, personal communication, 7th July) confirming the protocol for puromycin selection in HEK293T cells]. Briefly, UCMSC were seeded in a 24-well tissue culture plate (BD Falcon) until 80% confluence. UCMSC were incubated with increasing doses of puromycin (ThermoFisher) over 0-2μg/mL for 48 hours, before washing off non-adherent cells with PBS^+. Data were expressed as the percentage survival, as determined by the percentage of adherent cells remaining after 48 hours of puromycin treatment.

2.13.3. CRISPR/Cas9 transfections

HEK293T cells or UCMSC positive for PDPN expression were transfected using Lipofectamine 2000 (ThermoFisher) or P1 Primary Cell 4D-Nucleofector X Kit L (Lonza). Lipofectamine 2000 transfections were performed as per the manufacturer’s instructions. Briefly, cells were seeded in 6-well tissue culture plates (BD Falcon) at 4.2×10^3 cells/mm^2 in MSCLG. The cells were incubated at 37°C and 5% CO_2 till 80% confluence, upon which the custom plasmid (pSpCas9n(BB)-2A-Puro (PX459) V2.0 + gRNA1/2/3) was diluted to 0.1μg/μL in 150μL OptiMEM (ThermoFisher) and mixed with 150μL Lipofectamine 2000, then incubated at room temperature for 5 minutes. The DNA-lipid complex was added to the cells and incubated for 24 hours at 37°C and 5% CO_2 before replacing the medium with MSCLG containing 2.5 or 1.0μg/mL puromycin for HEK293T cells or UCMSC respectively and cultured for 48 hours at 37°C and 5% CO_2. MSCLG was replaced and cells cultured to 80% confluence before analysing PDPN protein expression by flow cytometry (Section 2.7.1).

Alternatively, cells were transfected by electroporation with a 4D-Nucleofector X Unit and P1 Primary Cell 4D-Nucleofector X Kit (both Lonza) as per the manufacturer's instructions. Briefly, the cells were subcultured and 500,000 were re-suspended in 100μL P1 Nucleofector solution (Lonza) with 5μg custom, commercial (U6-gRNA/CMV-Cas9-GFP; Hs0000333287; Sigma-Aldrich), or pmaxGFP control plasmid (Lonza). The re-suspended cells were transferred to a Nucleofector cuvette (Lonza) and electroporated using the FW-105 program on the 4D-Nucleofector X Unit. The electroporated cells were incubated for 10 minutes at room temperature to allow for plasmid uptake, prior to diluting in MSCLG and incubating at 37°C and 5% CO_2. At 72 hours post-transfection, PDPN protein expression was measured by flow cytometry (Section 2.7.1).

In some experiments the PDPN knockout population of HEK293T cells were isolated by fluorescence activated cell sorting (MoFlow Astrios; Beckman Coulter) using the flow cytometry staining protocol and the gating strategy described in Figure 2-12. The cells were subsequently cultured at 37°C and 5% CO_2 as described.

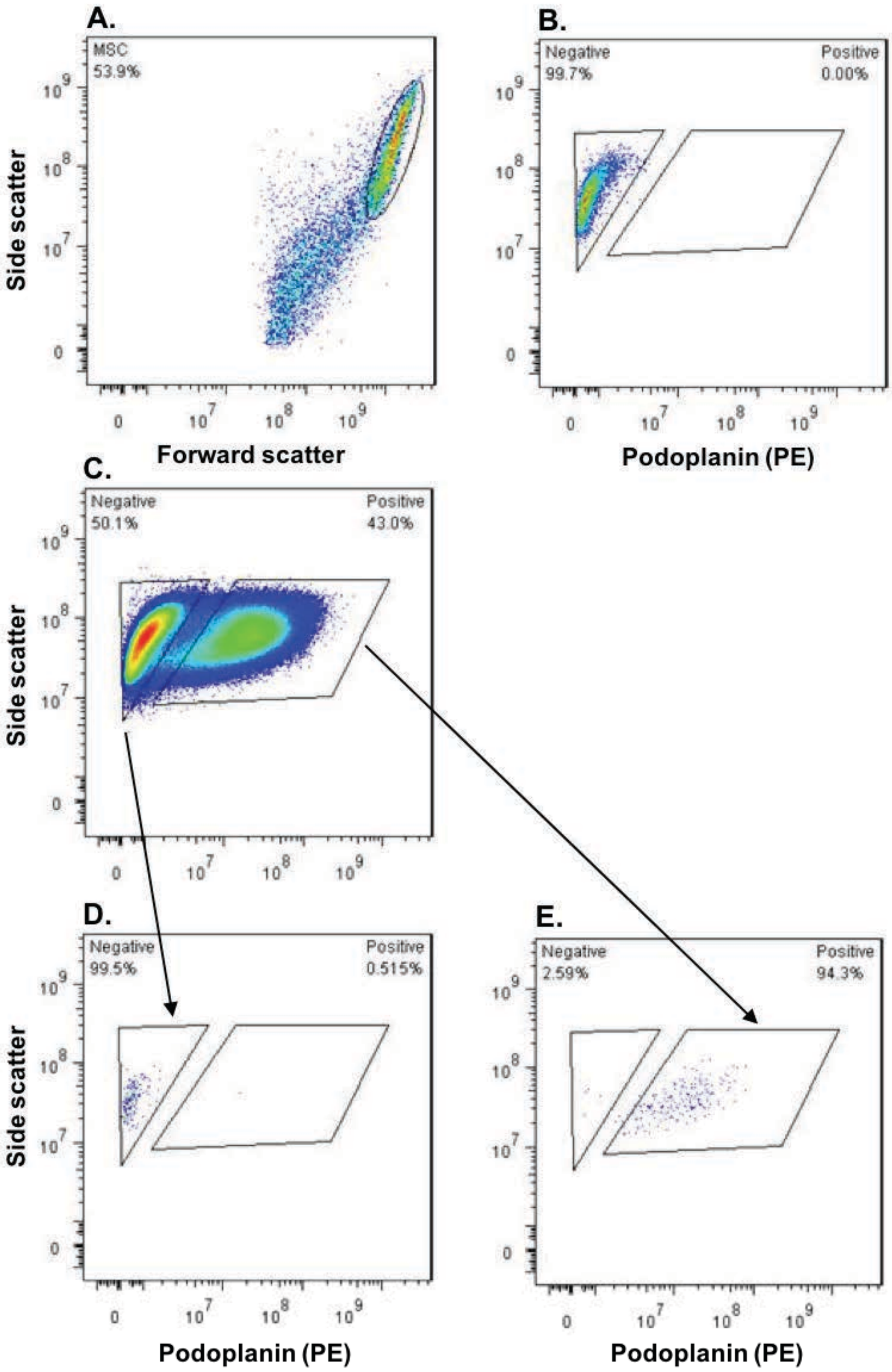

Figure 2-12 Fluorescence activated sorting of podoplanin expressing cells. HEK293T cells were stained with **(B)** rat IgG2a control or **(C)** anti-human podoplanin (NZ-1.3). Cells were gated by **(A)** side scatter vs forward scatter, and the **(C)** podoplanin populations selected using the **(B)** isotype control as a reference. Sorted cells were verified for podoplanin expression in the **(D)** negative and **(E)** positive populations. Images are from n=2 independent experiments using a HEK293T cell line.

2.14. Confocal microscopy

MSC (1.6×10^2 cells/mm^2) were seeded in Ibidi microslides (μ-Slide VI$^{0.4}$) for 24 hours in the presence or absence of 10μM NSC23766. Cells were fixed with 10% neutral-buffered formalin for 30 minutes, permeabilised with 0.5% Triton-X-100 (both Sigma-Aldrich) in PBS$^+$ for 10 minutes, followed by blocking with 1% BSA and 10% goat serum (Vector Laboratories) for 1 hour. Effects of PDPN on cytoskeletal structures were assessed by staining cells with 5μg/mL anti-human PDPN antibody and then 10μg/mL polyclonal goat anti-rat Alexa647 antibody (ThermoFisher) for 1 hour for each step. Cells were washed three times with PBS$^+$ between each step. Samples were counterstained with 16.5nM Alexa488-conjugated phalloidin (f-actin probe; ThermoFisher) for 30 minutes, and mounted in ProLong Gold Antifade Mountant with DAPI (ThermoFisher). Cells were imaged using Zen software on an LSM780 confocal microscope (both from Carl-Zeiss). Representative fluorescent images were taken of MSC to identify PDPN localisation with respect to cytoskeletal and nuclear staining. Images were false coloured using ImageJ software. Average cell area was expressed as the total area of f-actin staining divided by the number of nuclei. Average PDPN intensity was expressed as the integrated density function for the PDPN channel divided by the number of nuclei (both using ImageJ software). The percentage of cells expressing peripheral PDPN was determined by counting those with PDPN expression at the cell edge alone compared to the total number of cells.

2.15. Additional whole blood platelet aggregation assays

For cell suspension aggregation assays, HEK293T cells or UCMSC were subcultured and resuspended in whole blood at 500,000 cells/mL in round-bottomed Eppendorf tubes on the slow setting of a tube roller for 30 minutes at 37°C. The platelet count was measured using the ABX Pentra 60 (Horiba, Middlesex, UK). Data was expressed as the percentage reduction in platelet count in sample compared to platelet count in the whole blood-only control.

For static adhesion assays, CD41a-labelled whole blood was incubated for 1 hour 37°C and 5% CO_2 in the upper chamber of a 0.4, 3.0, or 8.0μm pore 6-well cell culture insert (all BD Falcon), with UCMSC monocultures on the basal surface of the filter. The filter was washed and the remaining adherent platelets were imaged by fluorescence microscopy and platelet adhesion and aggregation was expressed as average size using ImageJ software particle analysis.

2.16. Statistical analysis

Data are mean ± SEM of n independent experiments using individual biological replicates. In some instances, a biological replicate was taken as the mean of multiple technical replicates. In some data sets outliers where excluded using Grubbs' experimental outliers test. For modelling the relationship between two variables, linear regression was used. For non-parametric data sets, variation between multiple comparisons was evaluated by Friedman test. For parametric data sets, single treatments were compared using paired or unpaired t-test where appropriate. Variation between multiple comparisons was evaluated using a one-way or two-way analysis of variance (ANOVA), followed by Dunnett or Bonferroni post-test where appropriate. A p-value of <0.05 was considered statistically significant.

Chapter 3. ENABLING TECHNOLOGIES

3.1. Introduction

The underlying mechanisms of leukocyte recruitment have been widely studied, using techniques that range from simple adhesion assays to complex whole-tissue experiments and *in vivo* imaging systems (Munir et al. 2015; Jeffery et al. 2013; Chimen et al. 2015).

Static *in vitro* cell adhesion assays to endothelial monolayers present an ideal platform for analysing multiple variables through the prior addition of small molecule inhibitors or function-blocking antibodies to endothelial monolayers (Chimen et al. 2015). The disadvantage of such a simple assay is that it is far removed from physiological leukocyte recruitment in terms of cellular sedimentation by gravity and the absence of dynamic flow. A solution to this is to use flow-based assays. Whilst they still do not truly represent a physiological recruitment response, they allow the study of real-time leukocyte capture dynamics over recombinant protein or endothelium at different shear stress or turbulent flow (Navarro-Nunez et al. 2015; Munir et al. 2015). Indeed, flow-based systems enable researchers to scrutinise each individual step of the recruitment cascade from capture to transmigration. However, they lack the high-throughput nature of the static adhesion assay, and both assays fall short of being able to model leukocyte penetration into the underlying stroma.

Extracellular matrix components such as collagen have been used to create 3-D matrix models of the stromal microenvironment and study the inflammatory infiltrate. These can be combined with the static adhesion assay by culturing endothelium above the 3-D matrix and using Z-stacks to monitor leukocyte penetration over time, or their interactions with cocultured stromal cells (Jeffery et al. 2013). Indeed, coculture assays take us a step closer to understanding the crosstalk that occurs in a multicellular system during an inflammatory response. It is necessary to incorporate these coculture systems in both flow-based adhesion assays and 3-D matrices to develop an appropriate physiological model *in vitro*.

Here we describe a static 3-D matrix and two flow-based assays in which MSC can be cocultured with endothelium; of the latter, the Ibidi microchannel utilises multiple single surface channels whilst in the parallel-plate model cells can be cultured on either side of a porous filter. Thus, these models enable us to investigate how stromal cells modulate endothelial recruitment of leukocytes, and provide a platform for studying the effects of inflammatory stimuli on this system (Luu et al. 2013; Jeffery et al. 2013). Specifically, we aim to address which of these models is most suited for studying the result of stromal-endothelial crosstalk, and hypothesise that microvascular endothelium serves as a suitable and physiologically relevant alternative to HUVEC.

3.2. RESULTS

3.2.1. COMPARISON OF FLOW-BASED MODELS OF VASCULAR INFLAMMATION

Using TNF-α as a model for inflammation, we stimulated HUVEC in both the Ibidi microchannel and parallel plate models to determine whether there was any model variation using the same conditions. We tested its effect on the ability to recruit neutrophils from flow and analysed their subsequent behaviour in terms of rolling and transendothelial migration. In the microchannel model of flow, neutrophil adhesion was negligible in unstimulated HUVEC, but there was a dose-dependent increase in adhesion with TNF-α concentration (Figure 3-1). There was no effect of TNF-α concentration on neutrophil rolling over HUVEC at 2 minutes (Figure 3-2A), however a significant increase in neutrophil transmigration was observed with both TNF-α concentration and time post-perfusion (Figure 3-2B). Similarly, a significant dose-dependent increase in neutrophil adhesion to TNF-α treated HUVEC was observed in the parallel-plate model (Figure 3-3). In contrast to the microchannel model, there was no effect of TNF-α concentration or time on neutrophil behaviour (Figure 3-4). In future experiments, 100U/mL TNF-α allowed maximal neutrophil adhesion and therefore was selected to stimulate the endothelium. Furthermore, the parallel-plate model was chosen to establish cell coculture, as this model allows stromal cells to be seeded in a perivascular location and not to integrate into the endothelial monolayer.

Leukocyte recruitment typically occurs at the endothelium of the post-capillary venules (Goldsmith & Spain 1984). Historically numerous groups have analysed leukocyte recruitment using HUVEC, a macrovascular endothelial cell (Burns & DePaola 2005; Sheikh et al. 2005; Patel 1999). Here we compared HUVEC with human dermal blood microvascular endothelial cells (BEC) which more closely represent the endothelium of the post-capillary venules (i.e. where recruitment occurs physiologically). No difference was observed between neutrophil adhesion to TNF-α

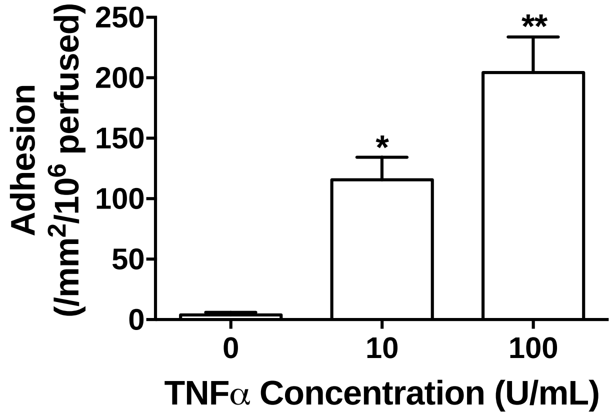

Figure 3-1 Effect of TNF-α stimulation on neutrophil adhesion from flow using Ibidi microchannels.
HUVEC were seeded into Ibidi microchannels for 24 hours prior to stimulation with 0, 10, or 100U/mL of TNF-α for 4 hours. A 4-minute neutrophil (1×10^6 cells/mL) bolus was perfused at 0.05Pa, and adhesion assessed at 2 minutes' post-perfusion. ANOVA showed a significant effect of treatment on adhesion; $p<0.01$. Data are mean ± SEM from n=3-5 independent experiments using at least three different donors for each cell type. * = $p<0.05$, ** = $p<0.01$ compared to untreated HUVEC (0U/ml) by Dunnett post-test.

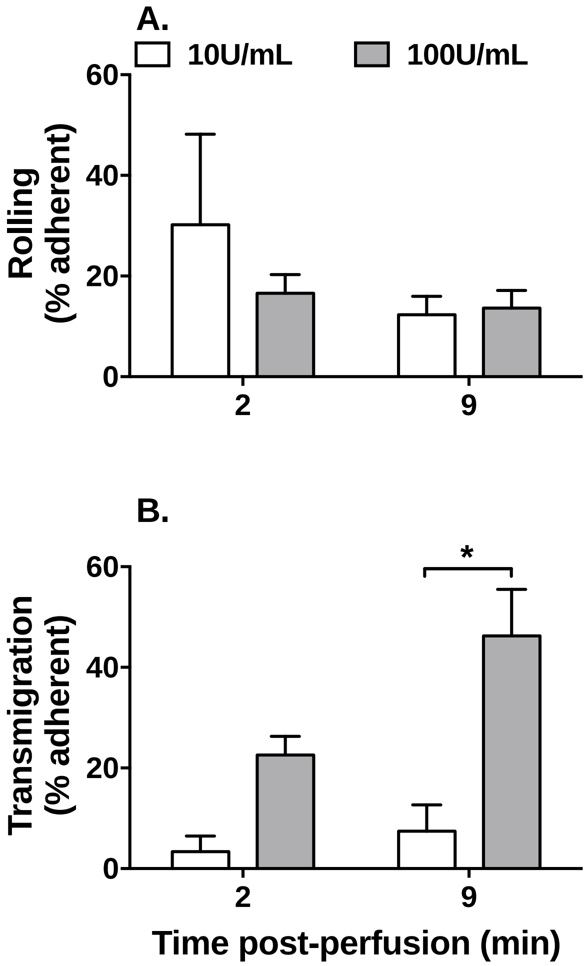

Figure 3-2 Effect of TNF-α stimulation on the behaviour of recruited neutrophils using Ibidi microchannels.
HUVEC were seeded into Ibidi microchannels for 24 hours prior to stimulation with 10 or 100U/mL of TNF-α for 4 hours. A 4-minute neutrophil ($1x10^6$ cells/mL) bolus was perfused at 0.05Pa, and neutrophil **(A)** rolling and **(B)** transmigration assessed at 2 and 9 minutes' post-perfusion. In B, ANOVA showed a significant effect of treatment, but not time, on transmigration; $p<0.01$. Data are mean ± SEM from n=3-5 independent experiments using at least three different donors for each cell type. * = $p<0.05$ by Bonferroni post-test.

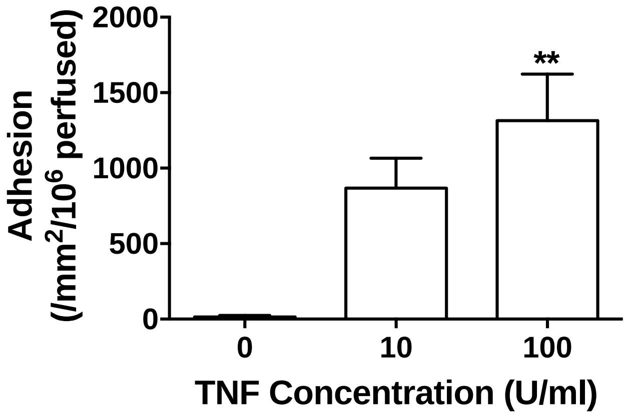

Figure 3-3 Effect of TNF-α stimulated HUVEC on neutrophil recruitment from flow using a filter-based assay.
HUVEC were seeded onto a 0.4μm transwell filter for 24 hours prior to stimulation with 0, 10, or 100U/mL of TNF-α for 4 hours. A 4-minute neutrophil ($1x10^6$ cells/mL) bolus was perfused at 0.1Pa, and adhesion assessed at 2 minutes' post-perfusion. ANOVA showed a significant effect of cytokine treatment on adhesion; $p<0.01$. Data are mean ± SEM from n=5-9 independent experiments using at least five different donors for each cell type. ** = $p<0.01$ compared to untreated HUVEC (0U/ml) by Dunnett post-test.

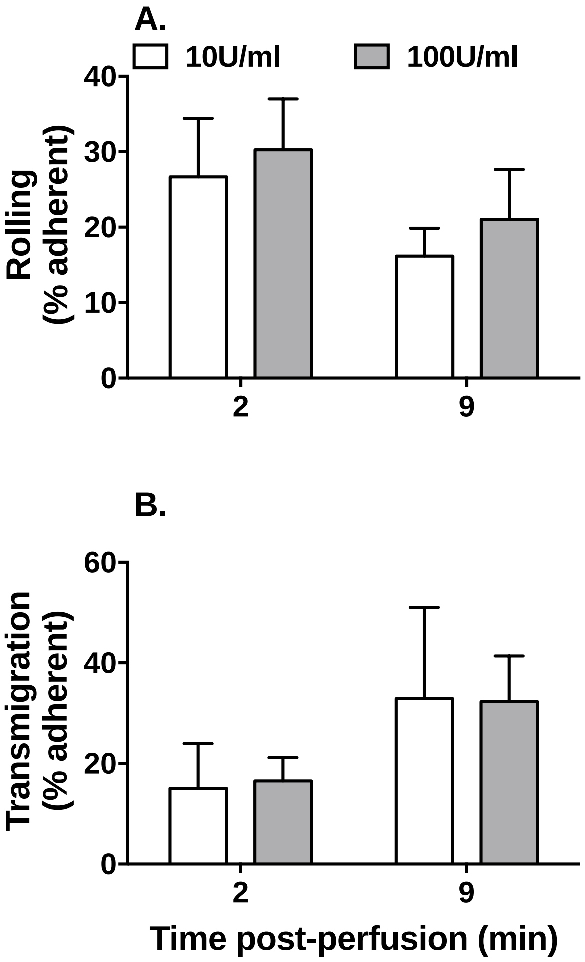

Figure 3-4 Effect of TNF-α stimulated HUVEC on the behaviour of recruited neutrophils using a filter-based assay.
HUVEC were seeded onto a 0.4μm transwell filter for 24 hours prior to stimulation with 10 or 100U/mL of TNF-α for 4 hours. A 4-minute neutrophil ($1x10^6$ cells/mL) bolus was perfused at 0.1Pa, and neutrophil **(A)** rolling and **(B)** transmigration assessed at 2 and 9 minutes' post-perfusion. Data are mean ± SEM from n=5-8 independent experiments using at least five different donors for each cell type.

treated HUVEC or BEC (Figure 3-5). However, both rolling and transmigration occurred at significantly lower levels on BEC compared to HUVEC at 2 and 9 minutes' post-perfusion respectively (Figure 3-6).

3.2.2. *Immunomodulatory potential of BMMSC*

Next, we established BMMSC coculture with HUVEC or BEC and compared neutrophil adhesion and behaviour against an endothelial monoculture control. MSC have previously been shown to suppress the responses of HUVEC (Luu et al. 2013; Munir et al. 2016), however, the immunosuppressive capacity of BMMSC on BEC was undefined. BMMSC coculture had no effect on neutrophil adhesion to HUVEC (Figure 3-7), nor their subsequent behaviour (Figure 3-8). However, BMMSC coculture significantly suppressed neutrophil recruitment to BEC in the presence of TNF-α (Figure 3-9). No effect was observed for neutrophil rolling with BMMSC coculture (Figure 3-10A), but neutrophil transmigration was significantly increased at both 2 and 9 minutes' post-perfusion (Figure 3-10B). As BEC coculture resulted in suppression of neutrophil adhesion, we used BEC as the endothelial source in future flow-based adhesion assays.

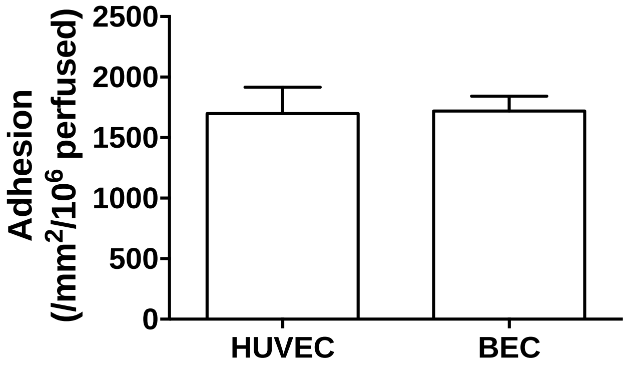

Figure 3-5 Effect of endothelial source on neutrophil recruitment from flow using a filter-based assay.
HUVEC or BEC were seeded onto a 0.4µm transwell filter for 24 hours prior to stimulation with 100U/mL of TNF-α for 4 hours. A 4-minute neutrophil ($1x10^6$ cells/mL) bolus was perfused at 0.1Pa, and adhesion assessed at 2 minutes' post-perfusion. Data are mean ± SEM from n=12-17 independent experiments using at least three different donors for each cell type.

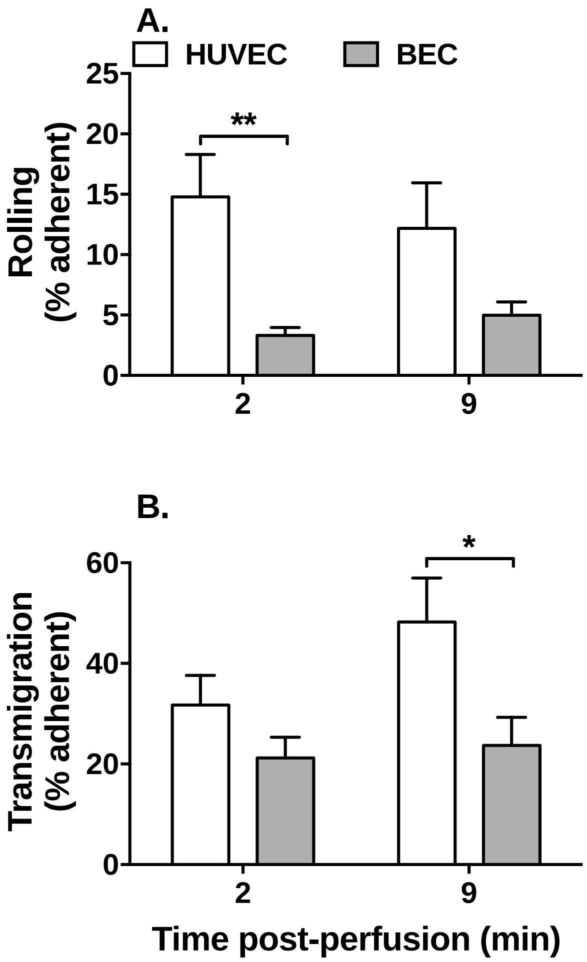

Figure 3-6 Effect of endothelial source on the behaviour of recruited neutrophils using a filter-based assay.
HUVEC or BEC were seeded onto a 0.4µm transwell filter for 24 hours prior to stimulation with 100U/mL of TNF-α for 4 hours. A 4-minute neutrophil ($1x10^6$ cells/mL) bolus was perfused at 0.1Pa, and neutrophil **(A)** rolling and **(B)** transmigration assessed at 2 and 9 minutes' post-perfusion. ANOVA showed a significant effect of endothelial source on (A) rolling and (B) transmigration; $p<0.01$ for both. Data are mean ± SEM from n=14-18 independent experiments using at least three different donors for each cell type. * = $p<0.05$, ** = $p<0.01$ by Bonferroni post-test.

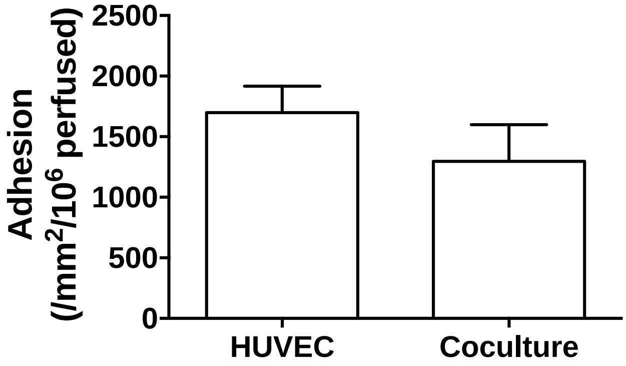

Figure 3-7 Effect of HUVEC:MSC coculture on neutrophil recruitment from flow using a filter-based assay.

HUVEC-BMSMC coculture (coculture) was established by seeding HUVEC on the opposite side of a 0.4μm transwell filter to BMMSC for 24 hours prior to stimulation with 100U/mL of TNF-α for 4 hours. HUVEC monocultures were seeded as controls (HUVEC). A 4-minute neutrophil ($1x10^6$ cells/mL) bolus was perfused at 0.1Pa, and adhesion assessed at 2 minutes' post-perfusion. Data are mean ± SEM from n=6-12 independent experiments using at least three different donors for each cell type.

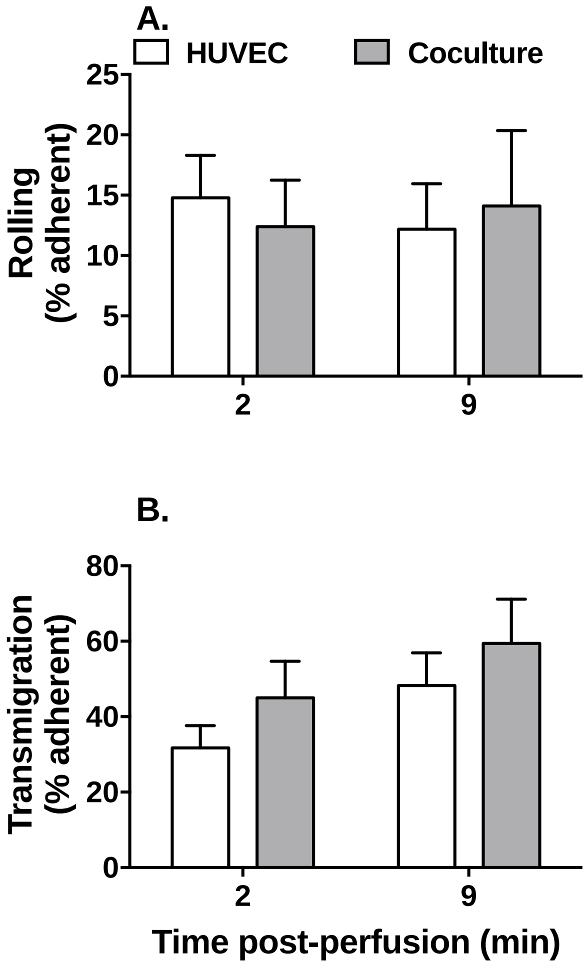

Figure 3-8 Effect of HUVEC:MSC coculture on the behaviour of recruited neutrophils using a filter-based assay.

HUVEC-BMMSC coculture (coculture) was established by seeding HUVEC on the opposite side of a 0.4μm transwell filter to BMMSC for 24 hours prior to stimulation with 100U/mL of TNF-α for 4 hours. HUVEC monocultures were seeded as controls (HUVEC). A 4-minute neutrophil ($1x10^6$ cells/mL) bolus was perfused at 0.1Pa, and neutrophil **(A)** rolling and **(B)** transmigration assessed at 2 and 9 minutes' post-perfusion. Data are mean ± SEM from n=6-12 independent experiments using at least three different donors for each cell type.

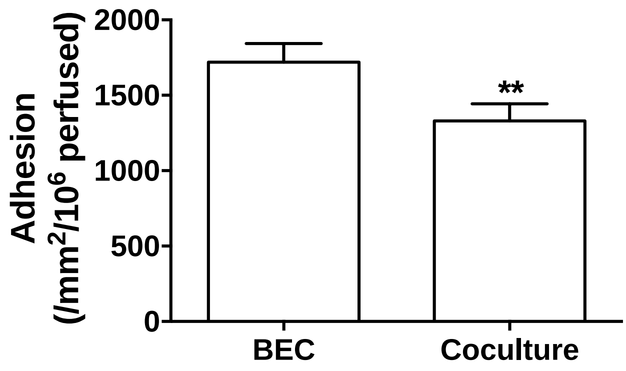

Figure 3-9 Effect of BEC:MSC coculture on neutrophil recruitment from flow using a filter-based assay.

BEC-BMMSC coculture (coculture) was established by seeding BEC on the opposite side of a 0.4µm transwell filter to BMMSC for 24 hours prior to stimulation with 100U/mL of TNF-α for 4 hours. BEC monocultures were seeded as controls (BEC). A 4-minute neutrophil ($1x10^6$ cells/mL) bolus was perfused at 0.1Pa, and adhesion assessed at 2 minutes' post-perfusion. Data are mean ± SEM from n=18-19 independent experiments using at least three different donors for each cell type. ** = $p<0.01$ by paired t-test compared to BEC mono-cultures.

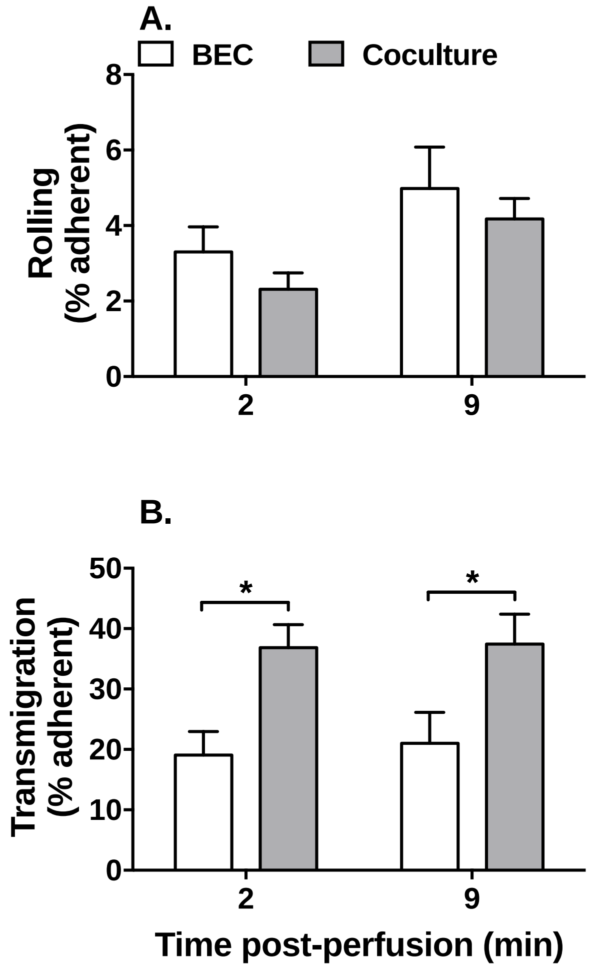

Figure 3-10 Effect of BEC:MSC coculture on the behaviour of neutrophils recruited from flow using a filter-based assay.

BEC-BMMSC coculture (coculture) was established by seeding BEC on the opposite side of a 0.4µm transwell filter to BMMSC for 24 hours prior to stimulation with 100U/mL of TNF-α for 4 hours. BEC monocultures were seeded as controls (BEC). A 4-minute neutrophil ($1x10^6$ cells/mL) bolus was perfused at 0.1Pa, and neutrophil **(A)** rolling and **(B)** transmigration assessed at 2 and 9 minutes' post-perfusion. In B, ANOVA showed a significant effect of culture conditions, but not time, on transmigration; p<0.01. Data are mean ± SEM from n=18-19 independent experiments using at least three different donors for each cell type. * = p<0.05 by Bonferroni post-test.

3.2.3. Neutrophil recruitment to 3-D collagen gels incorporating HUVEC and BMMSC coculture

3-D collagen matrices have previously been shown to be effective models of the inflammatory infiltrate (Jeffery et al. 2013). To confirm this HUVEC were stimulated with or without 100U/mL TNF-α and subsequent leukocyte adhesion, migration, and penetration recorded. Neutrophil adhesion was significantly increased with TNF-α-treatment of HUVEC (Figure 3-11A), but cytokine treatment had no effect on neutrophil migration or gel penetration (Figure 3-11B and Figure 3-11C). BMMSC coculture had no effect on neutrophil adhesion to TNF-α-treated HUVEC (Figure 3-12A). Coculture caused a significant decrease in neutrophil penetration of the gel at 20 minutes' post-incubation (Figure 3-12B), but this effect was lost by 2 hours (Figure 3-12C). BMMSC coculture also significantly reduced the depth of the collagen gel (Figure 3-12D). These data suggest that in static models MSC have little impact on neutrophil adhesion, but delayed their migration into the inflammatory sites at early time-points.

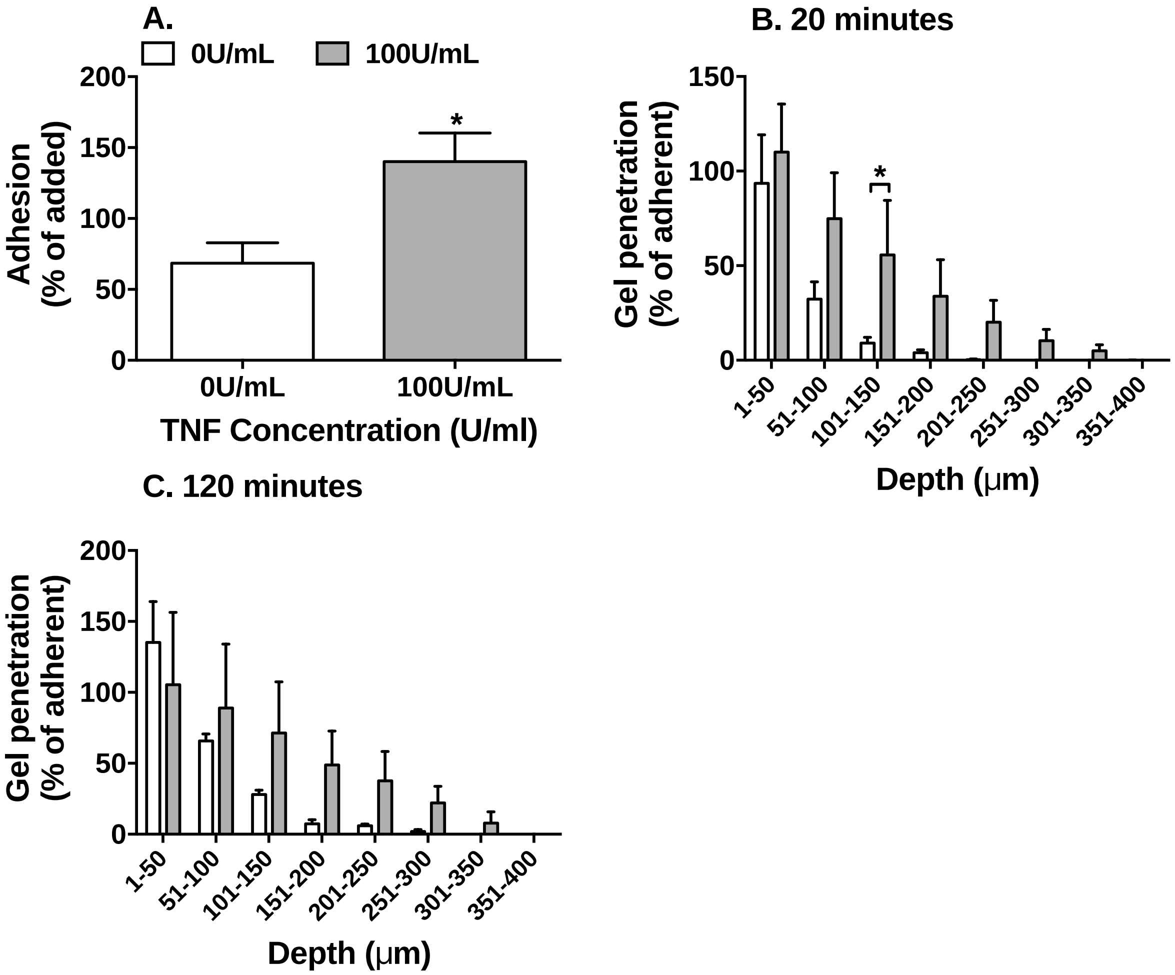

Figure 3-11 Effect of TNF-α stimulated HUVEC on neutrophil recruitment and infiltration into collagen gels.

HUVEC were seeded onto the surface of a collagen gel for 24 hours prior to stimulation with 100U/mL TNF-α for 4 hours. Neutrophils (1×10^6) were incubated with the endothelium for 20 minutes. **(A)** Adhesion was assessed immediately after neutrophil incubation. Gel penetration was assessed after both **(B)** 20 minutes and **(C)** 2 hours. In B and C, ANOVA showed a significant effect of treatment on gel penetration; $p<0.05$. Data are mean ± SEM from n=4 independent experiments using four different donors for each cell type. * = $p<0.05$ by **(A)** paired t-test or **(B)** Bonferroni post-test compared to untreated control (0U/ml).

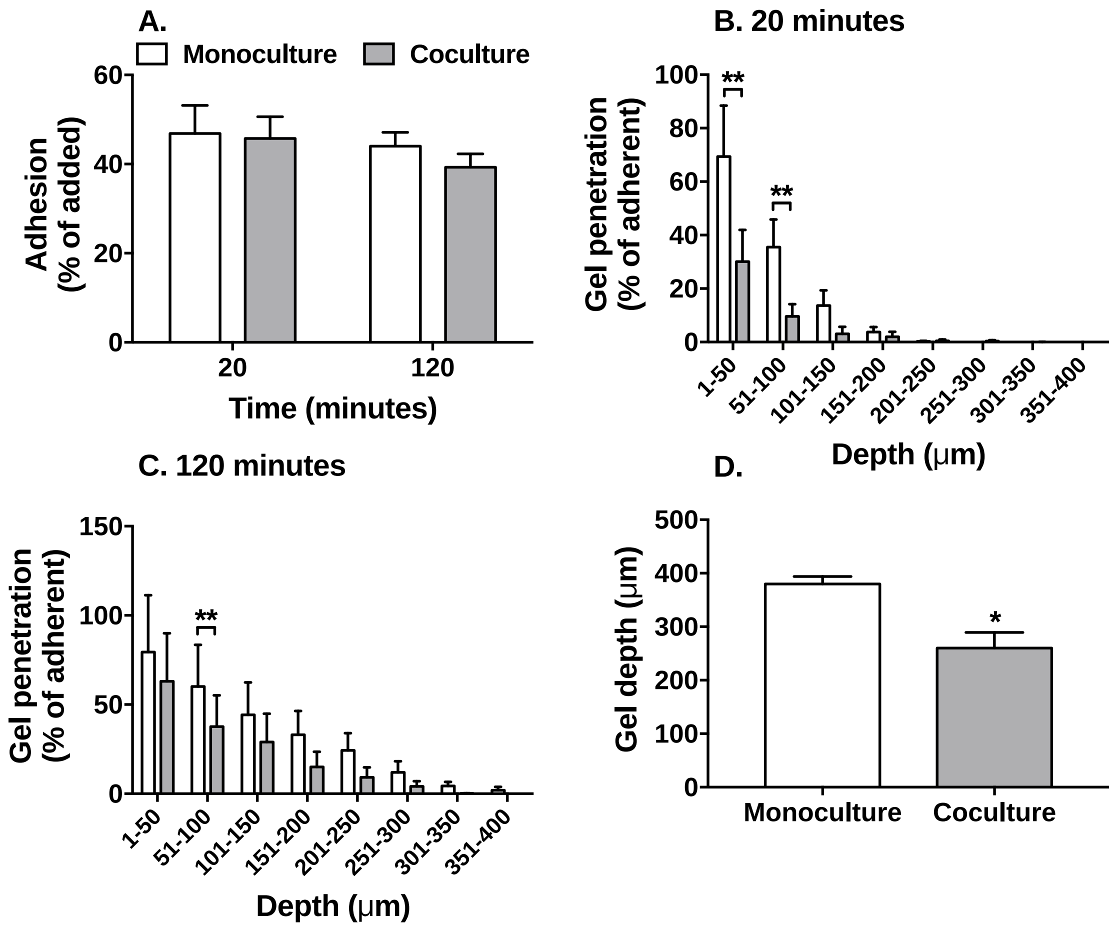

Figure 3-12 Effect of HUVEC:MSC coculture on neutrophil recruitment and infiltration into collagen gels.

BMMSC were incorporated into a collagen gel and HUVEC seeded on the surface for 24 hours prior to stimulation with 100U/mL TNF-α for 4 hours. Neutrophils (1×10^6) were incubated with the endothelium for 20 minutes. **(A)** Adhesion was assessed immediately after neutrophil incubation. Gel penetration was assessed after both **(B)** 20 minutes and **(C)** 2 hours. **(D)** Gel depth was assessed immediately after neutrophil incubation. In B and C, ANOVA showed a significant effect of coculture on gel penetration; $p<0.01$. Data are mean ± SEM from n=4 independent experiments using four different donors for each cell type. * = $p<0.05$, ** = $p<0.01$ by **(B, C)** Bonferroni post-test or **(D)** paired t-test compared to monoculture controls.

3.3. Discussion

In this chapter, we evaluated and optimised several adhesion assays to determine which was best suited for studying the interactions between MSC and inflamed endothelium. We observed a TNF-α dose dependent increase in neutrophil recruitment to HUVEC in the Ibidi microchannel, parallel-plate, and collagen gel models. An increase in neutrophil transmigration was also observed when we used the Ibidi microchannel and collagen gel model, but not the parallel-plate model. Whilst inflamed HUVEC and BEC supported comparable levels of binding, we observed less cells rolling and migrating on BEC compared to the HUVEC. Surprisingly, BMMSC had no effect on HUVEC responses, in the context of neutrophil recruitment when using the parallel-plate model. BMMSC did, however, impede neutrophil penetration into the collagen gel. In contrast, BMMSC suppressed BEC responses to TNF-α, such that fewer neutrophils were recruited. Collectively, we have explored the suitability of several different *in vitro* models, and shown that BMMSC suppress neutrophil recruitment to microvascular, but not macrovascular endothelium. We propose that the parallel-plate model allows the most flexibility in future experiments, and that MSC preferentially modulate the microvascular compartment during an inflammatory response.

The effect of TNF-α dose responses are well described for neutrophil recruitment in HUVEC; with the concentration of TNF-α describing a positive correlation for CD62, VCAM1, and β1-integrin surface expression by HUVEC (W. Y. Sun et al. 2010), as well as neutrophil adhesion and transmigration (Butler et al. 2005). We also observed the same response in HUVEC using the Ibidi microchannel model, however transmigration was unaffected by TNF-α stimulation in the parallel-plate model.

Regarding differences between the Ibidi microchannel and parallel-plate flow assays, we found that neutrophil adhesion was dramatically reduced in the Ibidi microchannel compared to the parallel-plate model. Though neutrophil rolling and transmigration were similar between models, the Ibidi microchannel was more sensitive to changes in TNF-α concentration regarding neutrophil transmigration. However, a lower wall shear stress was used to compensate for the resident time in which neutrophils are recruited to endothelium in the microchannel model. An equivalent wall shear stress would restrict neutrophil capture to the channel outlet. Adhesion of promyelocytic leukaemia cells (HL-60) to CD62 coated surfaces has been shown to exhibit a biphasic profile to increasing wall shear stress, with peak adhesion at 0.05Pa or 0.025Pa for CD62P or CD62E coatings respectively (Lawrence et al. 1997). Whilst contrary to our results, this study demonstrates that there isn't a simple negative correlation between increasing wall shear stress and neutrophil adhesion. Indeed, it may instead be the case that this biphasic adhesion profile is shifted toward higher wall shear rates in HUVEC than on recombinant selectin coatings, though more studies are required.

HUVEC are widely used in adhesion assays due to the accessibility of umbilical cords. However, leukocyte recruitment primarily takes place within the post-capillary venules; studies directly comparing endothelial-specific recruitment are scarce and show mixed results. CD62E is known to support neutrophil rolling during recruitment, however gene expression of CD62E was shown to be 40% lower in BEC compared to HUVEC when pre-stimulated with 10ng/mL TNF-α for 2 hours (Vora et al. 1996). This also agreed with our finding of significantly reduced neutrophil rolling in BEC compared to HUVEC. Indeed, wild-type mice stimulated with local injections of 0.5μg TNF-α for 2-3 hours also exhibited reduced leukocyte rolling in microvascular post-capillary venules when compared to the macrovasculature of the inferior vena cava (Eriksson et al. 2005). Conversely, another study showed that 5-20ng/mL TNF-α stimulation over 12 hours causes BEC to upregulate CD62E to a greater extent than HUVEC, but saw reductions in CD31 and VCAM1 (Murakami et al. 2001). Gene expression of ICAM1 and VCAM1 have also been shown to be greatly reduced in BEC compared with HUVEC when pre-stimulated with 25 ng/mL TNF-α over 4 hours, however no difference in lymphocyte rolling was observed (Oostingh et al. 2007). Though another study showed equivalent binding of HL-60 cells to TNF-α treated HUVEC and BEC (J. H. Li et al. 2003), agreeing with our observations for neutrophil adhesion. There appears to be no consensus within the literature on leukocyte rolling or adhesion at different vascular sites, though all used different methods of TNF-α stimulation.

Regarding leukocyte transmigration in macro versus microvasculature, Chimen *et al*., (2015) observed no difference in lymphocyte transmigration for HUVEC or BEC under static conditions (Chimen et al. 2015). This disagreed with our observations where we saw a significant reduction in the number of transmigrating neutrophils in

BEC compared to HUVEC. VE-cadherin expression is involved in maintaining vascular integrity through endothelial cell-cell adhesions, under 25 ng/mL TNF-α stimulation over 4 hours it was found to be reduced in BEC compared to HUVEC (Oostingh et al. 2007). Interestingly, antibody-mediated blockade of VE-cadherin interactions *in vivo* have proven to enhance neutrophil transmigration into inflamed mouse peritoneum (Gotsch et al. 1997). This would suggest that neutrophil transmigration was increased in BEC due to lower expression of VE-cadherin than HUVEC, however, we observed decreased transmigration. Intravital microscopy of TNF-α induced neutrophil transmigration in several mouse models, has shown to be also dependent on the actions of ICAM2, JAM-A, and PECAM1 (Woodfin et al. 2009). However, direct comparisons of the expression of these adhesion molecules in TNF-α stimulated HUVEC and BEC have yet to be made. These studies suggest that differential expression of endothelial adhesion molecules may have explicit outcomes on leukocyte recruitment at post-capillary venules compared to large veins.

Stromal coculture has been shown to regulate expression of these adhesion molecules by endothelium, as discussed below. Indeed, treating pulmonary endothelial cells with conditioned medium from BMMSC coculture inhibited leukocyte adhesion in a static adhesion assay through downregulation of ICAM1 and VCAM1, but had no effect on CD62E and CD62P surface expression (Pati, Gerber, et al. 2011). Indeed, BMMSC coculture with BEC suppressed adhesion, but had no effect on rolling of neutrophils in our flow-based assays. BMMSC coculture has previously been shown to suppress the adhesion of both neutrophils and lymphocytes to cytokine stimulated HUVEC, with reduced or equal neutrophil transmigration to stimulated HUVEC monoculture (Luu et al. 2013; Munir et al. 2016). Here we have shown that BMMSC coculture has no effect on neutrophil adhesion, rolling, or transmigration on HUVEC. Indeed, we also observed increased neutrophil transmigration in microvascular BEC in the presence of BMMSC coculture. However, the reasons behind these contrasting results are unclear without further interrogation of this system or the contribution of similar studies.

Other stromal cell populations have also been shown to regulate the inflammatory infiltrate. Human hepatocytes promote lymphocyte adhesion to liver sinusoidal endothelium through upregulation of VCAM1 and CD62E, with TNF-β stimulation further enhancing coculture-mediated induction of PECAM1 and ICAM1 expression (Edwards et al. 2005). Furthermore, pathogenic secretory smooth muscle cells (SMC) also display a pro-recruitment phenotype, with increased monocyte transmigration through aortic endothelium in the presence of SMC coculture, on the opposite side of a porous filter (Takaku et al. 1999) or underlying a collagen matrix (Navab et al. 1988). Whilst fibroblasts were observed to switch between a suppressive or pro-recruitment phenotype depending on the inflammatory state of the tissue (Filer et al. 2017). In contrast, coculture of podocytes with glomerular endothelium on opposite sides of a porous filter saw reduced neutrophil recruitment in response to stimulation with TNF-α (Kuravi et al. 2014). However, podocyte coculture with HUVEC saw no suppression of neutrophil recruitment indicating site-specific crosstalk (Kuravi et al. 2014). These studies have shown that the perivascular stromal compartment has a profound effect on the regulation of leukocyte recruitment, whether to promote or suppress the inflammatory infiltrate in a tissue and context specific manner.

The parallel-plate model closely resembles the perivascular inflammatory response, in such that MSC are proximal to the endothelial lining *in vivo* and are an appropriate model of the anti-inflammatory mesenchymal cell types residing within the tissue stroma (Méndez-Ferrer et al. 2010; McGettrick et al. 2012). It enables scrutiny of the process of leukocyte recruitment in a flow-based setting. However, static 3D gel models have the benefit of dissecting the interactions that occur between leukocytes and stromal cells within tissue. Indeed, the answer to which model is better largely depends on the experimental question being asked. Jeffery *et el.,* (2013) utilised collagen gels to study the infiltration of lymphocytes through inflamed tissue, and the effect of stromal cells on this process compared to transwell filter models (Jeffery et al. 2013). Coculture of dermal fibroblasts on the opposite side of a porous filter to HUVEC was found to have no effect on lymphocyte adhesion, but instead enhanced transmigration through HUVEC treated with TNF-α and IFN-γ (Jeffery et al. 2013). Whereas suspension of dermal fibroblasts within the collagen gel was found to have no effect on lymphocyte adhesion or transmigration across HUVEC treated with TNF-α and IFN-γ, nor the penetrance of adherent lymphocytes into the collagen gel (Jeffery et al. 2013). In a comparable study, neutrophil adhesion to HUVEC treated with TNF-α was shown to be suppressed in the presence of BMMSC coculture, to a similar extent in both the transwell filter and collagen gel models (Munir et al. 2017).

However, like the transwell filter model, the suppressive effect of BMMSC coculture on HUVEC in a collagen gel was also lost in our hands. Here we have shown that treatment of HUVEC with TNF-α increases adhesion and penetration into the collagen gel. In contrast, BMMSC coculture has no effect on adhesion, but impedes the penetration of recruited neutrophils into the gel. However, this could be a mechanical effect rather than a result of soluble factors as the depth of the collagen gel was contracted in the presence of BMMSC. These data also disagreed with another study reporting that substrate stiffness induces endothelial contraction, resulting in decreased endothelial cell-cell adhesion and increased neutrophil transmigration (Stroka & Aranda-Espinoza 2011). Collectively, these studies suggest a role for 3D gel models in understanding the process of leukocyte infiltration into the inflamed tissue.

In conclusion, the microchannel model was best suited for studying the capture dynamics of leukocytes to endothelial monocultures, whilst the parallel-plate model had advantages of being able to study the effect of coculture without disrupting the endothelial monolayer. The collagen gel model also allowed for coculture of cells in a physiologically relevant structure, with the benefit of investigating leukocyte infiltration into tissue, however the restriction to static leukocyte adhesion made it less suitable than the flow-based assays for investigating recruitment as a readout of endothelial function. The literature comparing leukocyte recruitment to micro and macrovascular endothelium was scarce and varied in their results as well as the methodology and readouts used. However, they do indicate differential leukocyte recruitment between these vessels. Indeed, we have shown similar levels of neutrophil adhesion, but reduced rolling and transmigration in BEC compared to HUVEC. Coculture of BMMSC with these sources of endothelium revealed preferential modulation of the microvascular compartment with suppression of neutrophil adhesion and increased transmigration compared to endothelial monoculture controls. However, we were unable to investigate the reasons behind a lack of response in HUVEC-BMMSC coculture compared to previous results in the literature nor the mechanisms governing the increased neutrophil transmigration in BEC-BMMSC coculture. We would suggest a comparison in the endothelial gene expression of adhesion molecules such as ICAM1 and VCAM1, in both coculture systems. Overall, we have shown that these models provide an effective means of observing site-specific functional changes within the inflammatory microenvironment brought forth by multicellular crosstalk.

Chapter 4. EFFECT OF THE INFLAMMATORY MICROENVIRONMENT ON MSC IMMUNOMODULATION

4.1. INTRODUCTION

The MSC field indicates that priming of MSC is required for enhanced function [reviewed by (Najar et al. 2017; Lee et al. 2015)]. However, this is not always the case. At sites of chronic inflammation, stromal cells acquire a pathogenic phenotype that allows them to perpetuate the disease state (Filer et al. 2017; Croft et al. 2016). Indeed, the context of the MSC microenvironment has been shown to directly modify the extent of their function (Munir et al. 2017; Munir et al. 2016; Kastrinaki et al. 2008). This leads us to hypothesise that mimicking the conditions of chronic inflammation alters MSC cross-talk with endothelium, such that it is no longer immunosuppressive.

4.2. RESULTS

Here we utilised the flow-based coculture adhesion model as a method of investigating the functional immunomodulatory actions of BMMSC on BEC, and how these responses might be perturbed in the context of either acute or prolonged TNF-α stimulation.

BMMSC coculture suppressed neutrophil recruitment to inflamed endothelium as described in the previous chapter. Priming BMMSC with 24 hours of TNF-α had no effect on neutrophil adhesion to inflamed BEC in coculture (Figure 4-1). Again, BMMSC coculture significantly increased neutrophil transmigration at 9 minutes' post-perfusion as described in the previous chapter, but 24-hour TNF-α-priming inhibited the increase in neutrophil migration observed with coculture (Figure 4-2B).

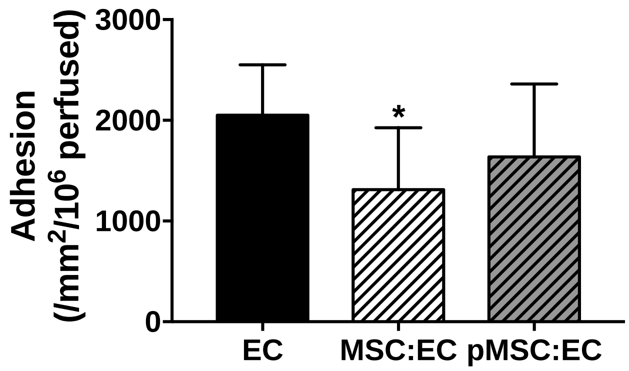

Figure 4-1 Effect of acute priming of MSC with TNF-α on their cross-talk with endothelium and recruitment of neutrophils from flow.
BMMSC were seeded onto the basal surface of a 0.4µm transwell filter for 24 hours, followed by TNF-α stimulation for 24 hours. Coculture was established by seeding BEC on the opposite side of the filter for 24 hours prior to stimulation with 100U/mL of TNF-α for 4 hours. A 4-minute neutrophil ($1x10^6$ cells/mL) bolus was perfused at 0.1Pa, and adhesion assessed at 2 minutes' post-perfusion. ANOVA showed a significant effect of culture conditions on neutrophil adhesion; $p<0.01$. Data are mean ± SEM from n=3 independent experiments using three different donors for each cell type. * = $p<0.05$ compared to BEC monoculture by Dunnett post-test.

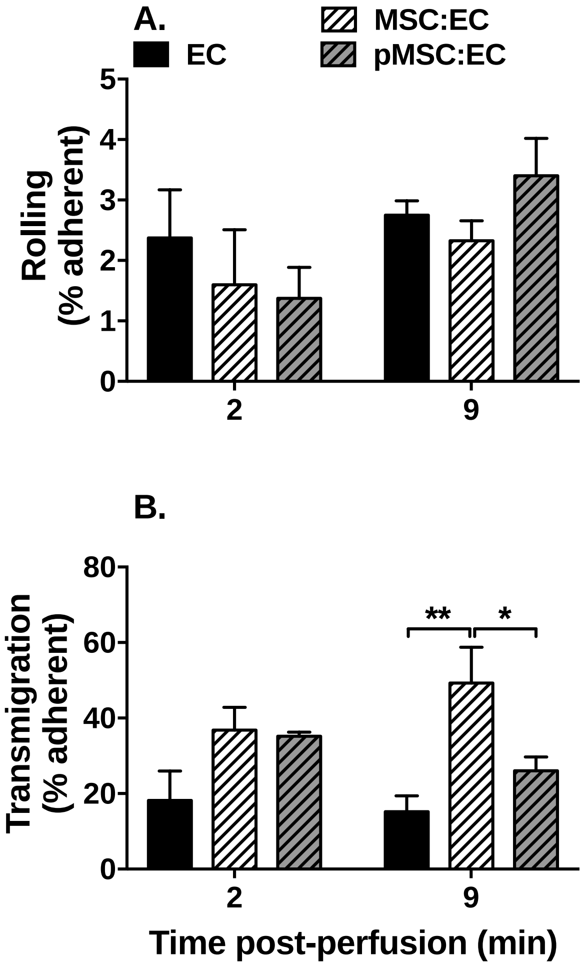

Figure 4-2 Effect of acute priming of MSC with TNF-α on their cross-talk with endothelium and modulation of neutrophil behaviour.
BMMSC were seeded onto the basal surface of a 0.4μm transwell filter for 24 hours, followed by TNF-α stimulation for 24 hours. Coculture was established by seeding BEC on the opposite side of the filter for 24 hours prior to stimulation with 100U/mL of TNF-α for 4 hours. A 4-minute neutrophil ($1x10^6$ cells/mL) bolus was perfused at 0.1Pa, and neutrophil **(A)** rolling and **(B)** transmigration assessed at 2 and 9 minutes' post-perfusion. In B, ANOVA showed a significant effect of culture conditions, but not time, on transmigration; $p<0.01$. Data are mean ± SEM from n=3 independent experiments using three different donors for each cell type. * = $p<0.05$, ** = $p<0.01$ by Bonferroni post-test.

Similar effects were observed for neutrophil recruitment when BMMSC were treated with TNF-α for prolonged periods (72 hours) prior to coculture (Figure 4-3 and Figure 4-4). TNF-α treatment increased IL-6 secretion in BMMSC monocultures when compared to the untreated BMMSC monoculture controls (Figure 4-5). However, this increase was lost upon coculture with BEC, with similar levels of IL-6 detected in cocultures incorporating primed or resting BMMSC (Figure 4-5). Furthermore, resting BMMSC coculture had no effect on the level of IL-6 compared to resting BMMSC monoculture controls (Figure 4-5).

TNF-α treatment has been shown to skew the phenotype of fibroblasts in culture from resolving to inflammation based on the differential expression of PDPN and CD248 (Croft et al. 2016). Indeed, inflamed stroma have been shown to express the cell adhesion molecules ICAM1 and VCAM1 in association with PDPN [reviewed by (Buckley et al. 2015)]. Whilst, IDO1 is involved in MSC immunomodulation (Ling et al. 2014), and fibroblast activation protein (FAP) is a protease expressed at sites of inflammation, and has also been shown to regulate BMMSC migration (Brokopp et al. 2011; Chung et al. 2014). We subsequently examined the effects of TNF-α priming on gene expression of the above molecules in BMMSC to determine whether these were modified. Comparisons were made to rheumatoid synovial fibroblasts (RASF) as a model for pro-inflammatory stromal cells in culture. Neither acute nor prolonged TNF-α treatment had any effect on BMMSC gene expression of PDPN, CD248, FAP, or VCAM1; or RASF gene expression of PDPN, CD248, FAP, IDO1, or VCAM1 (Figure 4-6 and Figure 4-7). However, IDO1 was significantly increased in response to TNF-α treatment in BMMSC, and ICAM1 was increased for both BMMSC and RASF in response to TNF-α at both 24 and 72 hours (Figure 4-6E and Figure 4-7E).

Next, we examined whether taking a pathogenically transformed cell from a chronically inflamed tissue might influence MSC functions (and vice-versa). We therefore cocultured BMMSC with RASF for 24 hours and analysed the expression of inflammation-associated genes compared to their respective monoculture controls. No significant changes were observed in PDPN, FAP, CD248, IDO1, or VCAM1 gene expression (Figure 4-8 and Figure 4-9). The exception was decreased ICAM1 gene expression for both BMMSC coculture with RASF (Figure 4-8E) and RASF coculture with BMMSC when compared to their respective monoculture controls (Figure 4-9E).

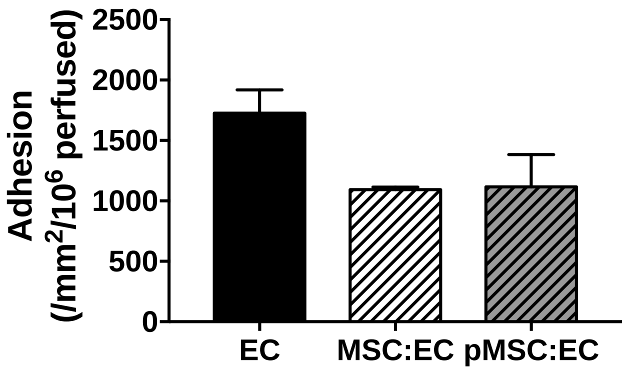

Figure 4-3 Effect of prolonged priming of MSC with TNF-α on their cross-talk with endothelium and recruitment of neutrophils from flow.
BMMSC were seeded onto the basal surface of a 0.4µm transwell filter for 24 hours, followed by TNF-α stimulation for 72 hours. Coculture was established by seeding BEC on the opposite side of the filter for 24 hours prior to stimulation with 100U/mL of TNF-α for 4 hours. A 4-minute neutrophil ($1x10^6$ cells/mL) bolus was perfused at 0.1Pa, and adhesion assessed at 2 minutes' post-perfusion. ANOVA showed no effect of culture conditions on neutrophil adhesion; p=0.12. Data are mean ± SEM from n=3 independent experiments using three different donors for each cell type.

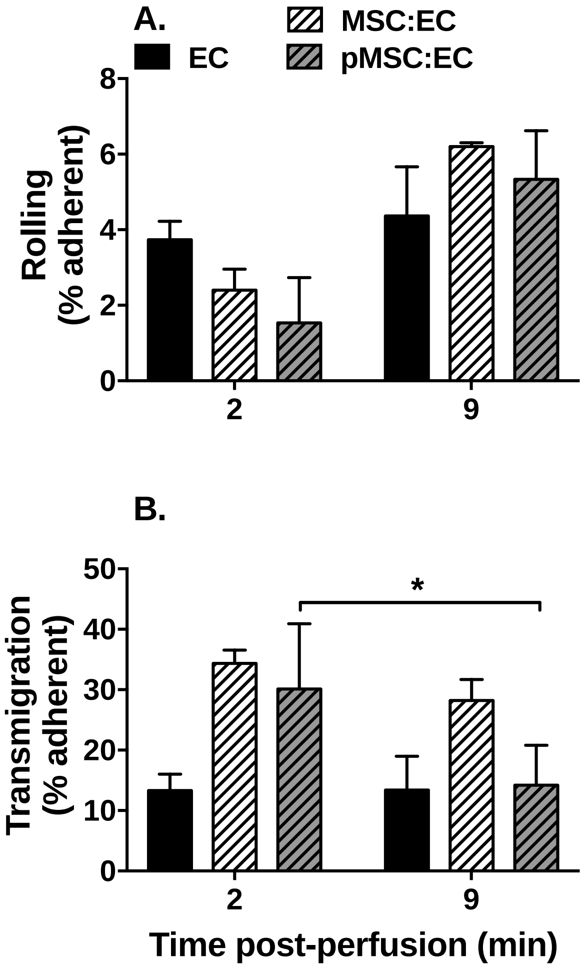

Figure 4-4 Effect of prolonged priming of MSC with TNF-α on their cross-talk with endothelium and modulation of neutrophil behaviour.
BMMSC were seeded onto the basal surface of a 0.4µm transwell filter for 24 hours, followed by TNF-α stimulation for 72 hours. Coculture was established by seeding BEC on the opposite side of the filter for 24 hours prior to stimulation with 100U/mL of TNF-α for 4 hours. A 4-minute neutrophil ($1x10^6$ cells/mL) bolus was perfused at 0.1Pa, and neutrophil **(A)** rolling and **(B)** transmigration assessed at 2 and 9 minutes' post-perfusion. In B, ANOVA showed a significant effect of time, but not culture conditions, on neutrophil transmigration; $p<0.01$. Data are mean ± SEM from n=3 independent experiments using three different donors for each cell type. * = $p<0.05$ by Bonferroni post-test.

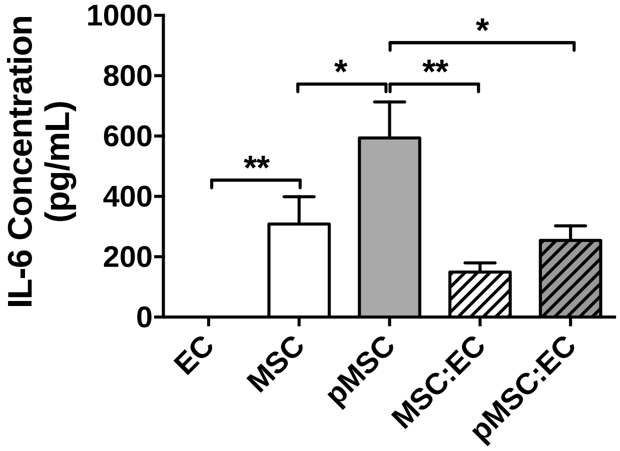

Figure 4-5 Effect of acute priming of MSC with TNF-α on their production of IL-6.

IL-6 concentration was measured by ELISA from BMMSC monocultures or cocultures with BEC. pMSC denotes 24-hour TNF-α stimulation of BMMSC monoculture. ANOVA showed a significant effect of culture conditions; $p<0.01$. Data are mean ± SEM from $n=4$-13 experiments using three different donors for each cell type. * = $p<0.05$, ** = $p<0.01$ by Bonferroni post-test.

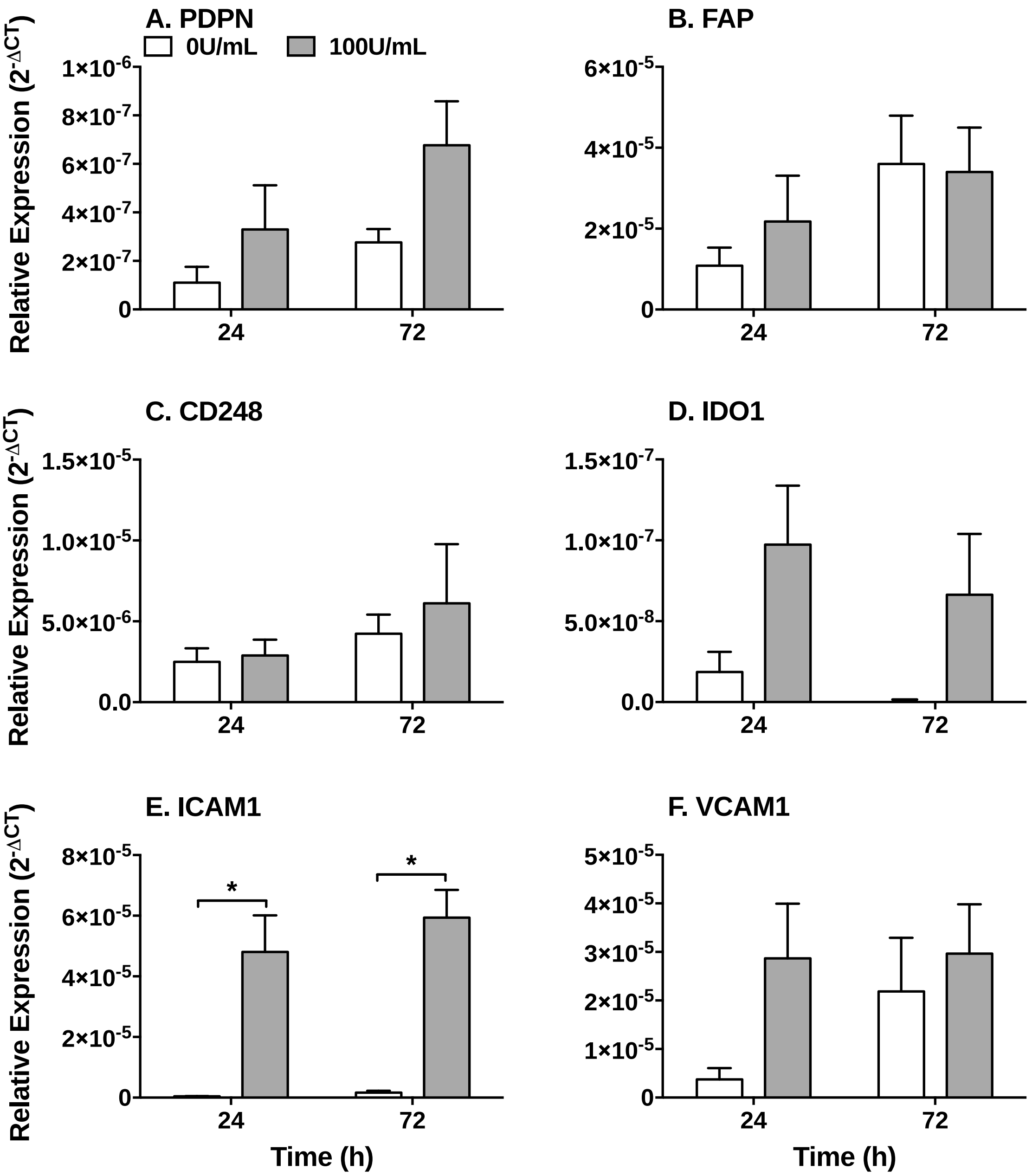

Figure 4-6 Effect of TNF-α priming on MSC gene expression.

BMMSC were stimulated with 0U/mL or 100U/mL TNF-α stimulation for 24 or 72 hours. Gene expression for **(A)** PDPN, **(B)** FAP, **(C)** CD248, **(D)** IDO1, **(E)** ICAM1, and **(F)** VCAM1 were examined by qPCR. ANOVA showed a significant effect of treatment, but not time, on **(D)** IDO1 and **(E)** ICAM1 gene expression; $p<0.05$. In **(F)**, ANOVA showed a borderline significant effect of treatment, but not time on VCAM-1 expression, $p=0.06$. * = $p<0.05$ by Bonferroni post-test. Data are mean ± SEM from n=3 independent experiments using three different donors.

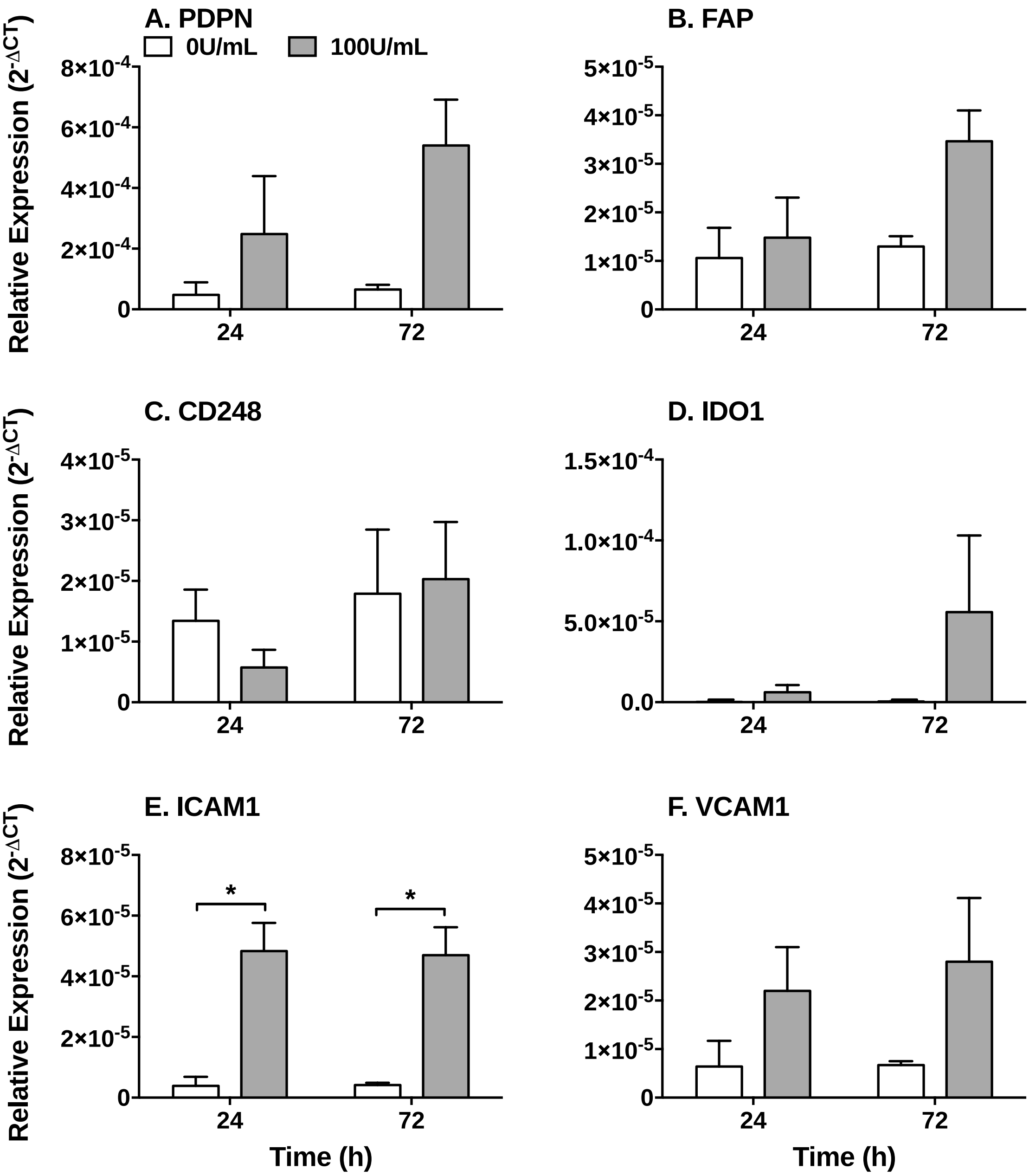

Figure 4-7 Effect of TNF-α priming on RASF gene expression.
RASF were stimulated with 0U/mL or 100U/mL TNF-α stimulation for 24 or 72 hours. Gene expression for **(A)** PDPN, **(B)** FAP, **(C)** CD248, **(D)** IDO1, **(E)** ICAM1, and **(F)** VCAM1 were examined by qPCR. ANOVA showed a significant effect of treatment, but not time, on **(E)** ICAM1 gene expression; $p<0.05$. * = $p<0.05$ by Bonferroni post-test. Data are mean ± SEM from n=3 independent experiments using three different donors.

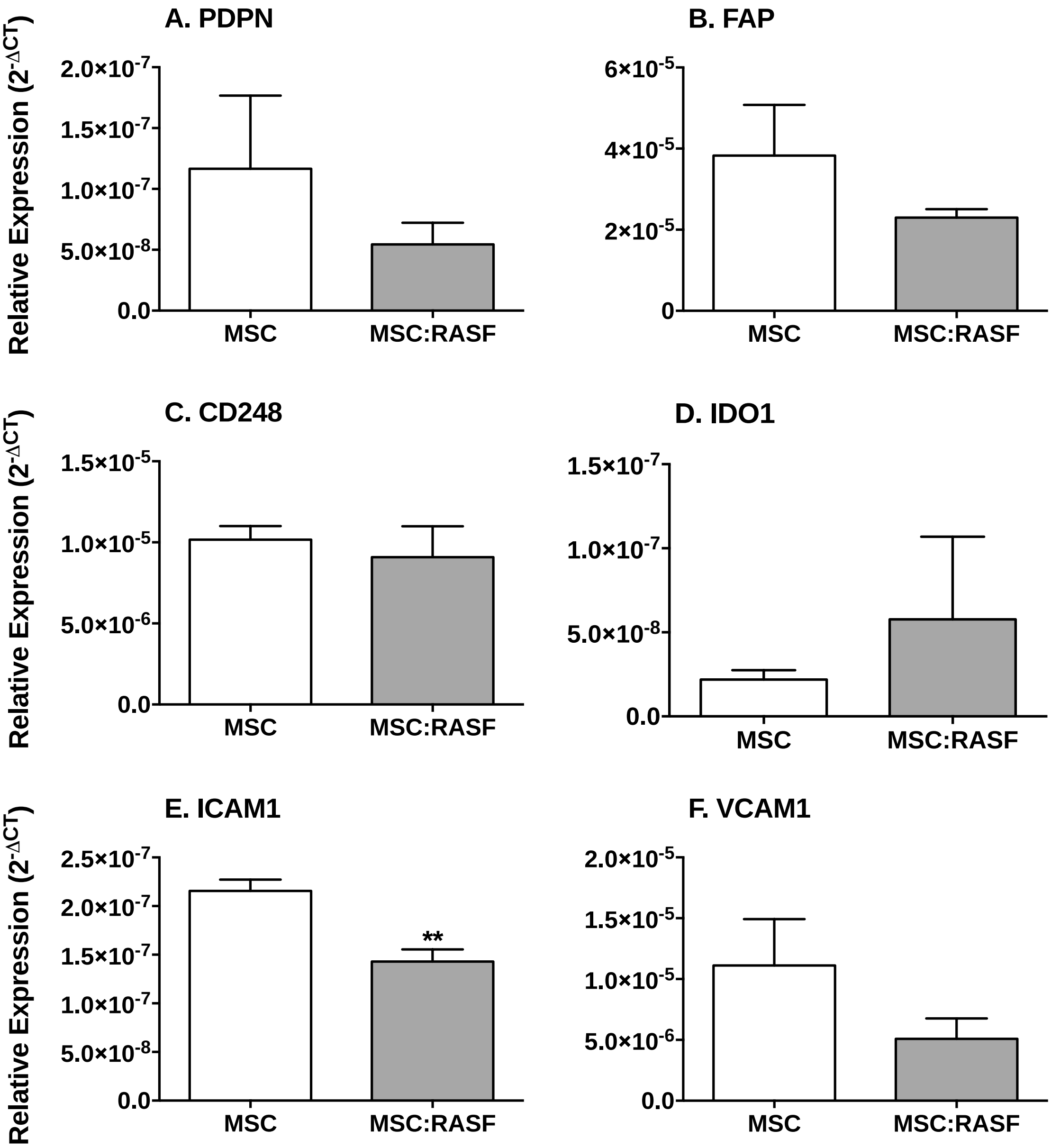

Figure 4-8 Effect of RASF coculture on MSC gene expression.
Stromal coculture was established by seeding BMMSC on the opposite side of a 0.4μm transwell filter to RASF for 24 hours. MSC monocultures were established as a control. MSC gene expression for **(A)** PDPN, **(B)** FAP, **(C)** CD248, **(D)** IDO1, **(E)** ICAM1, and **(F)** VCAM1 were examined by qPCR. Data are mean ± SEM from n=3 independent experiments using three different donors for each cell type. ** = p<0.01 by paired t-test compared to MSC monoculture.

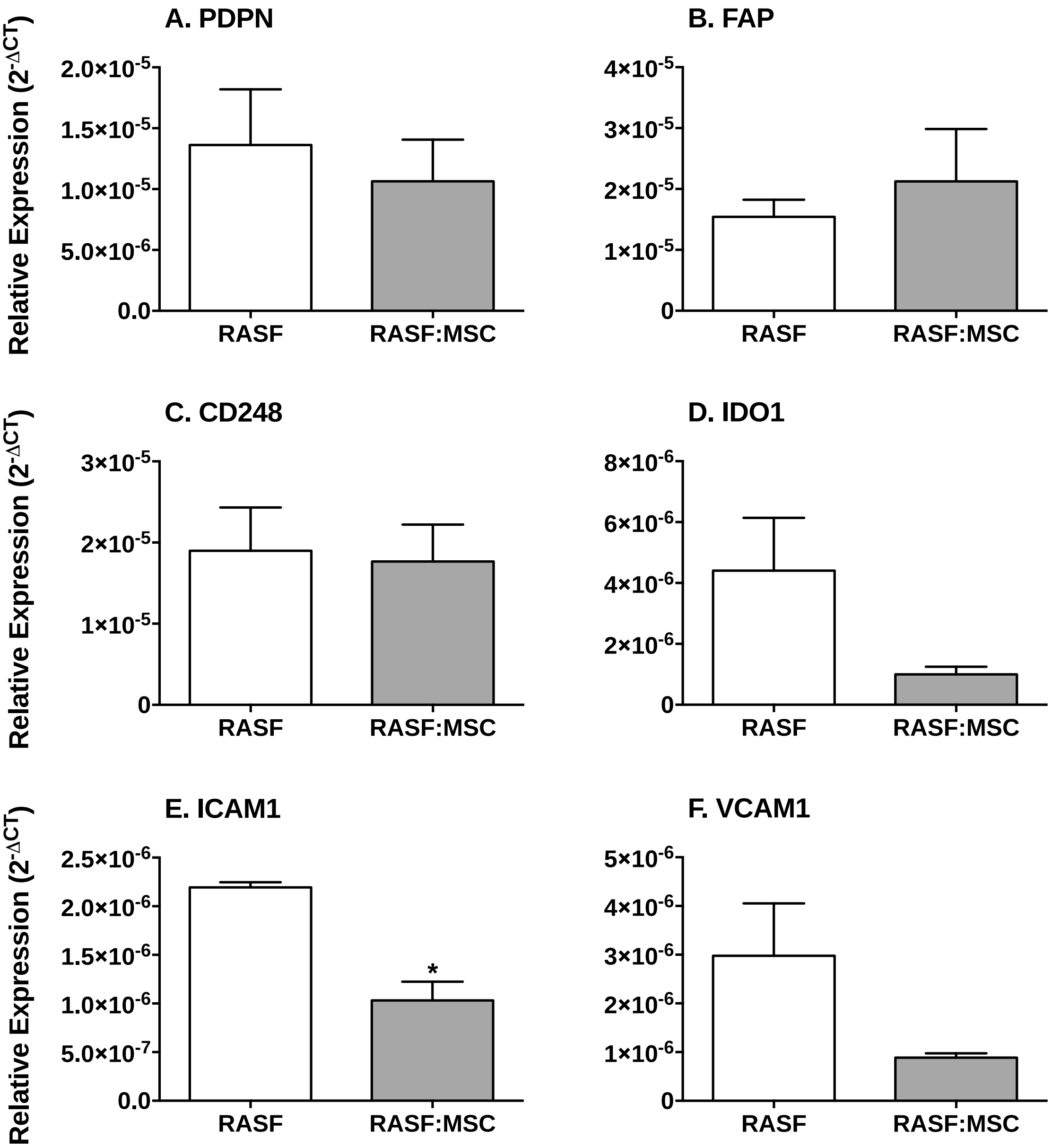

Figure 4-9 Effect of MSC coculture on RASF gene expression.
Stromal coculture was established by seeding BMMSC on the opposite side of a 0.4μm transwell filter to RASF for 24 hours. RASF monocultures were established as a control. MSC RASF gene expression for **(A)** PDPN, **(B)** FAP, **(C)** CD248, **(D)** IDO1, **(E)** ICAM1, and **(F)** VCAM1 were examined by qPCR. Data are mean ± SEM from n=3 independent experiments using three different donors for each cell type. * = $p<0.05$ by paired t-test compared to RASF monoculture control.

4.3. Discussion

Here we aimed to understand the effect of the inflammatory microenvironment on MSC phenotype and immunomodulation of endothelium. We observed that neither acute nor prolonged TNF-α priming affected the ability of BMMSC to suppress neutrophil recruitment to endothelium. BMMSC coculture increased neutrophil transmigration, whilst primed BMMSC coculture saw no difference in transmigration compared to endothelial monoculture. BMMSC secretion of IL-6 was increased by acute TNF-α priming. Coculture produced less IL-6 compared to BMMSC monoculture, independent of BMMSC priming. Acute and prolonged TNF-α priming upregulated ICAM-1 gene expression in both BMMSC and RASF, as well as IDO1 gene expression in BMMSC. BMMSC coculture with RASF, reduced ICAM-1 gene expression in RASF. We propose that the immunomodulatory capacity of BMMSC is unaltered by exposure to exogenous TNF-α stimulation, instead it would appear that BMMSC are still able to suppress neutrophil recruitment to microvascular endothelium. This has implications both in MSC cell-based therapy, and in understanding the pathogenesis of inflammatory disorders.

MSC are endogenous multipotent cells, enriched within the perivascular niche (Crisan et al. 2008). As such, they contribute to the maintenance, repair, and immunomodulation of the vascular compartment [reviewed by (Pankajakshan & Agrawal 2014)]. Indeed, adipose-derived MSC have been shown to support the formation of stable vessels in cardiac tissue through the upregulation of pro-angiogenic factors, such as VEGF and HGF (Rubina et al. 2009). MSC are also a migratory population of cells, enabling them to respond and move toward inflammatory stimuli where they can exert their immunosuppressive and reparative functions (see Chapter 5). This supportive phenotype is of importance for MSC-based therapeutics. By understanding the ways in which MSC respond to inflammatory stimuli we can effectively ‘prime’ these cells to amplify certain functions during treatment. Furthermore, investigations into the impact of the chronic inflammatory microenvironment on MSC function will benefit our understanding of progression of chronicity and failure to resolve.

The inflammatory microenvironment is composed of a large variety of different context specific stimuli, e.g. cytokines, chemokines, or pathogen- or damage-associated molecular patterns. The overall outcome of such signalling is an orchestrated response between different cell types that defines the switch between acute resolving and chronic persistent inflammation. Attempts to model these scenarios by stimulating MSC with pro-inflammatory cytokines are well documented, with some studies demonstrating that priming enhances MSC function (Table 1-2). However, other groups have reported conflicting data, where priming has no effect on MSC function. For example, treatment of murine BMMSC with TNF-α was shown to increase PGE_2 secretion and HGF expression whilst reducing TGF-β secretion (English et al. 2007), however, contradictory results saw decreased PGE_2 secretion and HGF expression but increased TGF-β1 expression (Wu et al. 2015; Prasanna et al. 2010). Likewise, the ability to polarise BMMSC to an anti- or pro-inflammatory phenotype was deemed possible through TLR3 or TLR4 priming with poly(I:C) or

LPS respectively (Waterman et al. 2010). TLR stimulation of BMMSC has also been shown to upregulate the expression of ICAM1 and VCAM1, promoting their adhesion to lymphocytes (Kota et al. 2014). Indeed, we found that TNF-α stimulation upregulated gene expression of ICAM1 on both BMMSC and RASF. Interestingly, increased expression of ICAM1 is suggested to be the mechanism by which MSC bind infiltrating leukocytes during the inflammatory response and exert their contact-dependent or local immunosuppressive factors (Kota et al. 2014; Ren et al. 2010; Schena et al. 2010). However, subsequent studies reported conflicting findings to those made by Waterman. Raicevic *et al*., (2011) showed no effect of TLR3 or TLR4 priming on TGF-β expression, suppression of T-cell proliferation, or PGE_2 secretion compared to unstimulated controls (Raicevic et al. 2011). Whilst, Liotta *et al*., (2008) demonstrated no effect of TLR3 or TLR4 priming on IDO activity, but equally impaired suppression of T-cell proliferation and increased IL-6, IL-8, and CXCL10 secretion regardless of which TLR was primed (Liotta et al. 2008). These studies would suggest that MSC describe a heterogeneous population of cells and that their responses to inflammatory stimuli differ greatly depending on environmental conditions.

Flow-based adhesion assays have previously demonstrated that MSC differ in their ability to modulate endothelial recruitment of neutrophils based on their tissue source (Munir et al. 2016). Indeed, *in vitro* adipogenic differentiation of these MSC, through prior exposure to a number of chemicals and growth factors, has caused them to lose their immunosuppressive capacity (Munir et al. 2017). This is of consequence in the physiological formation of ectopic fat at inflammatory sites (Goodpaster & D. Wolf 2004; Arend et al. 2013), and how this contributes to the failure to resolve the inflammatory response. However, we observed no effect of TNF-α priming on the ability of BMMSC to suppress neutrophil recruitment to endothelium. In fact, BMMSC coculture increased neutrophil transmigration as described in Chapter 3, whereas 24-hour priming inhibits this increase. This may be an attempt by MSC to limit the neutrophil infiltrate in response to an additional inflammatory stimulus. Indeed, RASF have been shown to prolong NF-κB pathway activation in response to re-stimulation with TNF-α, whilst the response from dermal fibroblasts remained unaltered (Crowley et al. 2017). However, the response of BMMSC to repeated inflammatory stimuli remains unknown within the literature, though our primed BMSMC undergo a 24-hour rest period during BEC coculture, prior to a secondary 4-hour stimulus of TNF-α and subsequent incorporation into the parallel-plate flow-based adhesion assay. Overall, these data indicate that stromal cells issue site-specific responses that are modified according to prior exposure.

MSC suppression of leukocyte recruitment to HUVEC is IL-6 dependent, with MSC:HUVEC coculture increasing the level of MSC IL-6 secretion (Luu et al. 2013; Munir et al. 2016). To determine the ability of BMMSC to secrete IL-6 in response to TNF-α priming, we measured its concentration in 24 hour conditioned medium by ELISA. Acute priming with TNF-α significantly increased the secretion of soluble IL-6 by BMMSC monoculture compared to untreated BMMSC. Comparisons with other studies showed that primed BMMSC monoculture secreted similar soluble IL-6 concentrations to those released by late-passage BMMSC (Munir et al. 2016). Contrary to previous reports, we also found that endothelial coculture reduced the concentration of soluble IL-6 compared to MSC monoculture, independent of prior priming (Munir et al. 2016; Luu et al. 2013). Indeed, the similarities in soluble IL-6 concentration between primed and unprimed coculture could account for the parallel observation in neutrophil adhesion. We also used microvascular BEC in place of macrovascular HUVEC, suggesting that different signalling factors may be involved in BMMSC-endothelial crosstalk. Furthermore, when scaffolds of BMMSC cocultured with HUVEC were subcutaneously implanted into non-obese diabetic/severe combined immunodeficient mice, reduced IL-6 gene and protein expression, as well as reduced CD11b-positive infiltrates were observed compared to BMMSC alone scaffolds (Bartaula-Brevik et al. 2014). Overall, these data suggest that endothelium can both upregulate or downregulate BMMSC secretion of soluble IL-6, though it doesn’t appear to be dependent on the source of endothelium. The impact of different concentrations of soluble IL-6 on leukocyte recruitment is unknown. Indeed, passage seven BMMSC and UCMSC secrete more soluble IL-6 than at passage three, yet BMMSC lose their suppressive function at passage seven (Munir et al. 2016). Furthermore, RASF from resolving arthritis patients secrete equivalent soluble IL-6 to those from joint replacement patients, however only resolving arthritis RASF were capable of upregulating SOCS3 and suppressing lymphocyte adhesion to cocultured endothelium (Filer et al. 2017). Indeed, differential secretion of soluble IL-6 may be important in determining the outcome of MSC immunomodulation of endothelium, as demonstrated by antibody blocking of soluble IL-6 or its receptor on BMMSC-HUVEC coculture no longer suppressing neutrophil recruitment (Munir et al.

2016; Luu et al. 2013). This leads us to speculate that stromal suppression of endothelium is dependent upon other factors, though further work is required to conclude what these may be.

The development of chronic inflammation requires that the immunosuppressive properties of endogenous stroma are overridden or transformed by their microenvironment, resulting in a failure to resolve the inflammatory response [reviewed by (McGettrick et al. 2012)]. However, the effect of prolonged exposure to the inflammatory microenvironment on stromal cell function is poorly defined, with very few studies approaching this longstanding question. Croft *et al*., (2016) showed that treating RASF with TNF-α or TGF-β1 for 72 hours was required for predominant expression of PDPN or CD248 respectively, with little change following 24 hours of exposure (Croft et al. 2016). These PDPN-positive RASF were also positive for FAP and VCAM1, and were associated with a pro-inflammatory phenotype as shown by cartilage destruction and transmigration from their site of origin to alternative sites of cartilage where they supported further damage (Croft et al. 2016). However, our data showed that TNF-α stimulation had no effect on PDPN, CD248, or FAP gene expression in either BMMSC or RASF. *Ex vivo* studies of BMMSC isolated from chronic inflammatory environments (RA, SLE, ITP), revealed a common theme of reduced proliferation and shortened telomeres, indicative of cellular senescence when compared to healthy controls (Nie et al. 2010; L. Sun et al. 2010; Kastrinaki et al. 2008; Pérez-Simón et al. 2009). However, with respect to cell function, only BMMSC from RA or ITP patients showed impaired ability to support of haematopoiesis or suppress T-cell proliferation respectively (Kastrinaki et al. 2008;

Papadaki et al. 2002; Pérez-Simón et al. 2009), whereas BMMSC from SLE patients showed normal function in terms of haematopoietic support and suppression of T-cell proliferation compared to healthy controls (Nie et al. 2010; L. Sun et al. 2007). In our functional assays, we found that prolonged TNF-α priming had no effect on the ability of BMMSC to suppress endothelial recruitment of neutrophils compared to acute priming. Interestingly, culture of healthy BMMSC in the presence of 20% osteoarthritis synovial fluid was capable of upregulating gene expression of the immunomodulatory components, IL-6 and IDO1 (van Osch 2012). We also observed upregulation of IDO1 gene expression by BMMSC but not transformed RASF, but in response to TNF-α stimulation. MSC secrete IDO as a potent suppressor of inflammation through induction of T-cell arrest and apoptosis in response to tryptophan depletion (François et al. 2012; Meisel et al. 2004; Ling et al. 2014). Endothelium has also been shown to upregulate IDO production in response to stimulation with IFN-γ (Mouratidis & George 2015), with its deletion resulting in pulmonary hypertension in mouse models (Xiao et al. 2013). Regardless of its immunosuppressive function, overexpression of endothelial IDO was shown to have no effect on T-cell transmigration in a static adhesion assay (Mouratidis & George 2015). Interestingly, upregulation of SOCS3 via IL-6 induces the degradation of IDO in dendritic cells (Orabona et al. 2008), however the connotations of a similar result in SOCS3-mediated MSC-endothelial crosstalk are unclear. Rather we speculate that MSC upregulation of ICAM1 and IDO1 by TNF-α stimulation have a similar role to the release of nitric oxide in their murine MSC counterparts, in binding tissue-infiltrating leukocytes and suppressing them through the local release of IDO (Ren et al. 2008; Ren et al. 2010). IL-6 is a pleiotropic cytokine, in that it has both anti- and pro-inflammatory functions [reviewed by (Scheller et al. 2011)]. With regard to the effects of IL-6 on endothelium, it is both able to induce SOCS3 resulting in suppressed leukocyte adhesion (Luu et al. 2013), whilst conversely promoting recruitment through upregulation of ICAM1, VCAM1, and CD62E in HUVEC (Watson et al. 1996). Overall, this evidence suggests that stromal cells are modified by chronic inflammation, however the mechanism by which these cells are permanently polarised toward an inflammatory phenotype or are transiently primed to promote resolution is still unclear. Whilst MSC appear resistant to taking on a pro-inflammatory phenotype, with upregulation of immunomodulatory factors such as IDO instead.

Finally, we tested a novel stromal coculture model of the inflammatory microenvironment, whereby RASF were cultured with BMMSC for an acute time-frame of 24 hours and their gene expression profile subsequently analysed. Interestingly, we found that BMMSC coculture with RASF reduces ICAM1 gene expression, suggesting an anti-inflammatory action of BMMSC based on the intrinsic link between ICAM1 and inflammation. Also of interest was that the same reduction was observed with BMMSC ICAM1 gene expression in the presence of RASF coculture. We suggest further enquiries into this system by prolonging the duration of culture and characterising the inflammatory profile and function of these cells compared to monocultures. Whilst BMMSC may suppress the inflammatory properties of RASF, adipose-derived MSC were found to promote pathogenesis by dramatically enhancing the viability, proliferation, and metastatic potential of a breast cancer cell line both in *in vitro* cocultures and *in vivo* mouse experiments (Kamat et al. 2015). Indeed, MSC are capable of homing to tumourigenic sites and where they can promote tumour angiogenesis, establish an anti-inflammatory microenvironment, and assist in tumour metastasis [reviewed by (Chang et al. 2015)]. Overall, these data suggest that the anti-inflammatory properties of healthy MSC may initially overpower that of inflamed tissue, with the result of slowing, halting, or even resolving inflammation. However, this phenotype is likely to the detriment of other conditions such as cancer and bacterial infections.

The literature on MSC priming varies greatly in the methodology used, making the data shown here one of few studies that have made direct comparisons on the effects of acute versus prolonged cytokine priming on MSC immunomodulatory function. The literature described within this chapter support the notion that tissue-resident stromal cells may be modified or transformed by their microenvironment, perhaps resulting in a change in function of these once regulatory cells and perpetuating either the drive of pathogenesis or the failure to resolve the inflammatory response. However, we have shown that BMMSC are resilient to these changes, at least when considering short exposures (72h or less), by retaining their suppressive function over endothelium. Whether this resistance is transient or permanent has yet to be determined, but deciphering the mechanisms by which these transformations occur in other stromal populations may prove useful in the development of new therapeutic targets. This is of importance in MSC-based therapies in determining how healthy cells might be influenced by the inflammatory environments they are being introduced to and what implications any changes have on disease pathogenesis.

Chapter 5. ROLE OF PERIVASCULAR PODOPLANIN IN THE INFLAMMATORY MICROENVIRONMENT

5.1. INTRODUCTION

PDPN is a mucin-type transmembrane glycoprotein, whose expression is normally restricted to a small number of stromal cells (Breiteneder-Geleff et al. 1997; Farr et al. 1992; Schacht et al. 2003), and it is typically associated with a migratory and invasive phenotype (Wicki et al. 2006; Tejchman et al. 2017; Suchanski et al. 2017; Martín-Villar et al. 2006). In a pathological setting PDPN is upregulated at inflammatory sites (Inoue et al. 2015; Croft et al. 2016; Cimini et al. 2017), particularly in the perivascular space (Payne et al. 2017; Hitchcock et al. 2015). MSC are also enriched within the perivascular niche (Crisan et al. 2008; Feng et al. 2011), and we have recently shown that UCMSC differentially express PDPN and interact with platelets when administered systemically, raising concerns over their use in therapy (Dr L Sheriff, University of Birmingham, 2017, personal communication). It remains unclear whether circulating platelet CLEC-2 can interact with PDPN expressed by stromal cells in the perivascular niche. This leads us to hypothesise that PDPN regulates UCMSC migration and has a role in the perivascular niche that may involve interactions with its receptor CLEC-2 on platelets.

5.2. RESULTS

5.2.1. PDPN REGULATES MSC MIGRATION

We have recently reported that cultured BMMSC lack PDPN expression, whilst UCMSC differentially express PDPN between donors (Figure 5-1) (Dr L Sheriff, University of Birmingham, 2017, personal communication). To determine the role of PDPN on MSC migration, we screened UCMSC donors for PDPN expression and

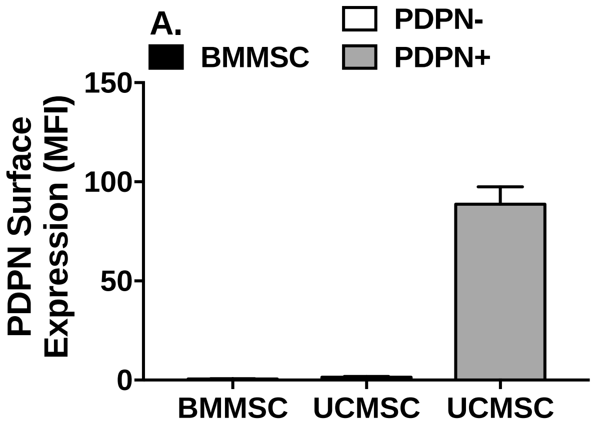

Figure 5-1 Characterisation of PDPN expression on MSC.
BMMSC and UCMSC donors were analysed for PDPN surface expression UCMSC were split based on PDPN expression into PDPN-negative (PDPN-) or -positive (PDPN+) isolates. Data are expressed as the MFI of PDPN staining subtracted from the isotype control. Data are mean ± SEM from n=4-9 independent experiments using four BMMSC, five PDPN-negative UCMSC and nine PDPN-positive UCMSC donors.

then analysed their migratory potential using two different *in vitro* models (transwell filter and spheroid collagen gel assay). Using a transwell migration model, significantly more PDPN-positive UCMSC migrated through the filter than PDPN-negative UCMSC or BMMSC (Figure 5-2A). In the collagen matrix invasion model, the percentage of PDPN-negative UCMSC migration did not change over time (Figure 5-2B). In contrast, significantly more PDPN-positive UCMSC had migrated into the collagen matrix compared to PDPN-negative UCMSC by 48 hours post-seeding (Figure 5-2B). Indeed, PDPN-positive UCMSC migration increased in a time-dependent manner between 24 and 48 hours (Figure 5-2B). These data suggest that expression of PDPN is associated with a pro-migratory phenotype in UCMSC.

To determine whether increased UCMSC migration was directly mediated by PDPN, we transfected MSC with siRNA against PDPN and observed a 41% and 29% reduction in PDPN gene and surface expression respectively at 24 hours compared to cells treated with scrambled siRNA (Figure 5-3). This reduction remained stable up to 72 hours, and at this time point resulted in a 55% reduction in gene expression (Figure 5-3A) and 34% reduction in surface protein expression (Figure 5-3B) when compared to scrambled controls. This partial knockdown of PDPN had no effect on UCMSC proliferation (Figure 5-4A), but was sufficient to cause a significant reduction in the migratory capacity of UCMSC within the siRNA-treated group (Figure 5-4B). This implies that PDPN directly regulates the migratory, but not the proliferative capacity, of MSC.

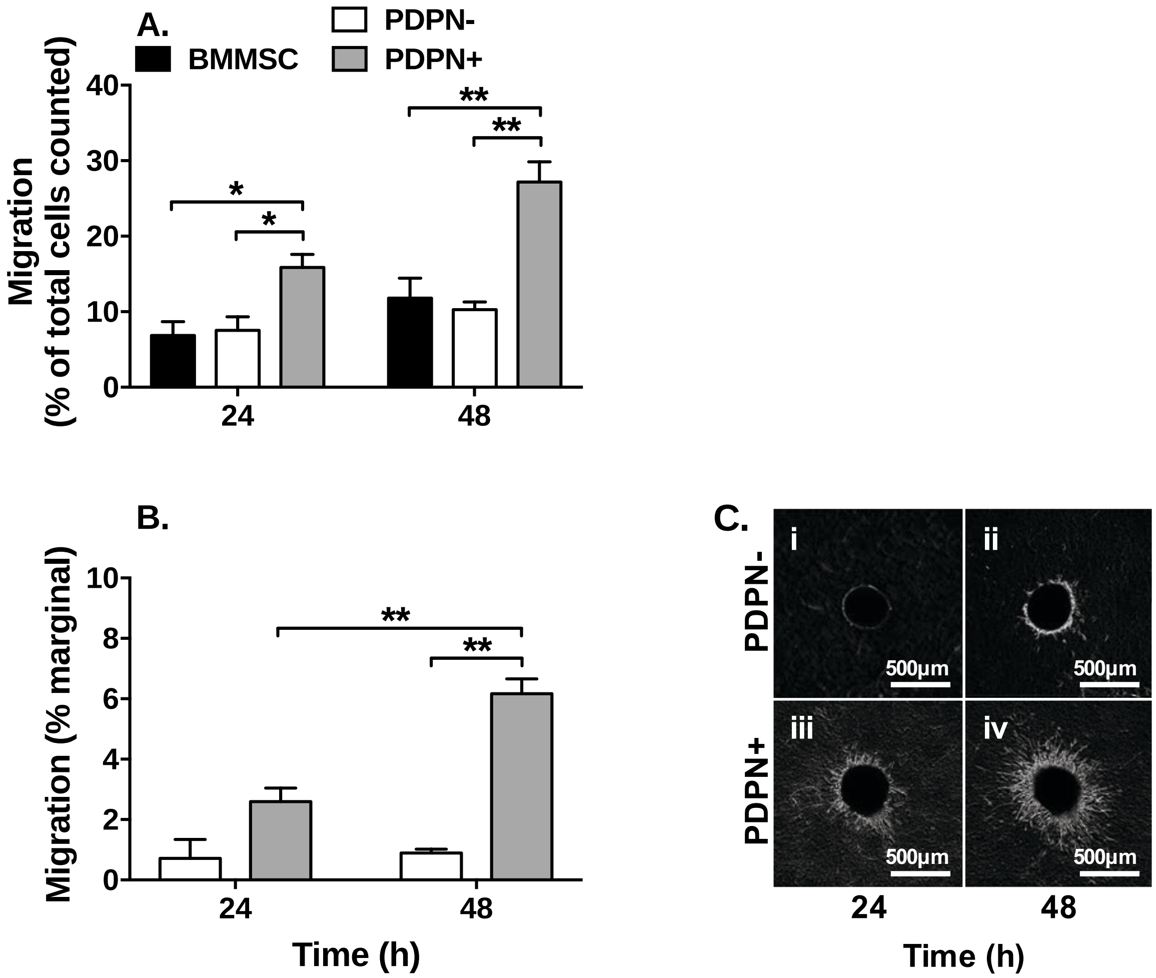

Figure 5-2 Effect of PDPN on UCMSC migration.

(A) MSC were seeded in an 8µm pore transwell filter and allowed to migrate through the filter for 48 hours. Cells were detached from the upper and lower chambers and counted. Data are expressed as the percentage migrated in the lower chamber compared to the total cell count for both chambers. ANOVA showed a significant effect of PDPN status on migration; $p<0.01$. **(B, C)** UCMSC donors, negative or -positive for PDPN were seeded to form a spheroid over 48 hours, prior to seeding on a collagen matrix and imaging at two 24 hour intervals. ANOVA showed a significant effect of time ($p<0.05$) and PDPN status on MSC migration ($p<0.01$). **(C)** Scale bar represents 500µm. Data are mean ± SEM from **(A)** n=4-9, or **(B, C)** n=2-4 independent experiments using **(A)** four BMMSC, five PDPN-negative UCMSC and nine PDPN-positive UCMSC donors, or **(B, C)** two PDPN-negative and four PDPN-positive UCMSC donors. * = $p<0.05$, ** = $p<0.01$ by Bonferroni post-test.

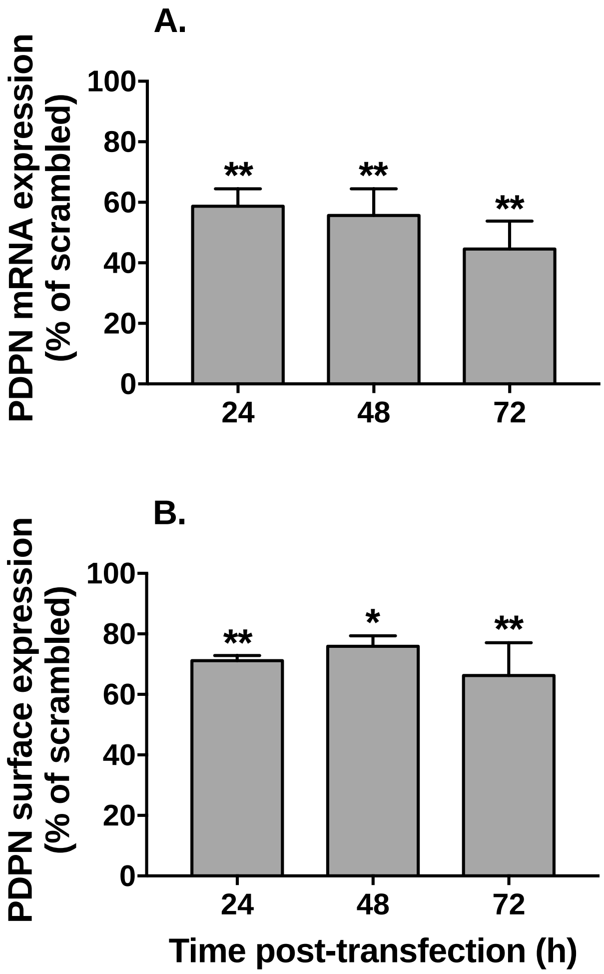

Figure 5-3 Effect of siRNA knockdown on PDPN expression over time. PDPN-positive UCMSC were transfected with siRNA against PDPN. **(A)** Gene expression assessed by qPCR and relative expression units normalised as a percentage of the scrambled control. **(B)** Surface protein expression assessed by flow cytometry and MFI expression normalised as a percentage of the scrambled MFI expression. ANOVA showed a significant effect of treatment, but not time, on PDPN mRNA and surface expression; $p<0.01$. Data are mean ± SEM from **(A)** n=3, **(B)** n=4-5 independent experiments using at least three different donors. * = $p<0.05$, ** = $p<0.01$ by Dunnett post-test compared to scrambled controls.

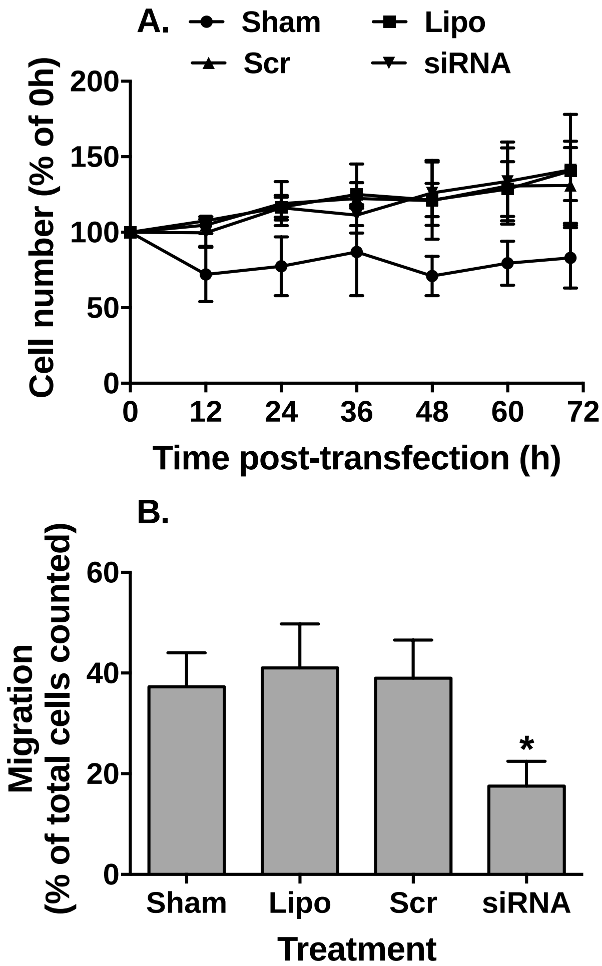

Figure 5-4 Effect of PDPN siRNA knockdown on UCMSC proliferation and migration.

PDPN-positive UCMSC were transfected with 50nM of two siRNA PDPN duplexes, a non-specific siRNA duplex control (Scr), lipofectamine alone (Lipo), or left untreated (Sham) for 24 hours. **(A)** Effect of PDPN expression on UCMSC proliferation was automatically recorded using the Cell-IQ Imagen system for six 12 hour intervals post-transfection. Data are expressed as the percentage of the number of cells at 0 hours **(B)** UCMSC were seeded in an 8µm pore transwell filter for 48 hours, then detached from the upper and lower chambers and counted. Data are expressed as the percentage migrated in the lower chamber compared to the total cell count for both chambers. ANOVA showed a significant effect of treatment on migration; p<0.05. Data are mean ± SEM from **(A)** n=2-3, **(B)** n=4 independent experiments using **(A)** at least two, **(B)** four different donors. * = p<0.05 by Dunnett post-test compared to sham.

We next wished to see whether absence of PDPN had a more pronounced effect on MSC migration. Initially we designed our own CRISPR/Cas9 construct and validated the procedure using a PDPN-positive cell line. Firstly, we generated three guide RNAs (gRNA) to different regions of the PDPN gene, with the intention of inducing a frameshift mutation and subsequent premature stop codon in the open reading frame for PDPN (Table 2-4). This occurs through non-homologous end joining when the Cas9 endonuclease is guided to the complimentary site and cleaves a double strand break in the target DNA. The custom CRISPR/Cas9 plasmid contained a puromycin resistance cassette enabling us to select cells that had been successfully transfected (Ran et al. 2013). The HEK293T cell line was chosen for validation as it is positive for PDPN expression (Figure 5-5A and Figure 5-6B). The minimum concentration of puromycin required to kill 100% of HEK293T cells was 2.5μg/mL (Dr P Noy, University of Birmingham, 2016, personal communication). For UCMSC, the minimum concentration of puromycin required to kill 100% of cells was found to be 1.0μg/mL, this was the concentration used after UCMSC transfection (Figure 5-7).

HEK293T cells and PDPN-positive UCMSC were transfected with the custom CRISR/Cas9 plasmid for each gRNA generated using Lipofectamine. Puromycin selection resulted in complete cell death of transfected UCMSC, suggesting an inability to transfect these cells using Lipofectamine. Puromycin-resistant HEK293T cells were analysed by flow cytometry for PDPN expression (Figure 5-5A), however no difference in surface expression was observed between each CRISPR/Cas9 construct used compared to the untreated control (Figure 5-5A). This suggests that

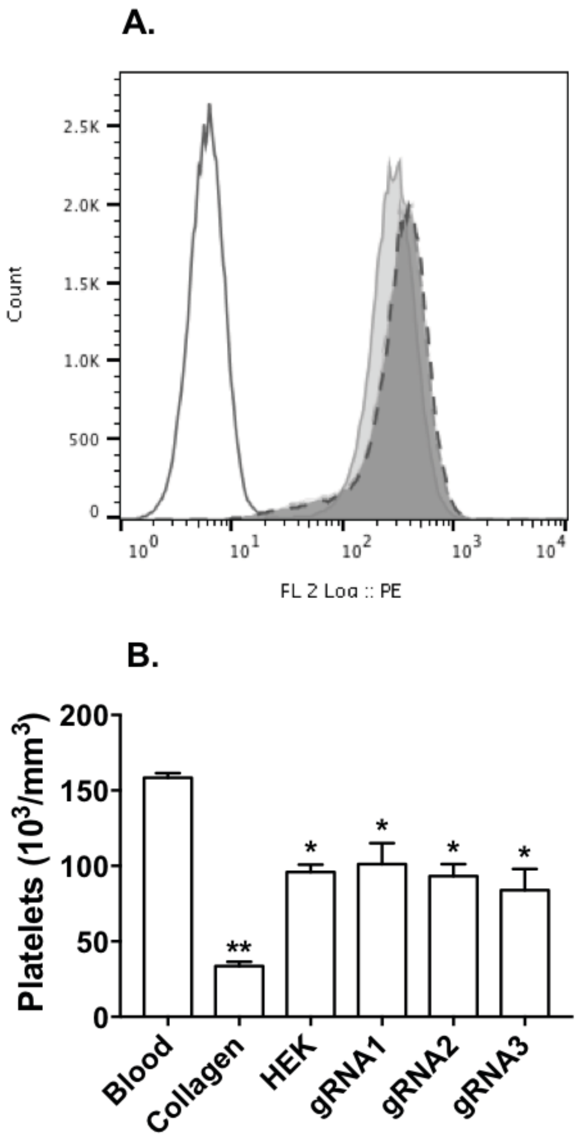

Figure 5-5 Effect of custom CRISPR/Cas9 plasmid transfection on HEK PDPN expression and platelet aggregation.

HEK293T cells were transfected with the custom CRISPR/Cas9 plasmid for gRNA1, gRNA2, or gRNA3 and selected with puromycin. **(A)** Cells were labelled with antibodies against PDPN (untreated HEK293T = shaded or transfected HEK293 = dashed line), isotype control (unshaded) and analysed by flow cytometry and shown as a representative histogram of frequency versus fluorescence intensity. **(B)** Ability of cells to aggregate platelets in whole blood was assessed by measuring the platelet count using the ABX Pentra 60 after a 30-minute incubation. Whole blood only negative control (blood); whole blood mixed with collagen positive control (collagen); untreated (HEK); transfected HEK293T cells (gRNA'n'). ANOVA showed a significant effect of treatment on platelet count; $p<0.01$. Data are mean ± SEM from n=3 independent experiments using one HEK293T cell donor and three whole blood donors. * = $p<0.05$, ** = $p<0.01$ by Dunnett post-test compared to the negative control (whole blood alone).

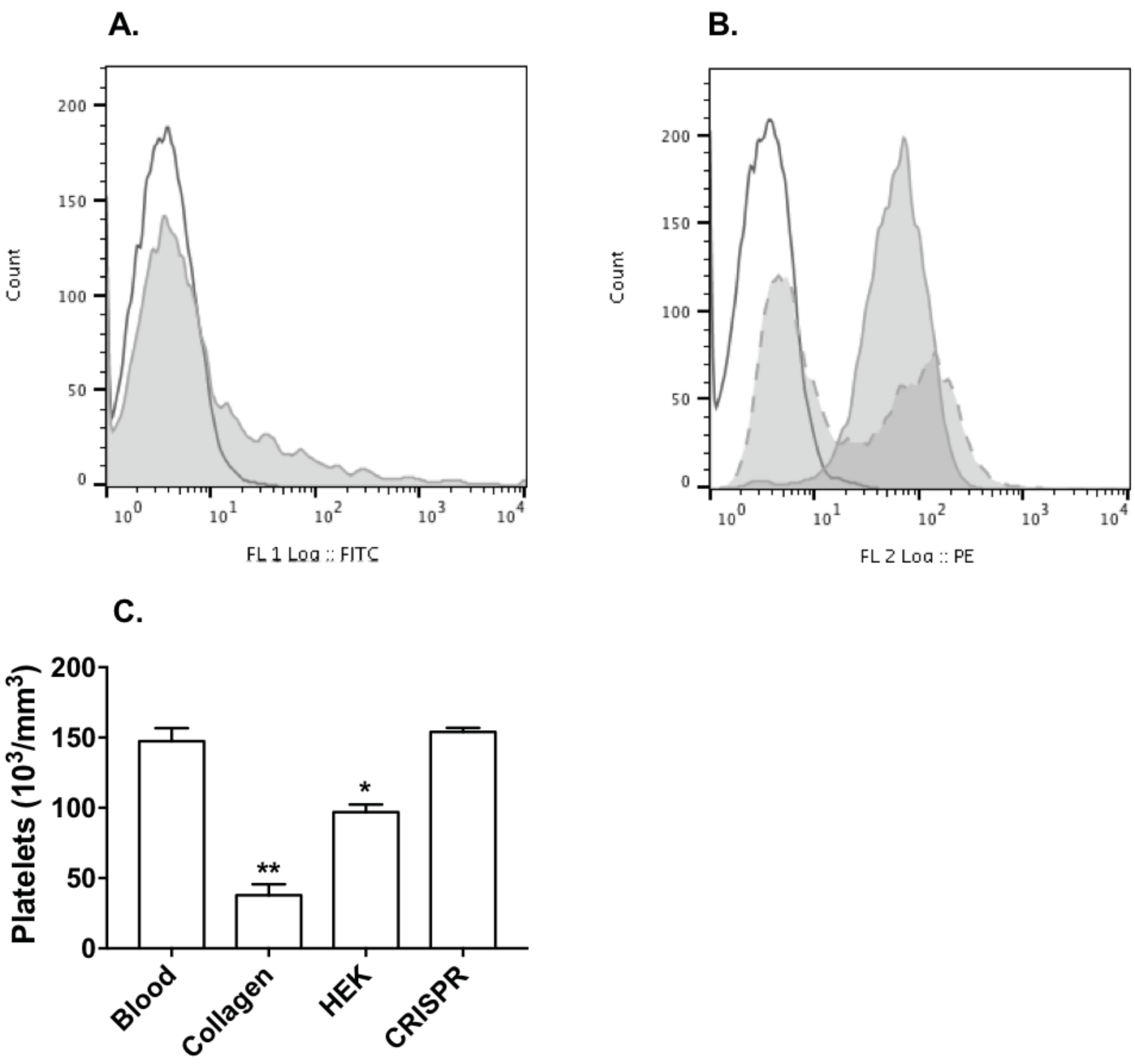

Figure 5-6 Effect of commercial CRISPR/Cas9 plasmid transfection on HEK PDPN expression and platelet aggregation.

HEK293T cells were transfected with the commercial CRISPR/Cas9 plasmid. **(A)** GFP expression in transfected cells (shaded) compared to untreated control (unshaded). **(B)** Untreated HEK293T were stained for PDPN surface expression and assessed by flow cytometry with rat anti-human (NZ-1.3) PDPN PE (shaded) or rat IgG2a isotype control (unshaded). Transfected HEK293T were stained with rat anti-human (NZ-1.3) PDPN PE (dashed line). **(C)** PDPN aggregation was assessed by suspending HEK293T in whole blood for 30 minutes and measuring the platelet count using the ABX Pentra 60. Whole blood only negative control (blood); whole blood mixed with collagen positive control (collagen); untreated (HEK); transfected and cell sorted PDPN-negative population (CRISPR). ANOVA showed a significant effect of treatment on platelet count; $p<0.01$. Data are mean ± SEM from n=3 independent experiments using one HEK293T donor and three whole blood donors. * = $p<0.05$, ** = $p<0.01$ by Dunnett post-test compared to the negative control (whole blood alone).

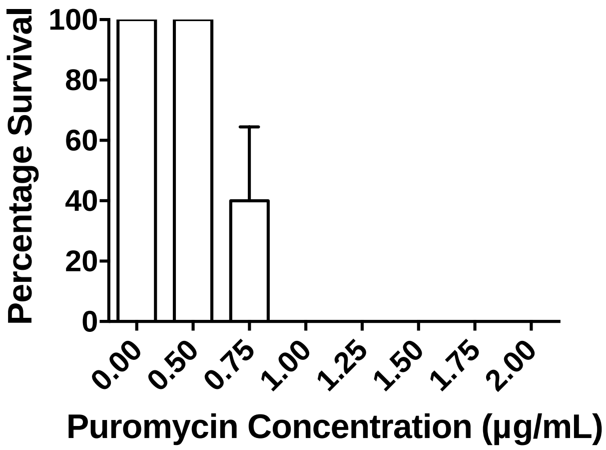

Figure 5-7 Effect of puromycin on UCMSC survival.
A kill curve depicting the minimum concentration of puromycin required to kill 100% of UCMSC. Friedman test showed a significant effect of treatment on percentage survival; $p<0.01$. Data are mean ± SEM from n=5 independent experiments using five different donors.

either all gRNAs generated were unsuccessful in inducing the deletion of PDPN or that the gRNAs did not sufficiently alter the binding epitope for our PDPN antibody (NZ-1.3).

We have previously shown that PDPN binds to CLEC-2 expressed on platelets inducing platelet aggregation (Dr L Sheriff, University of Birmingham, 2017, personal communication). Using this assay, we assessed whether PDPN CRISPR transfected cells could induce platelet aggregation when compared to the positive control, collagen. Puromycin-resistant HEK293T cells for each custom CRISPR/Cas9 construct reduced the platelet count to the same extent as untreated HEK293T cells (Figure 5-5B). This indicated that PDPN was still functional on these cells and that all gRNAs generated were unsuccessful in inducing a functional deletion of PDPN.

A recent publication had shown a commercial CRISPR/Cas9 plasmid targeting PDPN [with a green fluorescent protein (GFP) tag] to be successful in knocking out PDPN expression in HEK293T cells (Kaneko et al. 2017). We purchased this commercial construct and again validated its efficacy in HEK293T cells. The transfected cells were positive for GFP (Figure 5-6A) and expressed a bimodal PDPN distribution (Figure 5-6B), suggesting a successful deletion of PDPN within this population. The PDPN-negative population was isolated by fluorescence-activated cell sorting and assessed for their ability to induce platelet aggregation. The transfected and sorted PDPN-negative HEK293T cells were unable to aggregate platelets compared to the untreated control, indicating that PDPN function was also successfully deleted

(Figure 5-6C). Based on the success with the HEK293T cell validation, we transfected PDPN-positive UCMSC with the commercial CRISPR/Cas9 plasmid. Due to the problems we had previously experienced using Lipofectamine to transfect UCMSC, we decided to use an MSC-specific Nucleofector kit to electroporate the cells with the plasmid. Nucleofection of the commercial CRISPR/Cas9 plasmid into UCMSC resulted in very low transfection efficiencies (Figure 5-8), making them unsuitable to expand sufficiently to use experimentally without inducing senescence. Thus, we were unable to successfully delete PDPN in UCMSC.

To further validate the role of PDPN in UCMSC migration, we used an antibody crosslinking strategy to determine whether stimulation of PDPN resulted in increased migratory function. To achieve this, PDPN-positive UCMSC were incubated with rat anti-human PDPN (NZ-1.3) and in the presence or absence of goat anti-rat IgG to induce crosslinking of the PDPN receptor and their migration assessed using the Transwell model. We observed no effect of PDPN crosslinking on UCMSC migration (Figure 5-9), indicating that clustering of the PDPN receptor does not induce migration-related downstream signalling in UCMSC. In future experiments, we directly compared PDPN-positive and -negative UCMSC donors.

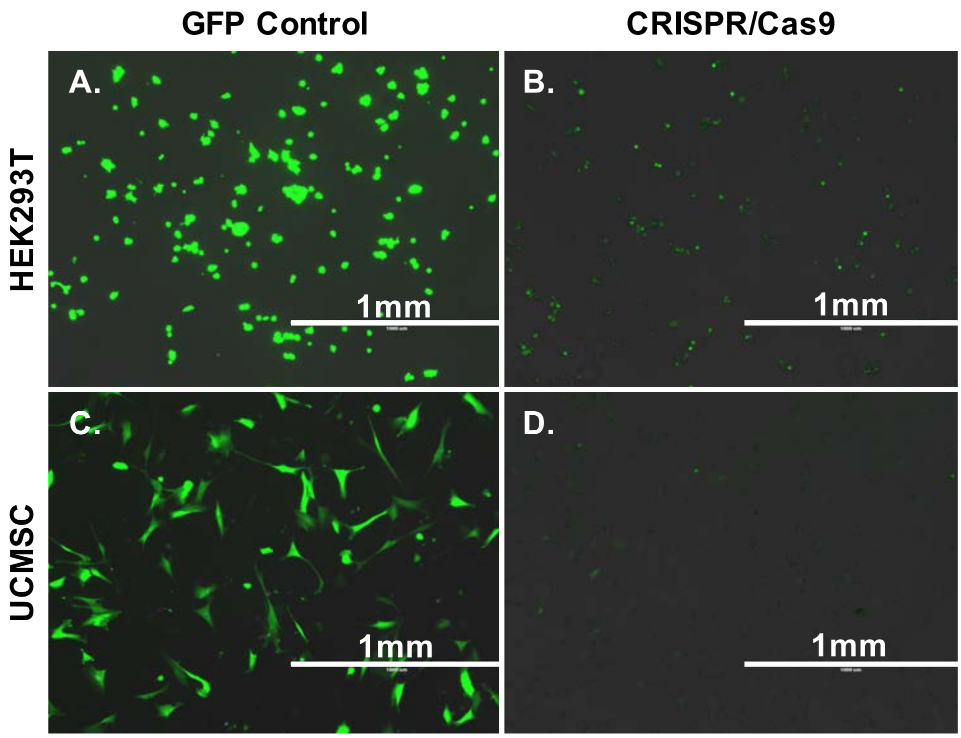

Figure 5-8 Effect of nucleofection on plasmid uptake by HEK and UCMSC. **(A, B)** HEK293T cells and **(C, D)** PDPN-positive UCMSC were transfected using the Lonza 4D-Nucleofector X unit with **(A, C)** pmaxGFP Vector control, or **(B, D)** commercial CRISPR/Cas9 plasmid with GFP cassette. Cells were seeded for 72 hours prior to imaging. Images are representative of 2-4 independent experiments using one HEK293T cell donor and four PDPN-positive UCMSC donors. Scale bar represents 1mm.

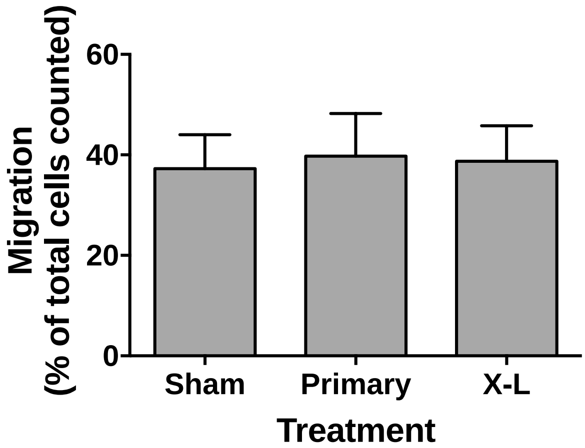

Figure 5-9 Effect of PDPN crosslinking on UCMSC transwell migration. PDPN-positive UCMSC were seeded in an 8μm pore transwell filter for 1 hour before the addition of anti-human PDPN for 30 minutes. Goat anti-rat IgG2a was subsequently added to induce crosslinking for 47 hours. The cells were detached and counted from the upper and lower chambers. Data are expressed as the percentage migrated in the lower chamber compared to the total cell count for both chambers. Untreated negative control (sham); treated with anti-human PDPN only (primary); treated with anti-human PDPN and goat anti-rat IgG2a (X-L). Data are mean ± SEM from n=4 independent experiments using four different donors.

5.2.2. PDPN-dependent migration is mediated through Rac1 signalling

The Rho GTPase family regulates cell migration through reorganisation of the actin cytoskeleton [reviewed by (Sahai & Marshall 2002)]. To determine which pathway was involved in PDPN-mediated MSC migration, we used inhibitors to block the activities of RhoA, RhoB, and RhoC (CT04), ROCK (Y27632), and Rac1 (NSC23766). Inhibition of Rho activation with CT04 significantly impaired UCMSC migration and cell number in a dose-dependent manner for both PDPN-positive and negative UCMSC (Figure 5-10). This suggests that Rho is a global positive regulator of UCMSC migration, and not specifically linked to PDPN signalling. In contrast, inhibition of ROCK significantly increased migration for both PDPN-positive and negative UCMSC, with the largest increase in the presence of 10μM of Y27632 (Figure 5-11A). Unexpectedly, an increase in cell number for PDPN-negative UCMSC was also observed in the presence of 10μM of Y27632 (Figure 5-11B). This implies that ROCK acts as a negative regulator of cell migration, and may have roles in regulating cell proliferation. Collectively these data suggest that signalling through Rho and ROCK both influence UCMSC migration, but are independent of PDPN expression.

Inhibition of Rac1 activity with NSC23766 caused a significant and dose-dependent decrease in the migration of PDPN-positive UCMSC, but not of PDPN-negative UCMSC (Figure 5-12A). Yet, high doses of NSC23766 were toxic with cell numbers drastically reduced (Figure 5-12B). Confocal imaging of UCMSC revealed that PDPN-positive UCMSC were significantly larger than their negative counterparts

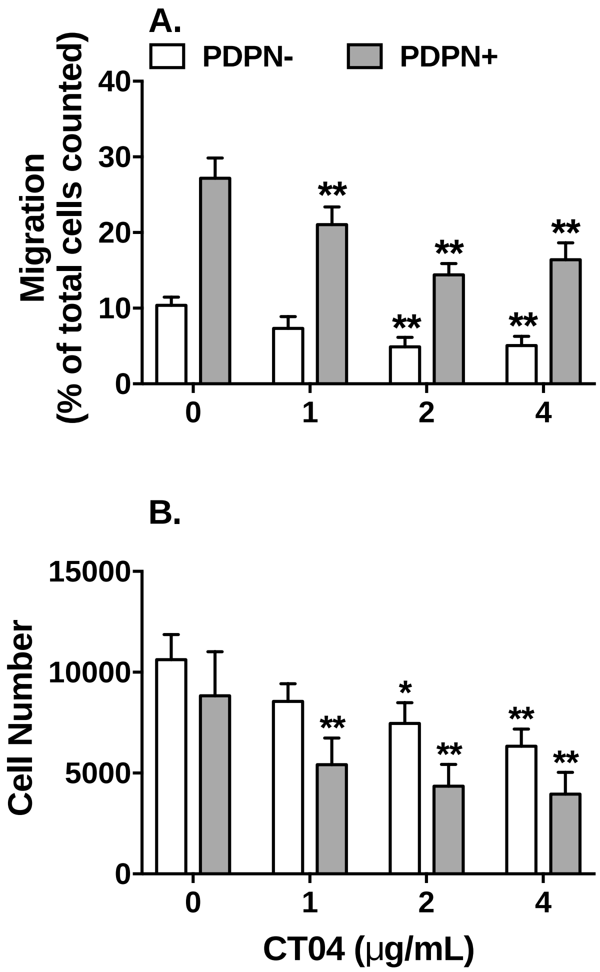

Figure 5-10 Effect of the Rho inhibitor CT04 on MSC transwell migration. PDPN-negative or -positive UCMSC were seeded in an 8µm pore transwell filter and treated with CT04 (0-4µg/mL) for 48 hours. The cells were detached and counted from the upper and lower chambers. Data are expressed as migration as a **(A)** percentage of total cells counted from both chambers, and **(B)** the total cell count of the upper and lower chambers. ANOVA showed a significant effect of treatment on migration and cell number; $p<0.01$. Data are mean ± SEM from n=4 independent experiments using four different UCMSC donors for each PDPN phenotype. * = $p<0.05$, ** = $p<0.01$ by Dunnett post-test compared to untreated control (0µg/mL).

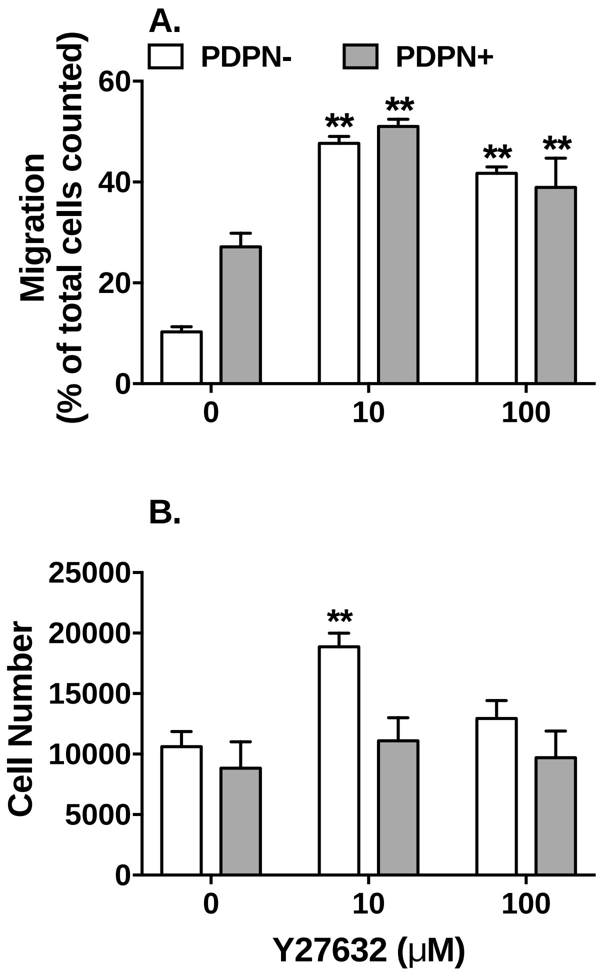

Figure 5-11 Effect of the ROCK inhibitor Y27632 on MSC transwell migration.

PDPN-negative or -positive UCMSC were seeded in an 8µm pore transwell filter and stimulated with Y27632 (0-100µM) for 48 hours. The cells were detached and counted from the upper and lower chambers. Data are expressed as the **(A)** percentage migrated in the lower chamber compared to the total cell count for both chambers, and **(B)** the total cell count of the upper and lower chambers. ANOVA showed a significant effect of treatment on migration and cell number; p<0.01. Data are mean ± SEM from n=4 independent experiments using four different UCMSC donors for each PDPN phenotype. * = p<0.05, ** = p<0.01 by Dunnett post-test compared to untreated control (0µg/mL).

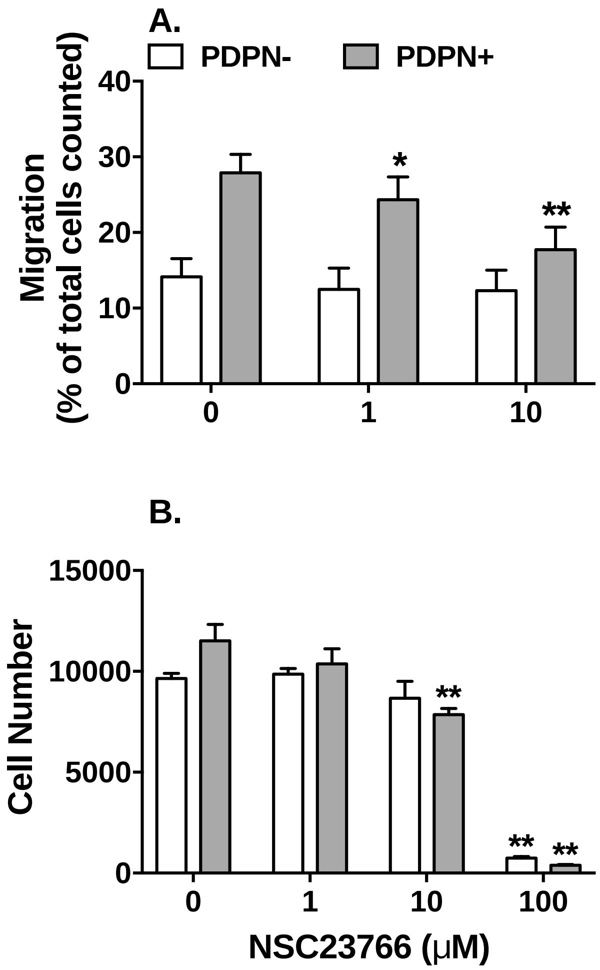

Figure 5-12 Effect of the Rac1 inhibitor NSC23766 on MSC transwell migration.

PDPN-negative or -positive UCMSC were seeded in an 8µm pore transwell filter and stimulated with NSC23766 (0-100µM) for 48 hours. The cells were detached and counted from the upper and lower chambers. Data are expressed as the **(A)** percentage migrated in the lower chamber compared to the total cell count for both chambers, and **(B)** the total cell count of the upper and lower chambers. ANOVA showed a significant effect of treatment on migration and cell number; $p<0.01$. Data are mean ± SEM from n=4 independent experiments using four different UCMSC donors for each PDPN phenotype. * = $p<0.05$, ** = $p<0.01$ by Dunnett post-test compared to untreated control (0µg/mL).

(Figure 5-13 and Figure 5-14A). However, Rac1 inhibition had no effect on either cell size (Figure 5-14A) or the intensity of PDPN expression (Figure 5-14B). Furthermore, analysis of PDPN location in positive UCMSC showed that in the presence of NSC23766, the number of cells expressing PDPN at the peripheral edges of the cell was significantly reduced (Figure 5-14C, D). These data suggest that PDPN-mediated migration of UCMSC is dependent on Rac1, and that Rac1 might be responsible for the peripheral localisation of PDPN, thus enabling PDPN to exert its pro-migratory function.

5.2.3. PDPN expressing MSC can protrude through endothelial barriers and capture platelets

Given the perivascular localisation of PDPN during inflammation (Payne et al. 2017; Hitchcock et al. 2015; Inoue et al. 2015), and that MSC are enriched within the perivascular niche (Feng et al. 2011; Crisan et al. 2008). We wondered what the localisation of PDPN-positive UCMSC was *in situ*. Immunohistochemistry staining for PDPN in umbilical cord cross-sections, showed PDPN to be localised to the perivascular space and fibrous areas of the amnion (Figure 5-15). This data implies that PDPN is positioned for involvement in the regulation of the vascular compartment rather than the underlying stroma.

We next considered whether PDPN-expressing MSC might activate platelets through the PDPN-CLEC-2 interactions. This would be possible if MSC could protrude from the perivascular space, presenting PDPN to the blood vessel lumen. To assess this

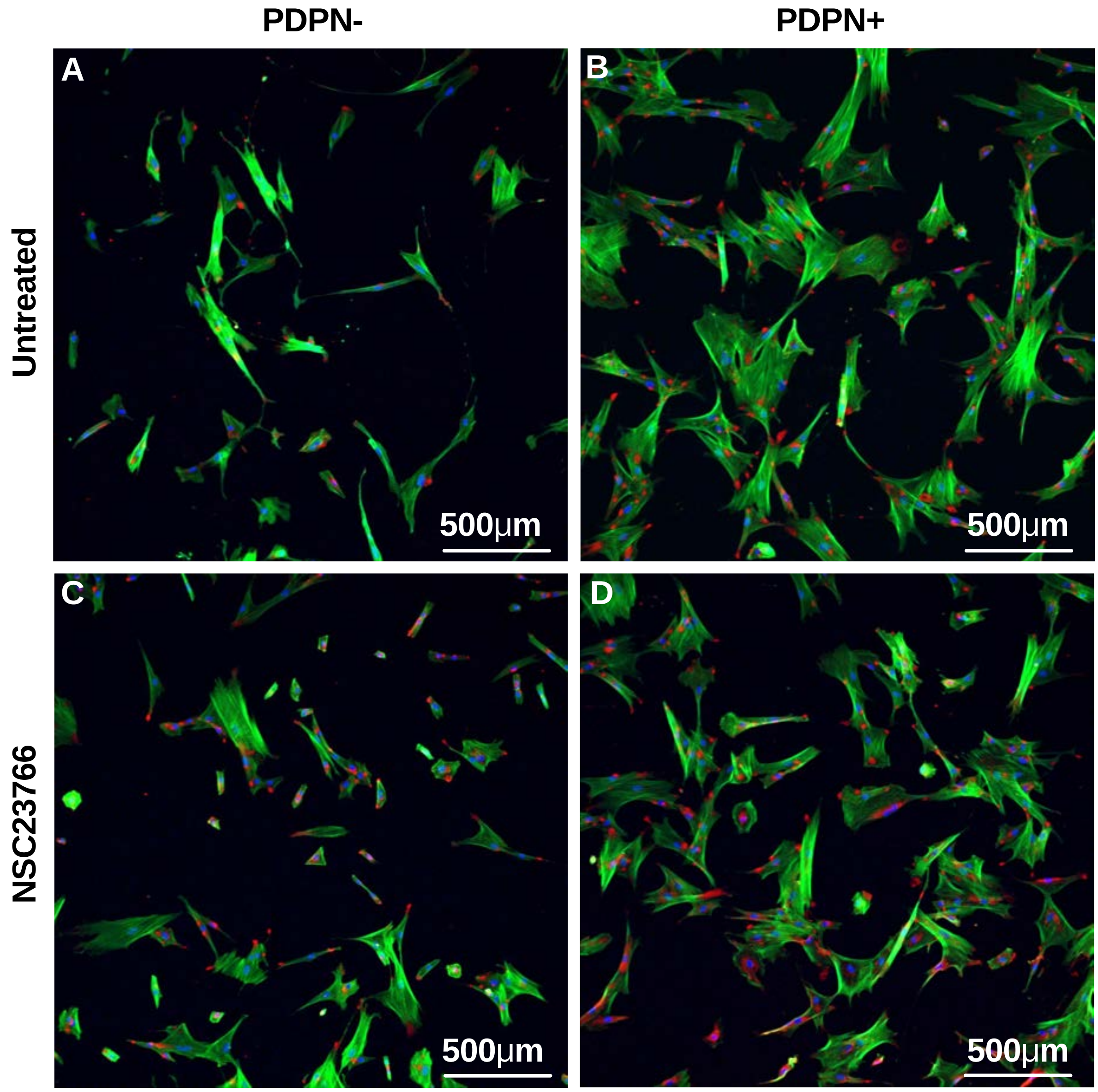

Figure 5-13 Micrograph analysis of the Rac1 inhibitor NSC23766.
UCMSC were treated with the Rac-1 inhibitor, (NSC23766) and subsequently stained for expression of PDPN (red), f-actin (green), and nuclei (blue), and analysed by confocal microscopy. Representative images were taken of **(A)** PDPN-negative, **(B)** PDPN-positive, **(C)** PDPN-negative NSC23766, **(D)** PDPN-positive NSC23766. Scale bar represents 500µm. Images are representative of n=4 independent experiments using four different UCMSC donors for each PDPN phenotype.

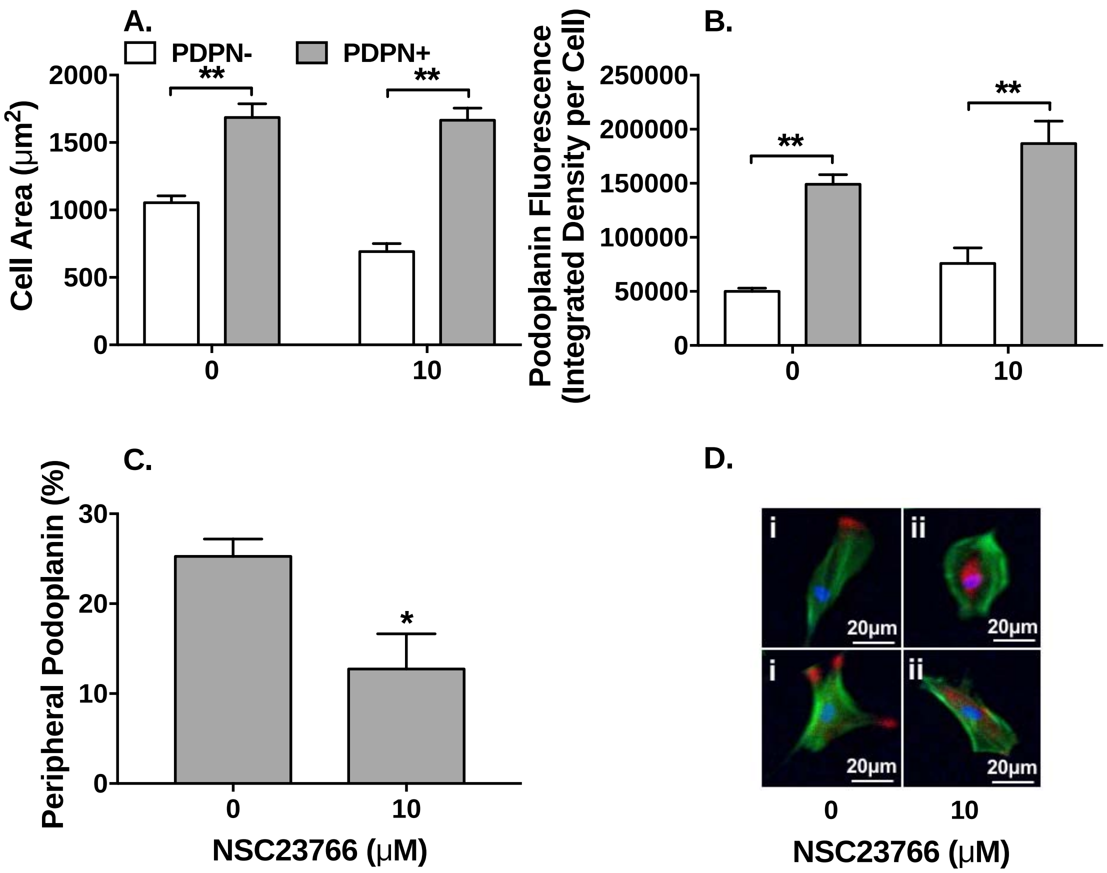

Figure 5-14 Effect of the Rac1 inhibitor NSC23766 on MSC morphology and PDPN localisation.

PDPN-negative or -positive UCMSC were seeded for 24 hours with or without the Rac-1 inhibitor, NSC23766. The cells were stained for f-actin (green), PDPN (red), and the nucleus (blue), then imaged by confocal microscopy. Data were expressed as **(A)** average cell area in μm^2, **(B)** PDPN fluorescence intensity as measured by the average integrated density for PDPN per cell, and **(C)** PDPN localisation as a percentage of cells expressing PDPN at the cell edge alone. **(D)** Representative images of single UCMSC expressing PDPN at **(i)** the cell edge alone in the absence of treatment or **(ii)** the centre of the cell in the presence of treatment. ANOVA showed a significant effect of treatment on cell area and PDPN fluorescence intensity; $p<0.01$. Data are mean ± SEM from n=4 independent experiments using four different UCMSC donors for each PDPN phenotype. **(A, B)** ** = $p<0.01$ by Bonferroni post-test, **(C)** * = $p<0.05$ by paired t-test.

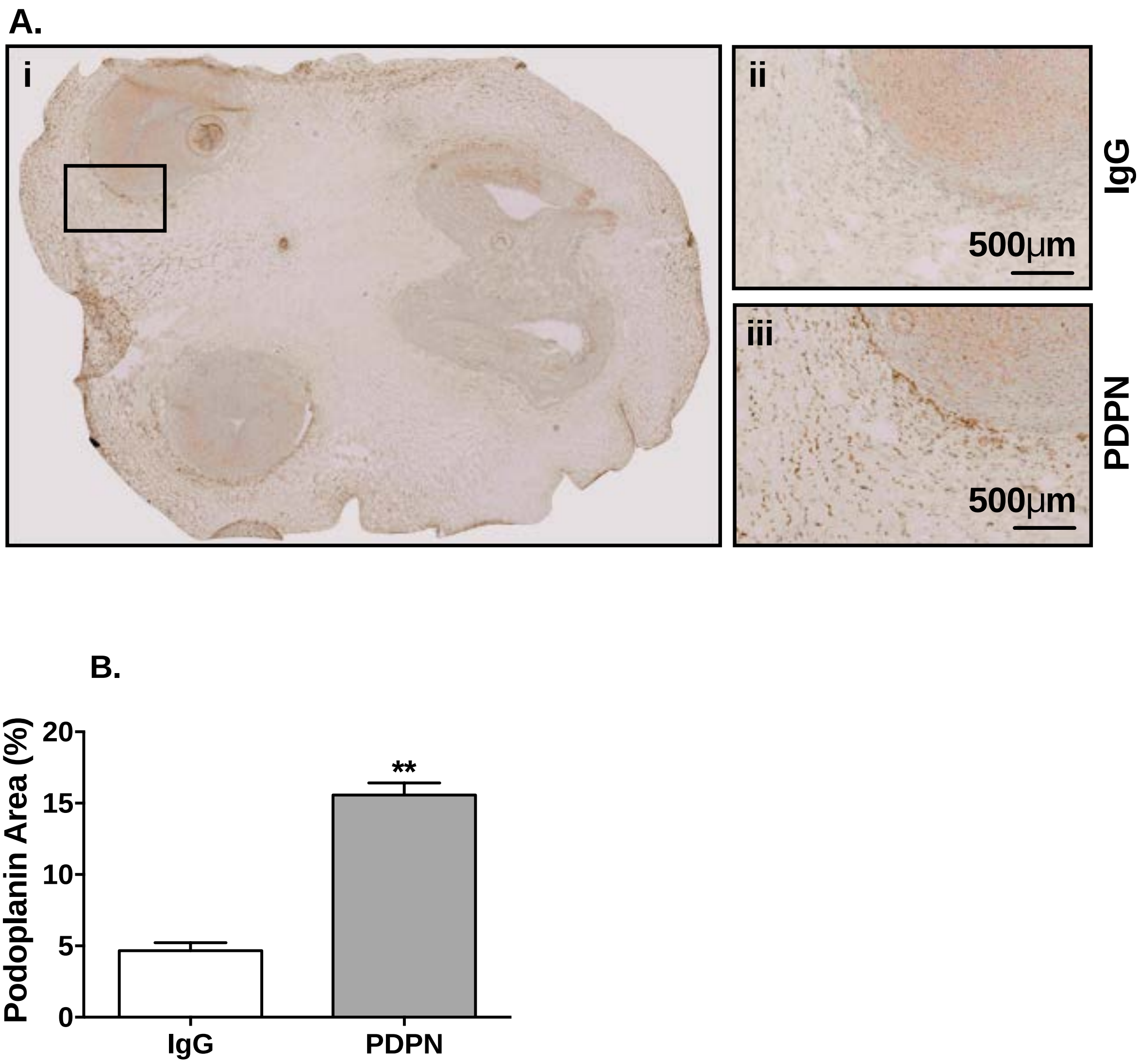

Figure 5-15 Micrograph analysis of PDPN expression in umbilical cords. Umbilical cord cross-sections were stained for PDPN by immunohistochemistry using rat IgG2a control or anti-human podoplanin (NZ-1.3) and nuclei stained with haematoxylin. **(A)** Representative images were taken of the; (i), whole umbilical cord cross-section or regions of interest (black box) stained with (ii), perivascular IgG control or (iii), perivascular PDPN stain. Scale bar represents 500µm. **(B)** Images were quantified for the percentage area of DAB staining in the whole umbilical cord cross-section. Data are mean ± SEM from n=6 independent experiments using six different UCMSC donors. ** = p<0.01 by paired t-test.

possibility, UCMSC were cultured on the basal surface of transwell filters with different pore sizes to determine the smallest gap that MSC could extend protrusions through. Whole blood was labelled with PE-conjugated anti-CD41 (specifically labelling platelets) and added to the apical surface of the filter, and interactions with MSC protrusions were assessed by fluorescence microscopy. Platelet adhesion to UCMSC protrusions could be detected on 3 and 8μm pore filters, but not 0.4μm (Figure 5-16), suggesting basally seeded MSC could extend cellular protrusions through gaps larger than 0.4μm. Moreover, platelet aggregates were significantly larger on the apical surface of filters with PDPN-positive UCMSC underneath compared to PDPN-negative UCMSC on 3μm pores (Figure 5-16B). Platelet aggregates for 8μm pores were of a similar size, but showed no difference between PDPN-positive and -negative UCMSC (Figure 5-16B). This is possibly explained by the ability of UCMSC to migrate from the basal surface to the apical surface on the 8μm filters over 24 hours, allowing whole cells to interact with the platelets. In contrast, UCMSC were unable to traverse across the 3μm pores (as assessed by cell counts from the upper chamber being below the limit of detection of the Coulter Counter), indicating that platelets were only able to interact with UCMSC that had formed protrusions through the 3μm pores. Of note, interaction with PDPN or a stimulating factor is required for platelet aggregation.

Subsequently we analysed the ability of PDPN-positive UCMSC protrusions to capture platelets from flowing blood using a flow-based adhesion assay. Recruitment of platelets was significantly more pronounced after 10 minutes of whole blood

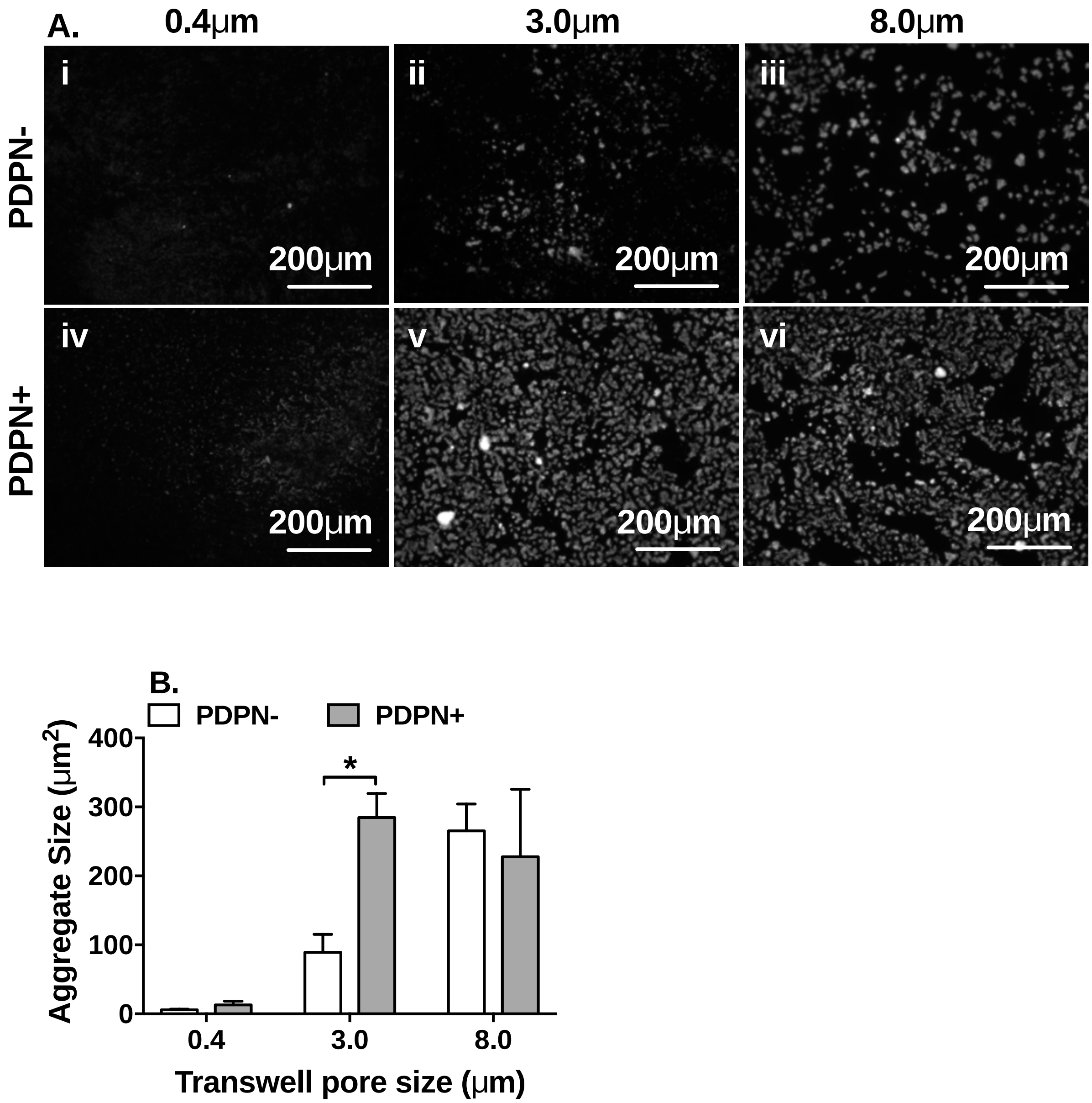

Figure 5-16 Effect of filter pore size on UCMSC protrusions.

PDPN-negative or -positive UCMSC were seeded on inverted 0.4μm, 3μm, 8μm pore culture inserts for 24 hours. CD41-labelled whole blood was incubated in the upper chamber of the insert for 1 hour. **(A)** Representative images were taken of fluorescent platelet aggregates; (i), 0.4μm PDPN-; (ii), 3μm PDPN-; (iii), 8μm PDPN-; (iv), 0.4μm PDPN-positive; (v), 3μm PDPN-positive; (vi), 8μm PDPN-positive. Scale bar represents 200μm. **(B)** Data are expressed as aggregate size in μm^2 as measured by the average size of fluorescent particles. ANOVA showed a significant effect of PDPN status, but not pore size, on aggregate size; $p<0.05$. Data are mean ± SEM from n=4 independent experiments using four different UCMSC donors for each PDPN phenotype. * = $p<0.05$ by Bonferroni post-test.

perfusion for the PDPN-positive than negative UCMSC, with lesser difference seen at the earlier 5-minute time point (Figure 5-17B). To establish whether platelet aggregates were a result of PDPN binding, we used human recombinant CLEC-2 (rCLEC-2) to competitively interfere with CLEC-2-PDPN interactions as previously described (Suzuki-Inoue et al. 2007). Pre-treatment of PDPN-positive UCMSC protrusions with rCLEC-2 prior to whole blood perfusion, resulted in a significant reduction in the average size of platelet aggregates compared to the untreated control (Figure 5-18). Platelet aggregation through platelet-platelet binding is mediated through αIIbβ3-integrin (Fullard 2004). We also utilised the αIIbβ3-integrin inhibitor integrilin (Thomas et al. 2011) to determine whether PDPN induces platelet activation and allows aggregates to form through platelet-platelet binding. Integrilin enables platelet adhesion to PDPN on MSC protrusions, but not platelet-platelet interactions. The presence of integrilin in the perfused whole blood significantly reduced the size of platelet aggregates compared to the untreated control (Figure 5-18). These data suggest that PDPN-positive UCMSC protrusions are capable of both capturing platelets from flow and of activating adherent platelets to aggregate in a PDPN-dependent manner.

Given that MSC are able to extend protrusions through pores in a filter, we next wanted to determine whether MSC were capable of protruding from the perivascular space into the vessel lumen. To do this we seeded a monolayer of BEC on the apical surface of the filter. In this model, MSC would need to extend through the BEC in order to come into contact with the flowing platelets. PDPN-positive UCMSC protrusions induced larger platelet aggregates than their negative counterparts

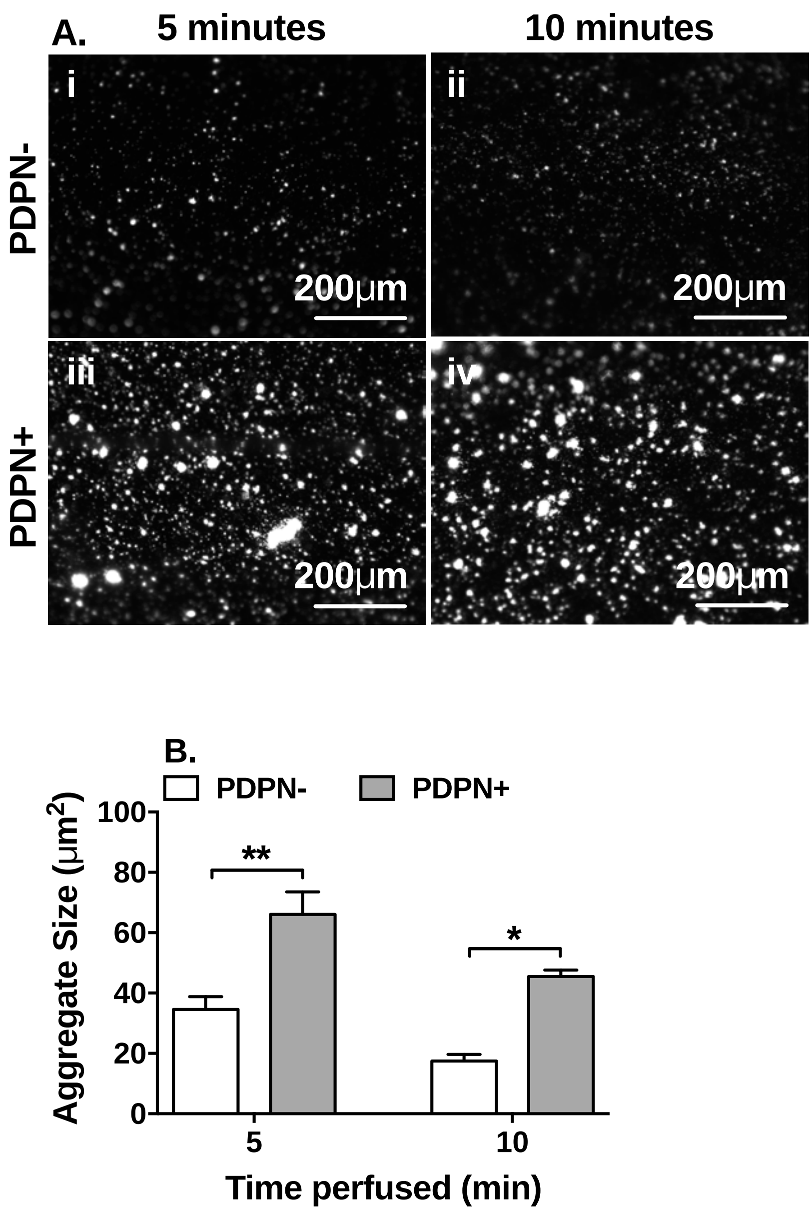

Figure 5-17 Effect of UCMSC protrusions on platelet aggregation in flow.
PDPN-negative or -positive UCMSC were seeded on inverted 3μm pore culture inserts for 24 hours. CD41-labelled whole blood was perfused over the apical surface of the filter in a parallel plate chamber for 5 or 10 minutes. **(A)** Representative images were taken of fluorescent platelet aggregates; (i), 5-minute perfusion PDPN-negative; (ii), 10-minute perfusion PDPN-negative; (iii), 5-minute perfusion PDPN-positive; (iv), 10-minute perfusion PDPN-positive. Scale bar represents 200μm. **(B)** Data are expressed as aggregate size in μm^2 as measured by the average size of fluorescent particles. ANOVA showed a significant effect of PDPN status, but not time, on aggregate size; $p<0.05$. Data are mean ± SEM from n=3-4 independent experiments using four different UCMSC donors for each PDPN phenotype. * = $p<0.05$, ** = $p<0.01$ by Bonferroni post-test.

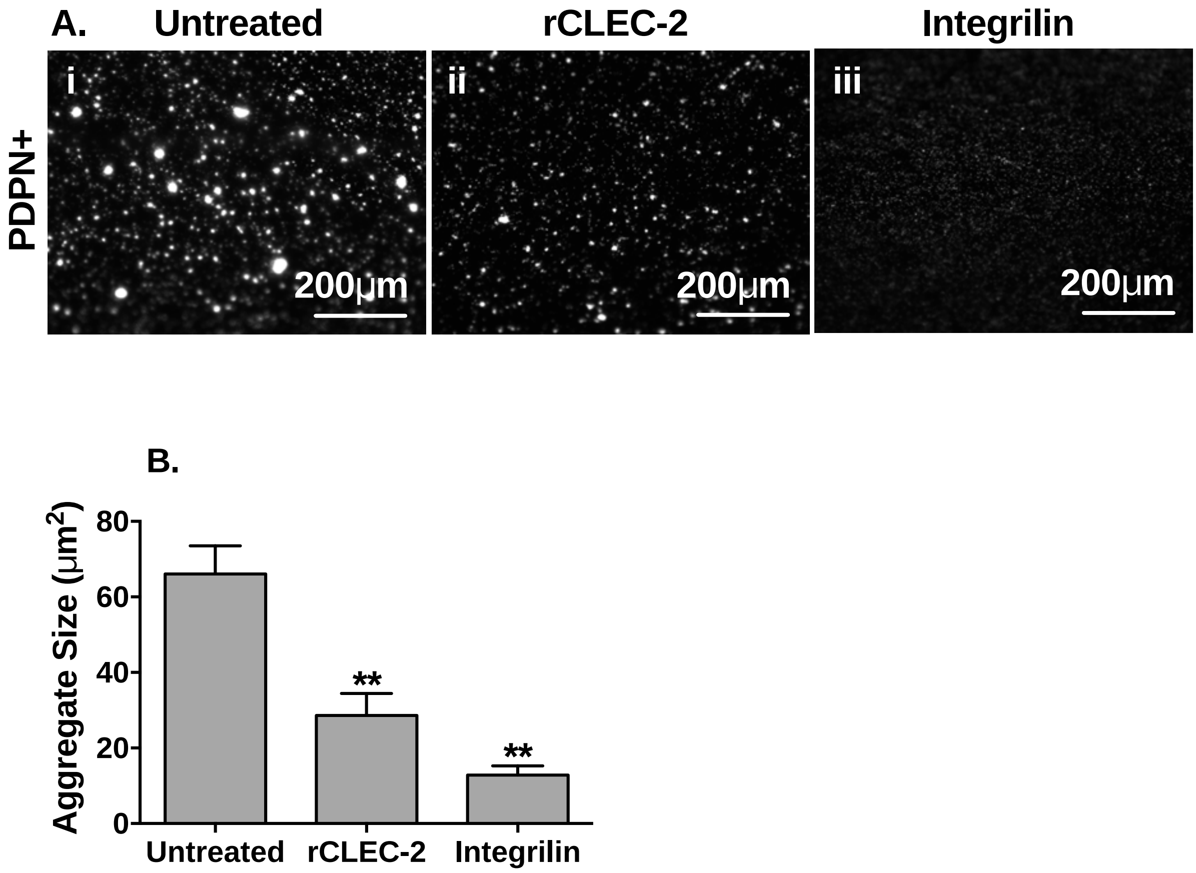

Figure 5-18 Effect of rCLEC-2 or integrilin on platelet aggregation on UCMSC protrusions.

PDPN-positive UCMSC were seeded on 3μm pore culture inserts for 24 hours. CD41-labelled whole blood was perfused over the apical surface of the filter in a parallel plate chamber for 5 minutes, with or without rCLEC-2 pre-treatment, or in the presence or absence of integrilin. **(A)** Representative images were taken of fluorescent platelet aggregates; (i), untreated; (ii), rCLEC-2 pre-treatment; (iii), integrilin treatment. Scale bar represents 200μm. **(B)** Data are expressed as aggregate size in μm^2 as measured by the average size of fluorescent particles. ANOVA showed a significant effect of treatment on aggregate size; $p<0.05$. Data are mean ± SEM from n=4 independent experiments using four different PDPN-positive UCMSC donors. ** = $p<0.01$ by Dunnett post-test compared to untreated.

(Figure 5-19). Furthermore, the presence of an endothelial monolayer had no effect on aggregate size (Figure 5-19). Endothelial monoculture (EC) adhered few very platelets (Figure 5-20). Again, we confirmed that the platelet aggregation was dependent on PDPN by using rCLEC-2 to block platelet-PDPN interactions. Pre-treatment of cocultures with rCLEC-2 significantly reduced platelet aggregate size to the same level as seen on endothelial monocultures (Figure 5-20). These data suggest that invasive perivascular MSC are capable of protruding through the endothelial vessel lining and activating platelets through PDPN and thus contributing to thrombosis.

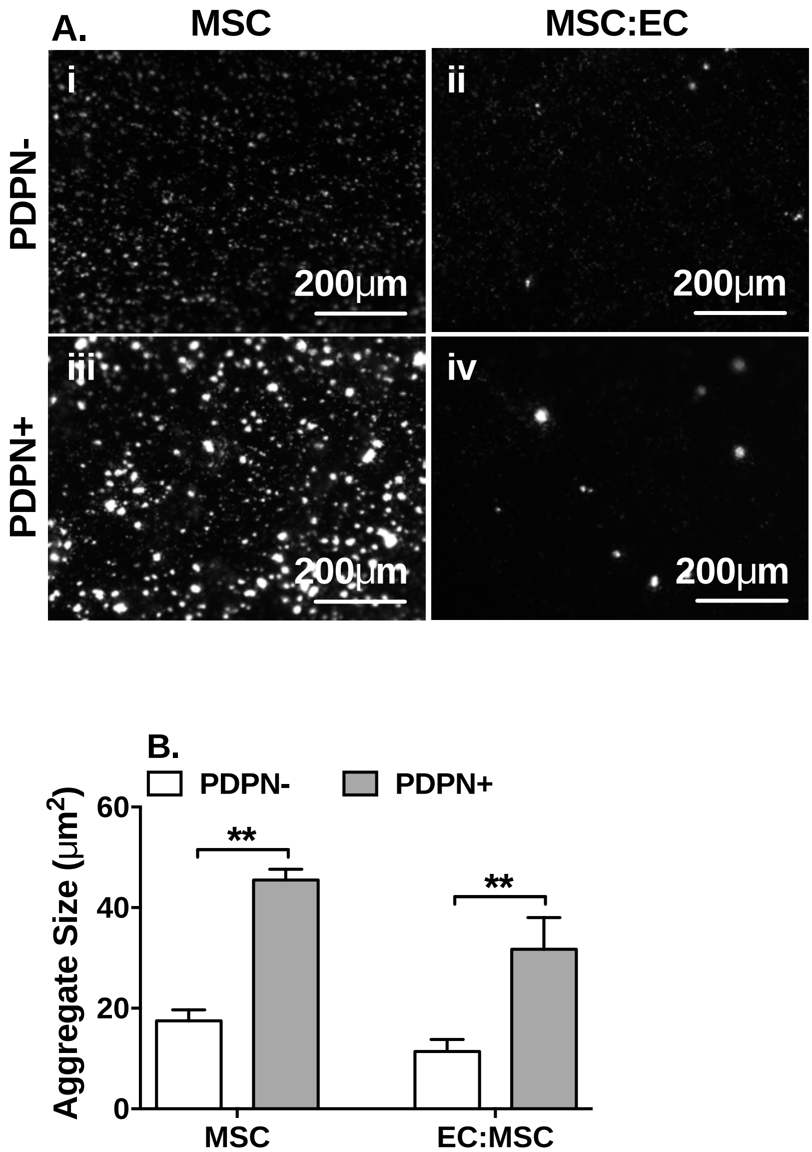

Figure 5-19 Effect of endothelial coculture on the ability of UCMSC protrusions to induce platelet aggregation.

PDPN-negative or -positive UCMSC were seeded on inverted 3µm pore culture inserts for 1 hour. The inserts were reinverted and the apical surface seeded with BEC to form coculture (EC:MSC). MSC monocultures were used as comparison. CD41-labelled whole blood was perfused over the apical surface of the filter in a parallel plate chamber for 10 minutes. **(A)** Representative images were taken of fluorescent platelet aggregates; (i), PDPN-negative MSC; (ii), PDPN-negative MSC:EC; (iii), PDPN-positive MSC; (iv), PDPN-positive MSC:EC. Scale bar represents 200µm. **(B)** Data are expressed as aggregate size in µm^2 as measured by the average size of fluorescent particles. ANOVA showed a significant effect of PDPN status, but not culture conditions, on aggregate size; $p<0.05$. Data are mean ± SEM from n=3 independent experiments using three different donors for each PDPN phenotype and cell type. ** = $p<0.01$ by Bonferroni post-test.

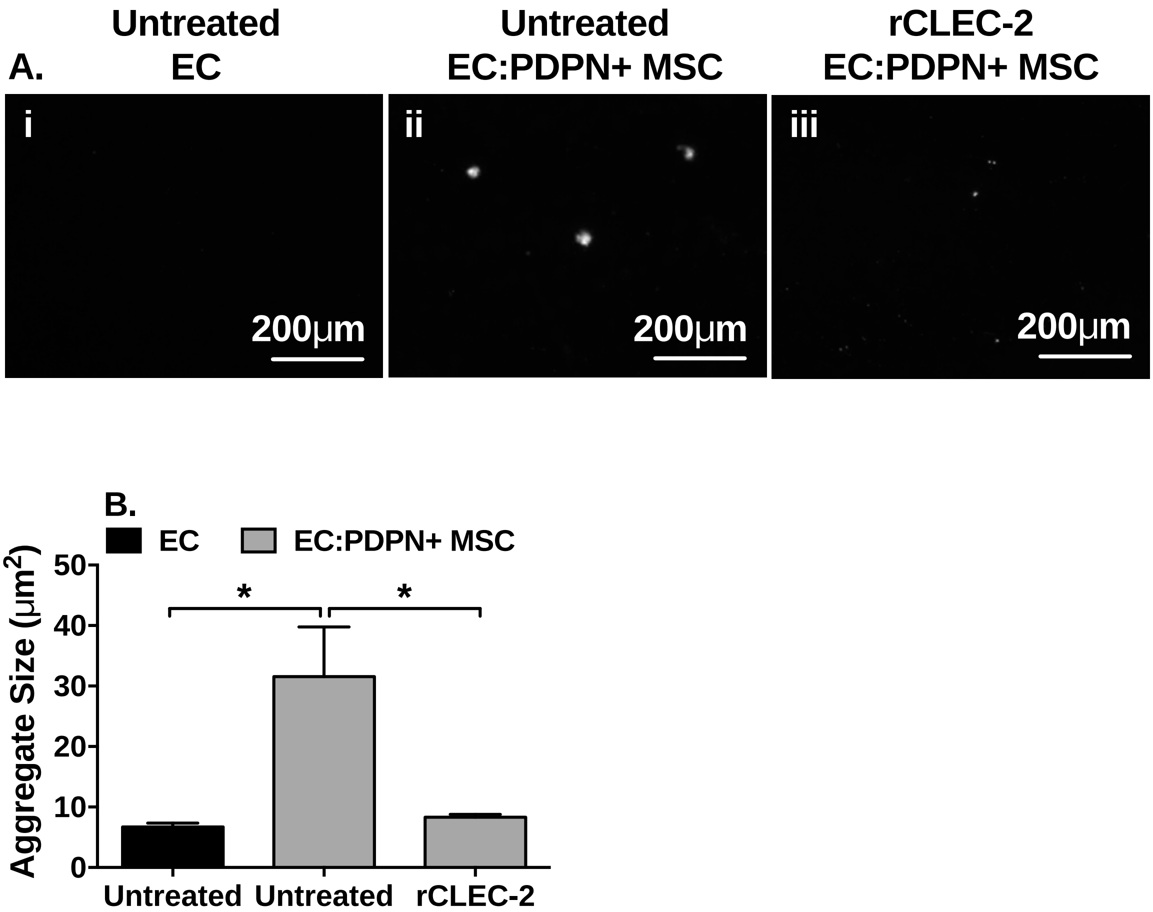

Figure 5-20 Effect of endothelial coculture on the ability of PDPN-positive UCMSC protrusions to induce platelet aggregation.

PDPN-positive UCMSC were seeded on inverted 3µm pore culture inserts for 1 hour. The inserts were reinverted and the apical surface seeded with BEC to form coculture (EC:MSC). BEC mono-cultures were used as a control (EC). CD41-labelled whole blood was perfused over the apical surface of the filter in a parallel plate chamber for 10 minutes, with or without rCLEC-2 pre-treatment. **(A)** Representative images were taken of fluorescent platelet aggregates; (i), EC; (ii), PDPN-positive MSC:EC; (iii), PDPN-positive MSC:EC with rCLEC-2 pre-treatment. Scale bar represents 200µm **(B)** Data are expressed as aggregate size in μm^2 as measured by the average size of fluorescent particles. ANOVA showed a significant effect of treatment on aggregate size; $p<0.05$. Data are mean ± SEM from n=4 independent experiments using four different donors for each cell type. * = $p<0.05$ by Bonferroni post-test.

5.3. Discussion

Here we aimed to understand the role of PDPN in MSC function, specifically looking at their migratory capacity and their ability to interact with circulating platelets given their perivascular location. Expression of PDPN by UCMSC promoted their ability to completely traverse a transwell filter and to migrate out of a spheroid and into a collagen gel when compared to UCMSC negative for PDPN. Knockdown of PDPN or inhibition of Rac1 significantly retarded UCMSC migration. We determined that both Rho and ROCK also played a role in UCMSC migration, but that this occurred independently of PDPN expression. From their perivascular location, PDPN-positive UCMSC were able to protrude through endothelial cells to interact with platelets, inducing platelet activation and aggregation. These processes could be reversed when we blocked either platelet-PDPN interactions, or platelet-platelet interactions with rCLEC-2 or integrilin respectively. We propose that this invasive phenotype facilitates the intravasation of stromal cells expressing PDPN, enabling interactions with circulating platelet CLEC-2 and presenting implications for the maintenance of vascular integrity, thromboembolism in inflammatory disorders, and cancer metastasis.

5.3.1. PDPN and cellular migration

Previous studies have also shown that PDPN is associated with a pro-migratory and invasive phenotype (Wicki et al. 2006; Martín-Villar et al. 2006; Takeuchi et al. 2017). Indeed, the ability to mediate cell contraction is integral for migration. Astarita *et al.*, (2015) demonstrated that PDPN regulates both cell size (by confocal microscopy) and contraction of fibroblastic reticular cells (by their ability to retract collagen matrices when suspended within) when compared to PDPN-negative counterparts, additionally, treatment with rCLEC-2 was shown to relax the contracted state of these cells (Astarita et al. 2015). We also observed an increase in cell size for the PDPN-positive compared to PDPN-negative UCMSC. Furthermore, transfection of a PDPN construct into an MCF7 breast cancer line conferred increased migratory and invasive potential compared to untransfected controls both *in vitro* and *in vivo*, with localisation of PDPN at cellular protrusions (Wicki et al. 2006; Petrie et al. 2012). This agrees with our data whereby we also observed PDPN localisation at peripheral protrusions of UCMSC. Indeed, cell migration studies in lymphatic endothelium and cancer cell lines have shown varied downstream signalling components for PDPN from ERM proteins to regulators of the actin cytoskeleton; Rho, ROCK, Cdc42, and Rac1 (Martín-Villar et al. 2006; Wicki et al. 2006; Navarro et al. 2011; Sahai & Marshall 2002). However, there are many discrepancies associated with the mechanism of action for PDPN in migration as discussed below.

Regarding signalling components involved in cell migration, Rho/ROCK signalling is used in amoeboid-like migration of tumour cells and leukocytes (Lämmermann & Sixt 2009; Sahai & Marshall 2003). Indeed, Martín-Villar *et al*., (2006) observed an increase in RhoA in MDCK tumour cells but no change for Cdc42 or Rac1 (Martín-Villar et al. 2006), suggesting that PDPN-mediated migration is promoted through RhoA signalling in MDCK cells. Interestingly, siRNA knockdown of PDPN in lymphatic endothelium reduced GTP-bound RhoA and migratory capacity (Navarro et al. 2011). Hence, also implying that RhoA is required for PDPN-mediated migration of lymphatic endothelium, but employed in amoeboid-like migration. In BMMSC, inhibition of Rho (C2I-C3) or ROCK (Y27632) both promoted their migratory capacity, suggesting Rho/ROCK signalling acts as a negative regulator of BMMSC migration (Jaganathan et al. 2007). This agrees with MSC migrating using mesenchymal-like processes. Conversely, we observed that inhibition of Rho resulted in a reduction of UCMSC migration, regardless of PDPN status, suggesting Rho may act as a global positive regulator of UCMSC migration.

Expression of PDPN by fibroblastic cell lines has been shown to increase their migratory properties in a ROCK-dependent manner when compared to PDPN-negative counterparts or in the presence of the ROCK inhibitor (Y27632) using a transwell assay (Suchanski et al. 2017). Conversely, in primary fibroblasts ROCK inhibition saw increased migration (Piltti et al. 2015), but again impaired migration in carcinoma cell lines (Z.-M. Wang et al. 2016). ROCK signalling has also been shown to promote BMMSC migration in response to CXCL12, but impair BMMSC transmigration through endothelium (Park et al. 2017; Lin et al. 2013). However, HIF-1α was also shown to promote BMMSC migration through both ROCK and Rac signalling (Choi et al. 2016). Again, we observed conflicting results with ROCK inhibition resulting in enhanced UCMSC migration, regardless of PDPN status, suggesting ROCK may act as a global negative regulator of UCMSC migration.

Interestingly, CLEC-2 activation via PDPN also promoted the migration of dendritic cells from the periphery to the lymph nodes through actin polymerisation and induction of membrane protrusions by Rac1 (Acton et al. 2012). Indeed, Rac1 has been shown to drive mesenchymal-like migration by stabilising lamellipodia formation at the leading edge (Ridley et al. 1992; Sanz-Moreno et al. 2008), with PDPN closely associated with these protrusions (Wicki et al. 2006; Petrie et al. 2012; Martin-Villar et al. 2015). Indeed, IL-17A stimulation induces migration of RASF in a Rac1-dependent manner (Moran et al. 2011). PI3K has been shown to signal through Rac1 (Henderson et al. 2015), with BMMSC transmigration through endothelium promoted in a PI3K-dependent manner. This disagrees with our data showing PDPN signals through Rac1, as we found BMMSC to be negative for PDPN expression. Indeed, Rac1 promoted CXCL12-induced UCMSC migration (Park et al. 2017), which agrees with our data showing that Rac1 inhibition selectively impairs PDPN-positive but not PDPN-negative UCMSC migration. This suggests that PDPN-mediated migration is Rac1 dependent and that Rac1 acts as a positive regulator of PDPN-mediated migration in UCMSC. These studies demonstrate that PDPN is strongly associated with a pro-migratory phenotype in stromal cells, but that the downstream signalling varies between cell types. Indeed, the differences observed in the signalling for MSC migration might be attributed to the tissue-specific sources of MSC, implying that differential migration-related signalling occurs as a result of their previous microenvironment.

Therapeutic administration of PDPN-positive MSC by intravenous injection has serious implications in their thrombotic potential (see below). However, the pro-migratory phenotype associated with PDPN expression is desirable for improving the efficiency of MSC homing to sites of tissue damage or inflammation. The data here highlights targeting ROCK inhibition in PDPN-negative MSC as a plausible method of increasing the migratory capacity of these cells. Indeed, inhibition of Rac1 is also a potential therapeutic target in preventing PDPN-positive tumour cell invasion and metastasis. The therapeutic potential of several Rac1 inhibitors is a topic of current scientific interest in the treatment of cancer, cardiovascular, and neurodegenerative diseases [reviewed by (Marei & Malliri 2017)].

5.3.2. PDPN AND THROMBOINFLAMMATION

Here we aimed to understand the mechanisms by which perivascular stromal cells present PDPN to circulating platelets and the effect of this interaction on platelet activation. Indeed, umbilical cord cross-sections revealed PDPN expression to be localised to the perivascular region, thus we hypothesised that these PDPN-positive pro-migratory MSC were capable of engaging platelet CLEC-2 by invading into the blood vessel lumen.

In normal human tissue, PDPN was expressed in discrete layers at the interface between dense regular and dense irregular connective tissue within the skin, cervix, esophagus, prostate, breast glands, salivary glands, and thymus (Schacht et al. 2005). Lymphoid tissue showed dispersed staining of PDPN by fibroblastic reticular cells, whilst PDPN was restricted to alveolar type I cells within the lung (Schacht et al. 2005). The physiological role of PDPN is still largely unknown. However, a common theme of PDPN deletion in mice was the leakage of blood into the lymphatics (Schacht et al. 2003; Bianchi et al. 2017; Fu et al. 2008). This might suggest an issue in the maintenance of vascular integrity. Indeed, Herzog et al., (2013) suggested that under basal conditions vascular integrity is continuously disrupted at high endothelial venules by circulating lymphocytes (Herzog et al. 2013). It was only through perivascular PDPN-mediated activation of platelets and their release of S1P that barrier function was restored through upregulation of VE-cadherin by endothelium (Herzog et al. 2013). However, it is unknown how platelets support vascular integrity during inflammation (Goerge et al. 2008). Platelet release of S1P has also been shown to promote the proliferation and survival of liver sinusoidal endothelium, as well as induce the secretion of VEGF and IL-6 (Nowatari et al. 2015). Such responses could enhance angiogenesis (Leung et al. 1989), but also have the potential to impede leukocyte recruitment through IL-6 induced expression of SOCS3 (Luu et al. 2013). Indeed, the release of S1P by endothelium has also been shown to impair memory T-cell transmigration through the inactivation of β2-integrin via S1P receptors 1/4 (Chimen et al. 2015). These studies would suggest a protective role for PDPN interactions with platelet CLEC-2 on vascular integrity. However, other protective functions may also be in place, as was the case in a mouse model of inflammatory arthritis whereby deletion of CLEC-2 resulted in increased inflammation and tissue damage through an undefined mechanism (Desanti et al. 2017).

With regard to pathology, expression of PDPN was strongly associated with metastasis in bladder tumours and oral ‘squamous cell carcinoma’ (SCC) (Yuan et al. 2006; Takagi et al. 2014). PDPN also correlates with a poor prognosis and aggressive tumours in liver, breast, lung and pancreatic cancers (Kawase et al. 2008; Hoshino et al. 2011; Pula et al. 2011; Yurugi et al. 2017). PDPN was also upregulated in skin and ovarian cancer, with staining limited to the dense regular but not dense irregular connective tissue (Schacht et al. 2005). This may explain the laminar appearance of PDPN in the inflamed perivascular space (Payne et al. 2017; Hitchcock et al. 2015; Inoue et al. 2015), with expression on stromal cells forming dense regular connective tissue. We also found expression of PDPN to be restricted to the dense regular areas of the umbilical cord surrounding the vasculature and along the amnion. However, its function in these areas is unclear. As discussed earlier, Astarita *et al*., (2015) showed PDPN to be an important contractile element of fibroblastic reticular cells, contact with its receptor CLEC-2 on dendritic cells inhibited this contraction and resulted in the overall expansion of the lymph node during an inflammatory response (Astarita et al. 2015). Another study also demonstrated PDPN to be expressed on different populations within the chronically infarcted myocardium, with their function divided into lymphangiogenesis or fibrosis and scar formation (Cimini et al. 2017). Expression of PDPN may correlate with a pro-fibrotic phenotype of stromal cells in certain contexts, this may have implications in vascular fibrosis during inflammation, given its perivascular expression profile.

A review by Wicki and Christofori has shown PDPN expression to be upregulated in the tumour mass periphery, where they indicated it was important for the collective invading edge of the tumour (Wicki & Christofori 2007). Indeed, intravasation of cells from the tissue stroma and into blood vessels is well described within the cancer field [reviewed by (Chiang et al. 2016)]. However, it remains unclear as to the mechanism by which circulating platelet CLEC-2 comes into contact with PDPN, due to the endothelial lining separating these two compartments (Suzuki-Inoue 2017). Here we have shown that perivascular UCMSC protrusions are able to partially intravasate through the endothelial lining and both recruit and activate platelets in a PDPN-dependent manner. The ability for PDPN to capture platelets has been previously described, with recombinant PDPN or PDPN-expressing lymphatic endothelium able to readily capture platelets from flow; Src/Syk platelet signalling was required for stable binding of CLEC-2 (Navarro-Nunez et al. 2015). These data suggest that in pathology, cells are capable of penetrating the endothelial lining and interacting with platelet CLEC-2 through PDPN.

In addition to the role of PDPN-CLEC-2 interactions in maintaining vascular integrity, a recent study has also demonstrated that PDPN activation of platelets by tumour cells induces the release of platelet TGF-β, which subsequently enhanced epithelial-mesenchymal transition (EMT) of tumour cells promoting metastasis (Takemoto et al. 2017). Martín-Villar *et al*., (2006) also reported that EMT was induced by PDPN, but through direct interactions with ERM proteins and activation of RhoA (Martín-Villar et al. 2006). Indeed, treatment of a PDPN expressing bladder SCC cell line with supernatants from PDPN-activated platelets significantly enhanced their invasiveness through a matrigel-overlaid transwell model (Takemoto et al. 2017). Suggesting that PDPN-CLEC-2 interactions may assist in driving stromal intravasation in a positive-feedback loop. Furthermore, metastasis could be blocked in mouse tumour models by therapeutic administration of a TGF-β neutralising antibody, implicating PDPN as a critical mediator of this process (Takemoto et al. 2017). However, the mechanism by which these PDPN-expressing cells breach the endothelial lining has not shown until this study. We have demonstrated for the first time that PDPN-positive UCMSC can breach the endothelial lining and activate platelet CLEC-2. However, the role of TGF-β in promoting the intravasation of non-tumourigenic cells, such as UCMSC, requires further investigation.

Excessive PDPN-mediated platelet activation may also lead to the pro-thrombotic phenotype seen in a number of inflammatory disorders [reviewed by (Aksu et al. 2012)]. Gestational vascular diseases, such as pre-eclampsia, are also closely associated with inflammation and thrombosis, posing a major cause of morbidity and mortality to the pregnancy (Kohli & Isermann 2017). Thromboembolism describes the process by which a thrombus breaks off and obstructs another vessel, resulting in local ischemia and potential fatalities. Indeed, patients with PDPN-positive brain tumours were shown to have significantly reduced platelet counts and increased risk of thromboembolism (Riedl et al. 2017). Indicating a role for PDPN-CLEC-2 interactions in thromboinflammation. Furthermore, scanning electron micrographs of the inferior vena cava in TNF-α-stimulated mice saw the formation of microthrombi at sites of increased leukocyte transmigration (Eriksson et al. 2005). Indeed, real-time observations in mouse models of deep vein thrombosis (DVT) link inflammation and leukocyte recruitment as an initiator of thrombosis (Brühl et al. 2012). This would agree with similar data whereby neutrophil transmigration over stiff substrates was shown to induce mechanical damage to the endothelial monolayer (Stroka & Aranda-Espinoza 2011). Indeed, perivascular PDPN-mediated contraction and fibrosis could promote vessel stiffness (Astarita et al. 2015; Cimini et al. 2017), thereby resulting in damage to endothelium during neutrophil recruitment. Indeed, vascular integrity was shown to be disrupted in a mouse model of systemic *Salmonella* Typhimurium infection, resulting in thrombosis at these sites through PDPN interactions (Hitchcock et al. 2015). Furthermore, it is unknown how vascular integrity is maintained during inflammation (Goerge et al. 2008), but it may the case that PDPN activation of CLEC-2 restores integrity through release of S1P as reported by Herzog *et al*., (2013) (Herzog et al. 2013). Indeed, the release of other pro-migratory stimuli by PDPN-activated platelets, namely FGF and TGF-β may assist stromal intravasation in a positive-feedback loop (Langer et al. 2009; Takemoto et al. 2017).

Overall, we propose that the following could occur during an inflammatory response: PDPN is upregulated on the underlying stroma, increasing vessel stiffness and impairing endothelial maintenance of integrity in response to neutrophil transmigration. This may or may not assist perivascular stroma protrusion into the vessel lumen. However, the presence of luminal PDPN could further enhance stromal intravasation through the release of FGF and TGF-β by PDPN-activated platelets in a positive-feedback loop. Ultimately, PDPN-activated platelet release of S1P could protect vascular integrity, as well as moderate the levels of leukocyte recruitment and migration as part of an endogenous stromal-platelet mediated regulatory pathway. However, further work is required to validate this concept and evaluate the role of this proposed pathway in chronic inflammatory diseases or cancer.

In conclusion, we have shown that expression of PDPN contributes a pro-migratory phenotype to MSC through Rac1 signalling, and that this function enables the presentation of PDPN through the endothelial lining to circulating platelets, inducing their activation via CLEC-2. We suggest that these invasive PDPN-expressing perivascular stromal cells are upregulated in pathology and may contribute to vascular integrity, immunosuppressive, metastatic, or thromboinflammatory processes.

Chapter 6. GENERAL DISCUSSION

6.1. Summary of the main findings

BMMSC responses to prolonged TNF-α priming were evaluated using an *in vitro* model of neutrophil recruitment and their transcriptional profile recorded for several inflammation-associated genes. Of which, the expression and function of PDPN was characterised using several models of cell migration. The downstream signalling pathways for PDPN-mediated migration were assessed with inhibitors against several members of the Rho GTPase family. Finally, the mechanism by which perivascular PDPN interacts with circulating platelet CLEC-2 was elucidated. The main findings of this thesis are:

- Prolonged priming of BMMSC with TNF-α had no effect on their ability to communicate with endothelium to suppress neutrophil adhesion.
- TNF-α priming also increased ICAM-1 gene expression and impaired the increased neutrophil transmigration observed by BMMSC coculture.
- PDPN expression increases UCMSC migration in a Rac1 dependent manner.
- PDPN-expressing cells are localised to the perivascular niche of the umbilical cord, and UCMSC protrusions are capable of platelet capture and activation through endothelium via PDPN.

6.2. Context of findings within the literature

6.2.1. *Effect of the inflammatory microenvironment on MSC*

We have previously shown that coculture of BMMSC with HUVEC suppresses neutrophil recruitment, but that this effect is varied with coculture contact, passage, and adipogenic differentiation according to the tissue microenvironment from which the MSC were isolated (Munir et al. 2016; Munir et al. 2017). Here, we found that using TNF-α priming as a model for the inflammatory microenvironment had no impact on the capacity of BMMSC to suppress neutrophil adhesion to BEC. Instead, BMMSC coculture increased neutrophil transmigration, with TNF-α priming reverting this response to levels seen in endothelial monocultures. This disagrees with previous reports showing that BMMSC-HUVEC coculture either suppresses (Luu et al. 2013), or has no effect on neutrophil transmigration (Munir et al. 2016). We speculate that the differences in neutrophil transmigration observed in the presence of BMMSC coculture are because of the different endothelial cell sources used. Indeed, MSC are capable of secreting neutrophil chemoattractants such as IL-8, CXCL1, and CXCL2 (Luu et al. 2013; Ren et al. 2008; Guijarro-Muñoz et al. 2014). However, the impact of endothelial coculture on these secretions are unknown. Perhaps these differences are to ensure preferential neutrophil transmigration across post-capillary venules over macrovascular veins. Interestingly, prior TNF exposure abolished the increase in neutrophil transmigration observed with BMMSC coculture. We suggest that this is a protective response to reduce neutrophil penetration into tissues already exposed to inflammation, though this warrants further functional comparisons with pro-inflammatory stromal cells such as RASF.

Overall, BMMSC do not appear to undergo a functional transformation with regard to their immunomodulatory capacity when exposed to exogenous TNF-α stimulation. Indeed, it would appear that BMMSC are initially able to dampen the pro-inflammatory microenvironment. As shown by BMMSC suppressing neutrophil recruitment in BEC coculture post-priming, and reducing inflammation-associated ICAM-1 gene expression in RASF coculture. Luu *et al*., demonstrated that BMMSC suppression of neutrophil transmigration through HUVEC was dependent on TGF-β (Luu et al. 2013). Future experiments should investigate whether TGF-β is increased in TNF-α primed compared to untreated BMMSC-BEC coculture, and hence explaining why we see a reduction in neutrophil transmigration in the primed coculture. Indeed, TGF-β appears to be differentially regulated in response to priming with TNF-α with one study seeing reduced secretion (English et al. 2007), and the other seeing increased gene expression compared to untreated MSC (Wu et al. 2015). However, the long-term repercussions of inflammation on MSC function cannot be modelled *in vitro*, with future work instead focussing on *ex vivo* functional comparisons between MSC isolated from a variety of chronic inflammatory conditions and healthy controls. Indeed, short-term exposure of MSC to inflammatory cytokines *in vitro* has been shown to have differential effects on MSC secretion of immunomodulatory factors and in their ability to suppress leukocyte proliferation and function (Prasanna et al. 2010; English et al. 2007; Waterman et al. 2010; Liotta et al. 2008; Raicevic et al. 2011). However, a greater proportion of studies overall report that MSC function is enhanced through cytokine priming. Few groups have investigated the effect of prolonged cytokine priming, and only a small number have characterised MSC from chronically inflamed sites, systemically they appear altered and there are conflicting reports on how this impacts their function (Table 1-3). More work is required in general, but in our assays with a relatively short priming we see little difference. Ideally, MSC should be isolated from chronic tissues to determine whether they exhibit the same epigenetic imprinting as their progeny and incorporated into these adhesion assays to investigate how the inflammatory microenvironment impacts MSC crosstalk with endothelium.

6.2.2. Role of PDPN expression in MSC

Here we have shown that UCMSC differentially express PDPN. PDPN is typically associated with sites of inflammation and cancer-supporting stroma, whereby it increases the metastatic capacity of these cells. In agreement with this, we show for the first time that PDPN signalling through Rac1 is responsible for MSC migration using several *in vitro* models. This is also of importance for the regenerative medicine field and understanding the relocalisation of MSC to sites of tissue damage where they exert their reparative function. PDPN also mediates the invasiveness of oral SCC cells through RhoA and Cdc42 activity, however, neither PDPN overexpression or knockdown had any impact on Rac1 activity (Y.-Y. Li et al. 2015). Yet, overexpression of PDPN in MCF7 cells resulted in reduced Rac1, RhoA, and Cdc42 (Wicki et al. 2006), but no change in Rac1 nor Cdc42 activity in MDCK cells (Martín-Villar et al. 2006). Even though ERM proteins (upstream of Rho GTPases) colocalise with PDPN at cell-surface protrusions (Martín-Villar et al. 2006). However, another study attributed activated Rac1 expression with increased metastatic potential in colorectal carcinoma (Zhong et al. 2009). The literature regarding PDPN downstream signalling is lacking, but overall these data suggest that the mechanism of PDPN-mediated migration and invasion greatly differ depending on the cell type. Further investigation is required in this area to better understand how PDPN regulates the migration of stromal cells both in health and disease.

Payne *et al*., (2017) recently identified that PDPN regulates the size but not the prevalence of thrombi in a sterile-inflammation deep vein thrombosis mouse model through interactions with platelet CLEC-2 (Payne et al. 2017). Indeed, confocal microscopy of thrombi in the inferior vena cava, showed extensive perivascular PDPN staining but the cells expressing it and the mechanism of contact were unknown (Payne et al. 2017). In a non-sterile mouse model of inflammation, Hitchcock *et al*., (2015) also saw perivascular PDPN expression driving thrombosis at sites of endothelial disruption, but this was attributed to inflammatory macrophages (Hitchcock et al. 2015). Here we investigated the upstream signalling of MSC PDPN and the mechanism by which it comes into contact with its receptor, CLEC-2 on circulating platelets. PDPN-expressing MSC were capable of capturing and activating platelets through 3μm pores, but not migrating through them. Since expression of PDPN is concentrated at cellular protrusions (Martin-Villar et al. 2010; Wicki et al. 2006), we speculated that these were infiltrating the pores and presenting PDPN to platelets. Indeed, immunohistochemistry staining of umbilical cord sections revealed PDPN to be localised to the perivascular niche and the fibrous areas of the amnion. With this in mind, we setup UCMSC cocultures with microvascular endothelium, and demonstrated that the size of platelet aggregates was determined by MSC expression of PDPN through the endothelial lining, albeit with reduced prevalence compared to UCMSC monocultures. These data pose particular importance to the field of thromboinflammation. Indeed, PDPN is found to be upregulated in a number of inflammatory disorders, including; RA, DVT, atherosclerosis, systemic infection, and cancer (Kawase et al. 2008; Shields et al. 2010; Inoue et al. 2015; Payne et al. 2017; Hitchcock et al. 2015; Del Rey et al. 2014; Croft et al. 2016; Ekwall et al. 2011; Hatakeyama et al. 2012). Whilst in brain cancer patients, platelet counts are reduced in associated with tumour expression of PDPN, these patients are also predisposed to thromboembolism (Riedl et al. 2017). The interaction between perivascular PDPN and CLEC-2 on circulating platelets has far reaching roles in understanding the mechanisms by which thrombosis, pulmonary embolism, and stroke occurs in inflammatory disorders [reviewed by (Aksu et al. 2012)]. Conversely, upregulation of PDPN in the perivascular space, and activation of platelets may also serve to protect vascular integrity during inflammation (Herzog et al. 2013).

Furthermore, this line of enquiry would also benefit from experiments addressing the role of Rac1 in PDPN-mediated MSC migration. Indeed, in the presence of the Rac1 inhibitor we observed a reduction in the number of UCMSC expressing PDPN at the cell periphery, suggesting that Rac1 may be involved in localising PDPN to the cell edge whereby it can exert its migratory function. It would also be prudent to acquire samples from mouse models of inflammation or patients with chronic inflammatory disorders to determine whether PDPN has a perivascular expression profile in these samples also and if this is associated with vessel fibrosis and or the presence of thrombi (Astarita et al. 2015; Cimini et al. 2017; Hitchcock et al. 2015; Payne et al. 2017). The work undertaken by Takemoto *et al*., (2017) should be verified here to determine whether PDPN-activation of platelet CLEC-2 induces the release of MSC invasion factors such as TGF-β and FGF and further enhances the intravasation of MSC into the vessel lumen (Langer et al. 2009; Takemoto et al. 2017). Lastly, the effect of S1P derived from PDPN-activated platelets should be investigated in its ability to enhance the integrity of inflamed endothelium and potentially suppress the transmigration of memory T-cell subsets (Herzog et al. 2013; Chimen et al. 2015).

6.3. Conclusion

In conclusion, we have shown that priming with TNF-α had no effect on the ability of BMMSC to communicate with microvascular endothelium and suppress neutrophil adhesion. BMMSC resisted functional transformation during TNF-α exposure, maintaining their immunomodulatory capacity and profile. Therefore, we support their use in MSC-based therapy in that they can retain their suppressive function over endothelium in the context of the inflammatory microenvironment and not further contribute toward disease pathogenesis through transformation as seen in endogenous stroma.

PDPN expression is known to be upregulated by the inflammatory microenvironment and was found to be differentially expressed by UCMSC. Expression of PDPN promoted MSC migration through Rac1-dependent signalling, enabling these perivascular MSC to potentially interact with CLEC-2-positive myeloid and dendritic cells (Lowe et al. 2015). Here we demonstrated that PDPN induced the activation of platelets from flow through UCMSC protrusions in the microvascular endothelial lining. These results implicate both detrimental roles for PDPN-CLEC-2 interactions in thromboinflammation or beneficial outcomes in the maintenance of vascular integrity and potential suppression of T-cell transmigration at inflammatory sites.

6.4. Future studies

The data presented within this thesis give rise to new questions and further studies to be performed. Possible suggestions of these experiments are listed below:

1. Investigate the mechanism by which TNF-α primed BMMSC-BEC coculture inhibits neutrophil transmigration compared to untreated. Attention should be drawn to the concentration of TGF-β in conditioned medium.
2. Identify differences in leukocyte recruitment to endothelium when cocultured with MSC isolated from patients with systemic chronic inflammation or those isolated from the site of inflamed tissue itself.
3. Characterise the effect of prolonged BMMSC coculture with RASF, and the impact on their ability to modulate leukocyte recruitment to endothelium.
4. Investigate the role of Rac1 in PDPN-mediated migration of MSC. Attention should be drawn to whether Rac1 localises PDPN to cellular protrusions.
5. Stain samples of inflamed vessels from mouse models or patient samples for perivascular PDPN, fibrosis, and thrombi, to determine the conditions under which PDPN is expressed and the effect on vessel stiffness. Attention should be drawn to samples from inflammatory disorders predisposed to thrombosis.
6. Determine whether platelet lysates enhance PDPN-positive UCMSC protrusion through the endothelial lining, and the subsequent impact on platelet recruitment and activation.
7. Investigate whether supernatant from PDPN-activated platelets contains S1P and if it enhances the integrity of inflamed endothelium or impairs T-cell transmigration.

Chapter 7. List of References

Abdel Aziz, M.T. et al., 2007. Therapeutic potential of bone marrow-derived mesenchymal stem cells on experimental liver fibrosis. *Clinical biochemistry*, 40(12), pp.893–899.

Acton, S.E. et al., 2012. Podoplanin-rich stromal networks induce dendritic cell motility via activation of the C-type lectin receptor CLEC-2. *Immunity*, 37(2), pp.276–289.

Aksu, K., Donmez, A. & Keser, G., 2012. Inflammation-induced thrombosis: mechanisms, disease associations and management. *Current pharmaceutical design*, 18(11), pp.1478–1493.

Alblazi, K.M.O. & Siar, C.H., 2015. Cellular protrusions--lamellipodia, filopodia, invadopodia and podosomes--and their roles in progression of orofacial tumours: current understanding. *Asian Pacific journal of cancer prevention : APJCP*, 16(6), pp.2187–2191.

Amano, M. et al., 1997. Formation of actin stress fibers and focal adhesions enhanced by Rho-kinase. *Science*, 275(5304), pp.1308–1311.

Arend, W.P. et al., 2013. Roles of adipocytes and fibroblasts in activation of the alternative pathway of complement in inflammatory arthritis in mice. *Journal of immunology (Baltimore, Md. : 1950)*, 190(12), pp.6423–6433.

Arnett, F.C. et al., 1988. The American Rheumatism Association 1987 revised criteria for the classification of rheumatoid arthritis. *Arthritis & Rheumatism*, 31(3), pp.315–324.

Astarita, J.L. et al., 2015. The CLEC-2-podoplanin axis controls the contractility of fibroblastic reticular cells and lymph node microarchitecture. *Nature Publishing Group*, 16(1), pp.75–84.

Astarita, J.L., Acton, S.E. & Turley, S.J., 2012. Podoplanin: emerging functions in development, the immune system, and cancer. *Frontiers in immunology*, 3, p.283.

Barhanpurkar-Naik, A. et al., 2017. Interleukin-3 enhances the migration of human mesenchymal stem cells by regulating expression of CXCR4. *Stem cell research & therapy*, 8(1), p.168.

Bartaula-Brevik, S. et al., 2014. Leukocyte transmigration into tissue-engineered constructs is influenced by endothelial cells through Toll-like receptor signaling. *Stem cell research & therapy*, 5(6), p.143.

Bernardo, M.E. & Fibbe, W.E., 2013. Mesenchymal Stromal Cells: Sensors and Switchers of Inflammation. *Stem Cell*, 13(4), pp.392–402.

Bianchi, R. et al., 2017. Postnatal Deletion of Podoplanin in Lymphatic Endothelium Results in Blood Filling of the Lymphatic System and Impairs Dendritic Cell Migration to Lymph Nodes. *Arteriosclerosis, thrombosis, and vascular biology*, 37(1), pp.108–117.

Boulaftali, Y. et al., 2013. Platelet ITAM signaling is critical for vascular integrity in inflammation. *Journal of Clinical Investigation*, 123(2), pp.908–916.

Brandau, S. et al., 2010. Tissue-resident mesenchymal stem cells attract peripheral blood neutrophils and enhance their inflammatory activity in response to microbial challenge. *Journal of leukocyte biology*, 88(5), pp.1005–1015.

Breiteneder-Geleff, S. et al., 1997. Podoplanin, novel 43-kd membrane protein of glomerular epithelial cells, is down-regulated in puromycin nephrosis. *The American journal of pathology*, 151(4), pp.1141–1152.

Brokopp, C.E. et al., 2011. Fibroblast activation protein is induced by inflammation and degrades type I collagen in thin-cap fibroatheromata. *European Heart Journal*, 32(21), pp.2713–2722.

Brühl, von, M.-L. et al., 2012. Monocytes, neutrophils, and platelets cooperate to initiate and propagate venous thrombosis in mice in vivo. *The Journal of experimental medicine*, 209(4), pp.819–835.

Buckley, C.D. et al., 2015. Stromal cells in chronic inflammation and tertiary lymphoid organ formation. *Annual review of immunology*, 33(1), pp.715–745.

Burns, M.P. & DePaola, N., 2005. Flow-conditioned HUVECs support clustered leukocyte adhesion by coexpressing ICAM-1 and E-selectin. *American journal of physiology. Heart and circulatory physiology*, 288(1), pp.H194–204.

Butler, L.M. et al., 2005. Prolonged culture of endothelial cells and deposition of basement membrane modify the recruitment of neutrophils. *Experimental cell research*, 310(1), pp.22–32.

Cassatella, M.A. et al., 2011. Toll-like receptor-3-activated human mesenchymal stromal cells significantly prolong the survival and function of neutrophils. *Stem Cells*, 29(6), pp.1001–1011.

Chang, A.I. et al., 2015. Involvement of mesenchymal stem cells in cancer progression and metastases. *Current cancer drug targets*, 15(2), pp.88–98.

Chauhan, A. et al., 2016. Platelets: No longer bystanders in liver disease. *Hepatology (Baltimore, Md.)*, 64(5), pp.1774–1784.

Chen, L. et al., 2008. Paracrine Factors of Mesenchymal Stem Cells Recruit Macrophages and Endothelial Lineage Cells and Enhance Wound Healing P. Bozza, ed. *PLoS ONE*, 3(4), pp.e1886–12.

Chiang, S.P.H., Cabrera, R.M. & Segall, J.E., 2016. Tumor cell intravasation. *American journal of physiology. Cell physiology*, 311(1), pp.C1–C14.

Chimen, M. et al., 2015. Homeostatic regulation of T cell trafficking by a B cell–derived peptide is impaired in autoimmune and chronic inflammatory disease. *Nature Medicine*, 21(5), pp.467–475.

Choi, J.H. et al., 2016. Hypoxia Inducible Factor-1α Regulates the Migration of Bone Marrow Mesenchymal Stem Cells via Integrin α 4. *Stem cells international*, 2016(1), pp.7932185–11.

Chung, K.-M. et al., 2014. Fibroblast activation protein (FAP) is essential for the migration of bone marrow mesenchymal stem cells through RhoA activation. *PLoS ONE*, 9(2), pp.e88772–11.

Cimini, M. et al., 2017. Phenotypically heterogeneous podoplanin-expressing cell populations are associated with the lymphatic vessel growth and fibrogenic responses in the acutely and chronically infarcted myocardium. D. K. Singla, ed. *PLoS ONE*, 12(3), p.e0173927.

Ciria, M. et al., 2017. Mesenchymal Stem Cell Migration and Proliferation Are Mediated by Hypoxia-Inducible Factor-1α Upstream of Notch and SUMO Pathways. *Stem cells and development*, 26(13), pp.973–985.

Colom, B. et al., 2015. Leukotriene B4-Neutrophil Elastase Axis Drives Neutrophil Reverse Transendothelial Cell Migration In Vivo. *Immunity*, 42(6), pp.1075–1086.

Crisan, M. et al., 2008. A perivascular origin for mesenchymal stem cells in multiple human organs. *Cell Stem Cell*, 3(3), pp.301–313.

Croft, A.P. et al., 2016. Rheumatoid synovial fibroblasts differentiate into distinct subsets in the presence of cytokines and cartilage. *Arthritis research & therapy*, 18(1), p.270.

Crowley, T. et al., 2017. Priming in response to pro-inflammatory cytokines is a feature of adult synovial but not dermal fibroblasts. *Arthritis research & therapy*, 19(1), p.35.

Del Rey, M.J. et al., 2014. Clinicopathological correlations of podoplanin (gp38) expression in rheumatoid synovium and its potential contribution to fibroblast platelet crosstalk. K. Freson, ed. *PLoS ONE*, 9(6), p.e99607.

Desanti, G.E. et al., 2017. 06.16 Platelet-derived clec-2 and its ligand podoplanin (gp38) inhibit synovial inflammation. In 37th European Workshop for Rheumatology Research 2–4 March 2017 Athens, Greece. BMJ Publishing Group Ltd and European League Against Rheumatism, pp. A66.2–A67.

Desilles, J.-P. et al., 2017. Exacerbation of Thromboinflammation by Hyperglycemia Precipitates Cerebral Infarct Growth and Hemorrhagic Transformation. *Stroke*, 48(7), pp.1932–1940.

Dominici, M. et al., 2006. Minimal criteria for defining multipotent mesenchymal stromal cells. The International Society for Cellular Therapy position statement. *Cytotherapy*, 8(4), pp.315–317.

Ed Rainger, G. et al., 2015. The role of platelets in the recruitment of leukocytes during vascular disease. *Platelets*, 26(6), pp.507–520.

Edwards, S. et al., 2005. Lymphocyte traffic through sinusoidal endothelial cells is regulated by hepatocytes. *Hepatology (Baltimore, Md.)*, 41(3), pp.451–459.

Ekwall, A.-K.H. et al., 2011. The tumour-associated glycoprotein podoplanin is expressed in fibroblast-like synoviocytes of the hyperplastic synovial lining layer in rheumatoid arthritis. *Arthritis research & therapy*, 13(2), p.R40.

El-Badri, N.S. et al., 2007. Autoimmune disease: is it a disorder of the microenvironment? *Immunologic Research*, 41(1), pp.79–86.

Engler, A.J. et al., 2006. Matrix elasticity directs stem cell lineage specification. *Cell*, 126(4), pp.677–689.

English, K. et al., 2007. IFN-γ and TNF-α differentially regulate immunomodulation by murine mesenchymal stem cells. *Immunology Letters*, 110(2), pp.91–100.

English, K., Barry, F.P. & Mahon, B.P., 2008. Murine mesenchymal stem cells suppress dendritic cell migration, maturation and antigen presentation. *Immunology Letters*, 115(1), pp.50–58.

Eriksson, E.E. et al., 2005. Powerful inflammatory properties of large vein endothelium in vivo. *Arteriosclerosis, thrombosis, and vascular biology*, 25(4), pp.723–728.

Farooqui, R. & Fenteany, G., 2005. Multiple rows of cells behind an epithelial wound edge extend cryptic lamellipodia to collectively drive cell-sheet movement. *Journal of cell science*, 118(Pt 1), pp.51–63.

Farr, A.G. et al., 1992. Characterization and cloning of a novel glycoprotein expressed by stromal cells in T-dependent areas of peripheral lymphoid tissues. *The Journal of experimental medicine*, 176(5), pp.1477–1482.

Feng, J., Mantesso, A. & De Bari, C., 2011. Dual origin of mesenchymal stem cells contributing to organ growth and repair. In Proceedings of the ….

Filer, A. et al., 2017. Identification of a transitional fibroblast function in very early rheumatoid arthritis. *Annals of the Rheumatic Diseases*, 76(12), pp.annrheumdis–2017–211286–2112.

Fischer, U.M. et al., 2009. Pulmonary passage is a major obstacle for intravenous stem cell delivery: the pulmonary first-pass effect. *Stem cells and development*, 18(5), pp.683–692.

Franco, A.T., Corken, A. & Ware, J., 2015. Platelets at the interface of thrombosis, inflammation, and cancer. *Blood*, 126(5), pp.582–588.

François, M. et al., 2012. Human MSC suppression correlates with cytokine induction of indoleamine 2,3-dioxygenase and bystander M2 macrophage differentiation. *Molecular Therapy*, 20(1), pp.187–195.

Friedl, P. & Wolf, K., 2010. Plasticity of cell migration: a multiscale tuning model. *The Journal of Cell Biology*, 188(1), pp.11–19.

Fu, J. et al., 2008. Endothelial cell O-glycan deficiency causes blood/lymphatic misconnections and consequent fatty liver disease in mice. *Journal of Clinical Investigation*, 118(11), pp.3725–3737.

Fullard, J.F., 2004. The role of the platelet glycoprotein IIb/IIIa in thrombosis and haemostasis. *Current pharmaceutical design*, 10(14), pp.1567–1576.

Garin-Shkolnik, T. et al., 2014. FABP4 attenuates PPARγ and adipogenesis and is inversely correlated with PPARγ in adipose tissues. *Diabetes*, 63(3), pp.900–911.

Goerge, T. et al., 2008. Inflammation induces hemorrhage in thrombocytopenia. *Blood*, 111(10), pp.4958–4964.

Goldsmith, H.L. & Spain, S., 1984. Margination of leukocytes in blood flow through small tubes. *Microvascular research*, 27(2), pp.204–222.

Goodpaster, B.H. & Wolf, D., 2004. Skeletal muscle lipid accumulation in obesity, insulin resistance, and type 2 diabetes. *Pediatric diabetes*, 5(4), pp.219–226.

Gotsch, U. et al., 1997. VE-cadherin antibody accelerates neutrophil recruitment in vivo. *Journal of cell science*, 110 (Pt 5), pp.583–588.

Grinnell, F., 2008. Fibroblast mechanics in three-dimensional collagen matrices. *Journal of bodywork and movement therapies*, 12(3), pp.191–193.

Guijarro-Muñoz, I. et al., 2014. Lipopolysaccharide activates Toll-like receptor 4 (TLR4)-mediated NF-κB signaling pathway and proinflammatory response in human pericytes. *The Journal of biological chemistry*, 289(4), pp.2457–2468.

Haddad, R. & Saldanha-Araujo, F., 2014. Mechanisms of T-cell immunosuppression by mesenchymal stromal cells: what do we know so far? *BioMed research international*, 2014(2), pp.216806–14.

Halfon, S. et al., 2011. Markers distinguishing mesenchymal stem cells from fibroblasts are downregulated with passaging. *Stem cells and development*, 20(1), pp.53–66.

Hatakeyama, K. et al., 2012. Podoplanin expression in advanced atherosclerotic lesions of human aortas. *Thrombosis research*, 129(4), pp.e70–6.

Henderson, V. et al., 2015. Snail promotes cell migration through PI3K/AKT-dependent Rac1 activation as well as PI3K/AKT-independent pathways during prostate cancer progression. *Cell adhesion & migration*, 9(4), pp.255–264.

Herzog, B.H. et al., 2013. Podoplanin maintains high endothelial venule integrity by interacting with platelet CLEC-2. *Nature*, 502(7469), pp.105–109.

Hitchcock, J.R. et al., 2015. Inflammation drives thrombosis after Salmonella infection via CLEC-2 on platelets. *Journal of Clinical Investigation*, 125(12), pp.4429–4446.

Ho-Tin-Noé, B., Demers, M. & Wagner, D.D., 2011. How platelets safeguard vascular integrity. *Journal of thrombosis and haemostasis : JTH*, 9 Suppl 1(s1), pp.56–65.

Hoshino, A. et al., 2011. Podoplanin-positive fibroblasts enhance lung adenocarcinoma tumor formation: podoplanin in fibroblast functions for tumor progression. *Cancer research*, 71(14), pp.4769–4779.

Huang, N.F. & Li, S., 2008. Mesenchymal stem cells for vascular regeneration. *Regenerative medicine*, 3(6), pp.877–892.

Hyun, Y.-M. & Hong, C.-W., 2017. Deep insight into neutrophil trafficking in various organs. *Journal of leukocyte biology*, 102(3), pp.617–629.

Inoue, O. et al., 2015. Vascular Smooth Muscle Cells Stimulate Platelets and Facilitate Thrombus Formation through Platelet CLEC-2: Implications in Atherothrombosis. F. Miller, ed. *PLoS ONE*, 10(9), p.e0139357.

Jaganathan, B.G. et al., 2007. Rho inhibition induces migration of mesenchymal stromal cells. *Stem Cells*, 25(8), pp.1966–1974.

Jang, W.-G. et al., 2012. BMP2 protein regulates osteocalcin expression via Runx2-mediated Atf6 gene transcription. *The Journal of biological chemistry*, 287(2), pp.905–915.

Jeffery, H.C. et al., 2013. Analysis of the effects of stromal cells on the migration of lymphocytes into and through inflamed tissue using 3-D culture models. *Journal of immunological methods*, 400-401, pp.45–57.

Jiang, X.-X. et al., 2005. Human mesenchymal stem cells inhibit differentiation and function of monocyte-derived dendritic cells. *Blood*, 105(10), pp.4120–4126.

Jones, B.J. et al., 2007. Immunosuppression by Placental Indoleamine 2,3-Dioxygenase: A Role for Mesenchymal Stem Cells. *Placenta*, 28(11-12), pp.1174–1181.

Kamat, P. et al., 2015. Human Adipose-Derived Mesenchymal Stromal Cells May Promote Breast Cancer Progression and Metastatic Spread. *Plastic and reconstructive surgery*, 136(1), pp.76–84.

Kaneko, M.K. et al., 2017. Development and characterization of anti-glycopeptide monoclonal antibodies against human podoplanin, using glycan-deficient cell lines generated by CRISPR/Cas9 and TALEN. *Cancer medicine*, 6(2), pp.382–396.

Kastrinaki, M.-C. et al., 2008. Functional, molecular and proteomic characterisation of bone marrow mesenchymal stem cells in rheumatoid arthritis. *Annals of the Rheumatic Diseases*, 67(6), pp.741–749.

Kato, Y. et al., 2003. Molecular identification of Aggrus/T1alpha as a platelet aggregation-inducing factor expressed in colorectal tumors. *The Journal of biological chemistry*, 278(51), pp.51599–51605.

Kawase, A. et al., 2008. Podoplanin expression by cancer associated fibroblasts predicts poor prognosis of lung adenocarcinoma. *International journal of cancer. Journal international du cancer*, 123(5), pp.1053–1059.

Kern, S. et al., 2006. Comparative analysis of mesenchymal stem cells from bone marrow, umbilical cord blood, or adipose tissue. *Stem Cells*, 24(5), pp.1294–1301.

Kerrigan, A.M. et al., 2012. Podoplanin-expressing inflammatory macrophages activate murine platelets via CLEC-2. *Journal of thrombosis and haemostasis : JTH*, 10(3), pp.484–486.

Khan, M. et al., 2011. Repair of senescent myocardium by mesenchymal stem cells is dependent on the age of donor mice. *Journal of Cellular and Molecular Medicine*, 15(7), pp.1515–1527.

Kinne, R.W., Stuhlmüller, B. & Burmester, G.-R., 2007. Cells of the synovium in rheumatoid arthritis. Macrophages. *Arthritis research & therapy*, 9(6), p.224.

Kohli, S. & Isermann, B., 2017. Placental hemostasis and sterile inflammation: New insights into gestational vascular disease. *Thrombosis research*, 151 Suppl 1, pp.S30–S33.

Kolaczkowska, E. & Kubes, P., 2013. Neutrophil recruitment and function in health and inflammation. *Nature Reviews Immunology*, 13(3), pp.159–175.

Kota, D.J. et al., 2014. Differential MSC activation leads to distinct mononuclear leukocyte binding mechanisms. *Scientific Reports*, 4, p.4565.

Kundrotas, G., 2012. Surface markers distinguishing mesenchymal stem cells from fibroblasts. *Acta medica Lituanica*, 19(2).

Kunita, A. et al., 2007. The platelet aggregation-inducing factor aggrus/podoplanin promotes pulmonary metastasis. *The American journal of pathology*, 170(4), pp.1337–1347.

Kuravi, S.J. et al., 2014. Podocytes regulate neutrophil recruitment by glomerular endothelial cells via IL-6-mediated crosstalk. *Journal of immunology (Baltimore, Md. : 1950)*, 193(1), pp.234–243.

Lamouille, S., Xu, J. & Derynck, R., 2014. Molecular mechanisms of epithelial-mesenchymal transition. *Nature reviews. Molecular cell biology*, 15(3), pp.178–196.

Langan, S.A. et al., 2017. Modulation of VEGF-induced migration and network formation by lymphatic endothelial cells: Roles of platelets and podoplanin.

Platelets, 116(300), pp.1–10.

Langer, H.F. et al., 2009. Platelet derived bFGF mediates vascular integrative mechanisms of mesenchymal stem cells in vitro. *Journal of molecular and cellular cardiology*, 47(2), pp.315–325.

Lawrence, M.B. et al., 1997. Threshold levels of fluid shear promote leukocyte adhesion through selectins (CD62L,P,E). *The Journal of Cell Biology*, 136(3), pp.717–727.

Lämmermann, T. & Sixt, M., 2009. Mechanical modes of “amoeboid” cell migration. *Current Opinion in Cell Biology*, 21(5), pp.636–644.

Lee, M.W. et al., 2015. Strategies to improve the immunosuppressive properties of human mesenchymal stem cells. *Stem cell research & therapy*, 6(1), p.179.

Leung, D.W. et al., 1989. Vascular endothelial growth factor is a secreted angiogenic mitogen. *Science*, 246(4935), pp.1306–1309.

Lhoumeau, A.-C. et al., 2015. Overexpression of the Promigratory and Prometastatic PTK7 Receptor Is Associated with an Adverse Clinical Outcome in Colorectal Cancer. A. W. I. Lo, ed. *PLoS ONE*, 10(5), p.e0123768.

Li, J.H. et al., 2003. TRAIL induces apoptosis and inflammatory gene expression in human endothelial cells. *The Journal of Immunology*, 171(3), pp.1526–1533.

Li, L. et al., 2008. Mesenchymal stem cell transplantation attenuates cardiac fibrosis associated with isoproterenol-induced global heart failure. *Transplant international : official journal of the European Society for Organ Transplantation*, 21(12), pp.1181–1189.

Li, Y.-Y., Zhou, C.-X. & Gao, Y., 2015. Podoplanin promotes the invasion of oral squamous cell carcinoma in coordination with MT1-MMP and Rho GTPases. *American Journal of Cancer Research*, 5(2), pp.514–529.

Lin, M.-N. et al., 2013. Involvement of PI3K and ROCK signaling pathways in migration of bone marrow-derived mesenchymal stem cells through human brain microvascular endothelial cell monolayers. *Brain research*, 1513, pp.1–8.

Ling, W. et al., 2014. Mesenchymal stem cells use IDO to regulate immunity in tumor microenvironment. *Cancer research*, 74(5), pp.1576–1587.

Liotta, F. et al., 2008. Toll-Like Receptors 3 and 4 Are Expressed by Human Bone Marrow-Derived Mesenchymal Stem Cells and Can Inhibit Their T-Cell Modulatory Activity by Impairing Notch Signaling. *Stem Cells*, 26(1), pp.279–289.

Liu, C.-F. & Lefebvre, V., 2015. The transcription factors SOX9 and SOX5/SOX6 cooperate genome-wide through super-enhancers to drive chondrogenesis. *Nucleic acids research*, 43(17), pp.8183–8203.

Lotfinegad, P. et al., 2014. Immunomodulatory nature and site specific affinity of mesenchymal stem cells: a hope in cell therapy. *Advanced pharmaceutical bulletin*, 4(1), pp.5–13.

Lowe, K.L. et al., 2015. The expression of mouse CLEC-2 on leucocyte subsets varies according to their anatomical location and inflammatory state. *European Journal of Immunology*, 45(9), pp.2484–2493.

Luu, N.T. et al., 2013. Crosstalk between mesenchymal stem cells and endothelial cells leads to downregulation of cytokine-induced leukocyte recruitment. *Stem Cells*, 31(12), pp.2690–2702.

Luu, N.T., Rainger, G.E. & Nash, G.B., 1999. Kinetics of the Different Steps during Neutrophil Migration through Cultured Endothelial Monolayers Treated with Tumour Necrosis Factor-α. *Journal of Vascular Research*, 36(6), pp.477–485.

Ma, S. et al., 2013. Immunobiology of mesenchymal stem cells. *Cell Death and Differentiation*, 21(2), pp.216–225.

Marei, H. & Malliri, A., 2017. Rac1 in human diseases: The therapeutic potential of targeting Rac1 signaling regulatory mechanisms. *Small GTPases*, 8(3), pp.139–163.

Martin-Villar, E. et al., 2010. Podoplanin Associates with CD44 to Promote Directional Cell Migration. *Molecular biology of the cell*, 21(24), pp.4387–4399.

Martin-Villar, E. et al., 2015. Podoplanin mediates ECM degradation by squamous carcinoma cells through control of invadopodia stability. *Oncogene*, 34(34), pp.4531–4544.

Martín-Villar, E. et al., 2006. Podoplanin binds ERM proteins to activate RhoA and promote epithelial-mesenchymal transition. *Journal of cell science*, 119(Pt 21), pp.4541–4553.

McEver, R.P., 2002. Selectins: lectins that initiate cell adhesion under flow. *Current Opinion in Cell Biology*, 14(5), pp.581–586.

McGettrick, H.M. et al., 2012. Tissue stroma as a regulator of leukocyte recruitment in inflammation. *Journal of leukocyte biology*, 91(3), pp.385–400.

Meesuk, L. et al., 2016. The immunosuppressive capacity of human mesenchymal stromal cells derived from amnion and bone marrow. *Biochemistry and biophysics reports*, 8, pp.34–40.

Meisel, R. et al., 2004. Human bone marrow stromal cells inhibit allogeneic T-cell responses by indoleamine 2,3-dioxygenase-mediated tryptophan degradation. *Blood*, 103(12), pp.4619–4621.

Méndez-Ferrer, S. et al., 2010. Mesenchymal and haematopoietic stem cells form a unique bone marrow niche. *Nature*, 466(7308), pp.829–834.

Moran, E.M. et al., 2011. Interleukin-17A induction of angiogenesis, cell migration, and cytoskeletal rearrangement. *Arthritis & Rheumatism*, 63(11), pp.3263–3273.

Mould, A.P. & Humphries, M.J., 2004. Regulation of integrin function through conformational complexity: not simply a knee-jerk reaction? *Current Opinion in Cell Biology*, 16(5), pp.544–551.

Mouratidis, P.X. & George, A.J., 2015. Regulation of indoleamine 2,3-dioxygenase in primary human saphenous vein endothelial cells. *Journal of inflammation research*, 8, pp.97–106.

Muir, K.W. et al., 2011. Prevalence, Predictors and Prognosis of Post-Stroke Hyperglycaemia in Acute Stroke Trials: Individual Patient Data Pooled Analysis from the Virtual International Stroke Trials Archive (VISTA). *Cerebrovascular Diseases Extra*, 1(1), pp.17–27.

Munir, H. & McGettrick, H.M., 2015. Mesenchymal Stem Cell Therapy for Autoimmune Disease: Risks and Rewards. *Stem cells and development*, 24(18), pp.2091–2100.

Munir, H. et al., 2017. Adipogenic Differentiation of Mesenchymal Stem Cells Alters Their Immunomodulatory Properties in a Tissue-Specific Manner. *Stem Cells*, 35(6), pp.1636–1646.

Munir, H. et al., 2015. Analyzing the effects of stromal cells on the recruitment of leukocytes from flow. *Journal of visualized experiments : JoVE*, (95), p.e52480.

Munir, H. et al., 2016. Comparative Ability of Mesenchymal Stromal Cells from Different Tissues to Limit Neutrophil Recruitment to Inflamed Endothelium. Z. Ivanovic, ed. *PLoS ONE*, 11(5), p.e0155161.

Murakami, S. et al., 2001. Expression of adhesion molecules by cultured human glomerular endothelial cells in response to cytokines: comparison to human umbilical vein and dermal microvascular endothelial cells. *Microvascular research*, 62(3), pp.383–391.

Najar, M. et al., 2017. Mesenchymal Stromal Cells and Toll-Like Receptor Priming: A Critical Review. *Immune network*, 17(2), pp.89–102.

Nakazawa, Y. et al., 2008. Tetraspanin family member CD9 inhibits Aggrus/podoplanin-induced platelet aggregation and suppresses pulmonary metastasis. *Blood*, 112(5), pp.1730–1739.

Navab, M. et al., 1988. Monocyte migration into the subendothelial space of a coculture of adult human aortic endothelial and smooth muscle cells. *Journal of Clinical Investigation*, 82(6), pp.1853–1863.

Navarro, A. et al., 2011. Polarized migration of lymphatic endothelial cells is critically dependent on podoplanin regulation of Cdc42. *American journal of physiology. Lung cellular and molecular physiology*, 300(1), pp.L32–42.

Navarro-Nunez, L. et al., 2015. Platelet adhesion to podoplanin under flow is mediated by the receptor CLEC-2 and stabilised by Src/Syk-dependent platelet signalling. *Thrombosis and haemostasis*, 113(5), pp.1109–1120.

Neri, S. et al., 2015. Podoplanin-expressing cancer-associated fibroblasts lead and enhance the local invasion of cancer cells in lung adenocarcinoma. *International journal of cancer. Journal international du cancer*, 137(4), pp.784–796.

Nie, Y. et al., 2010. Defective phenotype of mesenchymal stem cells in patients with systemic lupus erythematosus. *Lupus*, 19(7), pp.850–859.

Nitzsche, F. et al., 2017. Concise Review: MSC Adhesion Cascade-Insights into Homing and Transendothelial Migration. *Stem Cells*, 35(6), pp.1446–1460.

Nobes, C.D. & Hall, A., 1999. Rho GTPases control polarity, protrusion, and adhesion during cell movement. *The Journal of Cell Biology*, 144(6), pp.1235–1244.

Nowatari, T. et al., 2015. Sphingosine 1-phosphate has anti-apoptotic effect on liver sinusoidal endothelial cells and proliferative effect on hepatocytes in a paracrine manner in human. *Hepatology research : the official journal of the Japan Society of Hepatology*, 45(11), pp.1136–1145.

Oostingh, G.J. et al., 2007. Impaired induction of adhesion molecule expression in immortalized endothelial cells leads to functional defects in dynamic interactions with lymphocytes. *The Journal of investigative dermatology*, 127(9), pp.2253–2258.

Orabona, C. et al., 2008. SOCS3 drives proteasomal degradation of indoleamine 2,3-dioxygenase (IDO) and antagonizes IDO-dependent tolerogenesis. *Proceedings of the National Academy of Sciences of the United States of America*, 105(52), pp.20828–20833.

Otsu, K. et al., 2009. Concentration-dependent inhibition of angiogenesis by mesenchymal stem cells. *Blood*, 113(18), pp.4197–4205.

Pankajakshan, D. & Agrawal, D.K., 2014. Mesenchymal Stem Cell Paracrine Factors in Vascular Repair and Regeneration. *Journal of biomedical technology and research*, 1(1).

Papadaki, H.A. et al., 2002. Bone marrow progenitor cell reserve and function and stromal cell function are defective in rheumatoid arthritis: evidence for a tumor necrosis factor alpha– …. *Blood*, 99(5), pp.1610–1619.

Park, S. et al., 2017. Directional migration of mesenchymal stem cells under an SDF-1α gradient on a microfluidic device. N. D. Leipzig, ed. *PLoS ONE*, 12(9), p.e0184595.

Patel, K.D., 1999. Mechanisms of selective leukocyte recruitment from whole blood on cytokine-activated endothelial cells under flow conditions. *The Journal of*

Immunology, 101(11), pp.4437–4445.

Pati, S., Gerber, M.H., et al., 2011. Bone Marrow Derived Mesenchymal Stem Cells Inhibit Inflammation and Preserve Vascular Endothelial Integrity in the Lungs after Hemorrhagic Shock C. Schulz, ed. *PLoS ONE*, 6(9), pp.e25171–14.

Pati, S., Khakoo, A.Y., et al., 2011. Human mesenchymal stem cells inhibit vascular permeability by modulating vascular endothelial cadherin/β-catenin signaling. *Stem cells and development*, 20(1), pp.89–101.

Payne, H. et al., 2017. Mice with a deficiency in CLEC-2 are protected against deep vein thrombosis. *Blood*, 129(14), pp.2013–2020.

Petrie, R.J. et al., 2012. Nonpolarized signaling reveals two distinct modes of 3D cell migration. *The Journal of Cell Biology*, 197(3), pp.439–455.

Petrova, T.V., 2002. Lymphatic endothelial reprogramming of vascular endothelial cells by the Prox-1 homeobox transcription factor. *The EMBO journal*, 21(17), pp.4593–4599.

Pérez-Simón, J.A. et al., 2009. Mesenchymal stem cells are functionally abnormal in patients with immune thrombocytopenic purpura. *Cytotherapy*, 11(6), pp.698–705.

Phillipson, M. et al., 2006. Intraluminal crawling of neutrophils to emigration sites: a molecularly distinct process from adhesion in the recruitment cascade. *The Journal of experimental medicine*, 203(12), pp.2569–2575.

Piltti, J. et al., 2015. Rho-kinase inhibitor Y-27632 increases cellular proliferation and migration in human foreskin fibroblast cells. *PROTEOMICS*, 15(17), pp.2953–2965.

Prasanna, S.J. et al., 2010. Pro-Inflammatory Cytokines, IFNγ and TNFα, Influence Immune Properties of Human Bone Marrow and Wharton Jelly Mesenchymal Stem Cells Differentially C. M. Verfaillie, ed. *PLoS ONE*, 5(2), pp.e9016–16.

Proebstl, D. et al., 2012. Pericytes support neutrophil subendothelial cell crawling and breaching of venular walls in vivo. *The Journal of experimental medicine*, 209(6), pp.1219–1234.

Pula, B. et al., 2011. Podoplanin expression by cancer-associated fibroblasts predicts poor outcome in invasive ductal breast carcinoma. *Histopathology*, 59(6), pp.1249–1260.

Raicevic, G. et al., 2011. The source of human mesenchymal stromal cells influences their TLR profile as well as their functional properties. *Cellular Immunology*, 270(2), pp.207–216.

Ran, F.A. et al., 2013. Genome engineering using the CRISPR-Cas9 system. *Nature protocols*, 8(11), pp.2281–2308.

Ren, G. et al., 2010. Inflammatory Cytokine-Induced Intercellular Adhesion Molecule-1 and Vascular Cell Adhesion Molecule-1 in Mesenchymal Stem Cells Are Critical for Immunosuppression. *The Journal of Immunology*, 184(5), pp.2321–2328.

Ren, G. et al., 2008. Mesenchymal Stem Cell-Mediated Immunosuppression Occurs via Concerted Action of Chemokines and Nitric Oxide. *Cell Stem Cell*, 2(2), pp.141–150.

Reyat, J.S., Tomlinson, M.G. & Noy, P.J., 2017. Utilizing Lentiviral Gene Transfer in Primary Endothelial Cells to Assess Lymphocyte-Endothelial Interactions. In *T-Cell Trafficking*. Methods in Molecular Biology. New York, NY: Springer New York, pp. 155–168.

Ridley, A.J., 2003. Cell Migration: Integrating Signals from Front to Back. *Science*, 302(5651), pp.1704–1709.

Ridley, A.J. et al., 1992. The small GTP-binding protein rac regulates growth factor-induced membrane ruffling. *Cell*, 70(3), pp.401–410.

Riedl, J. et al., 2017. Podoplanin expression in primary brain tumors induces platelet aggregation and increases risk of venous thromboembolism. *Blood*, 129(13), pp.1831–1839.

Rodriguez, R. et al., 2014. Human bone marrow stromal cells lose immunosuppressive and anti-inflammatory properties upon oncogenic transformation. *Stem Cell Reports*, 3(4), pp.606–619.

Rosen, E.D. et al., 2002. C/EBPalpha induces adipogenesis through PPARgamma: a unified pathway. *Genes & development*, 16(1), pp.22–26.

Ross, J.J. et al., 2006. Cytokine-induced differentiation of multipotent adult progenitor cells into functional smooth muscle cells. *Journal of Clinical Investigation*, 116(12), pp.3139–3149.

Rubina, K. et al., 2009. Adipose stromal cells stimulate angiogenesis via promoting progenitor cell differentiation, secretion of angiogenic factors, and enhancing vessel maturation. *Tissue engineering. Part A*, 15(8), pp.2039–2050.

Sadik, C.D., Kim, N.D. & Luster, A.D., 2011. Neutrophils cascading their way to inflammation. *Trends in Immunology*, 32(10), pp.452–460.

Sahai, E. & Marshall, C.J., 2003. Differing modes of tumour cell invasion have distinct requirements for Rho/ROCK signalling and extracellular proteolysis. *Nature cell biology*, 5(8), pp.711–719.

Sahai, E. & Marshall, C.J., 2002. RHO-GTPases and cancer. *Nature reviews. Cancer*, 2(2), pp.133–142.

Salmon, M. et al., 1997. Inhibition of T cell apoptosis in the rheumatoid synovium. *Journal of Clinical Investigation*, 99(3), pp.439–446.

Sanz-Moreno, V. et al., 2008. Rac activation and inactivation control plasticity of tumor cell movement. *Cell*, 135(3), pp.510–523.

Schacht, V. et al., 2003. T1alpha/podoplanin deficiency disrupts normal lymphatic vasculature formation and causes lymphedema. *The EMBO journal*, 22(14), pp.3546–3556.

Schacht, V. et al., 2005. Up-regulation of the lymphatic marker podoplanin, a mucin-type transmembrane glycoprotein, in human squamous cell carcinomas and germ cell tumors. *The American journal of pathology*, 166(3), pp.913–921.

Scheller, J. et al., 2011. The pro- and anti-inflammatory properties of the cytokine interleukin-6. *Biochimica et biophysica acta*, 1813(5), pp.878–888.

Schena, F. et al., 2010. Interferon-γ-dependent inhibition of B cell activation by bone marrow-derived mesenchymal stem cells in a murine model of systemic lupus erythematosus. *Arthritis & Rheumatism*, 62(9), pp.2776–2786.

Schmidt, A. et al., 2006. Basic fibroblast growth factor controls migration in human mesenchymal stem cells. *Stem Cells*, 24(7), pp.1750–1758.

Selmani, Z. et al., 2008. Human leukocyte antigen-G5 secretion by human mesenchymal stem cells is required to suppress T lymphocyte and natural killer function and to induce CD4+CD25highFOXP3+ regulatory T cells. *Stem Cells*, 26(1), pp.212–222.

Semedo, P. et al., 2009. Mesenchymal Stem Cells Attenuate Renal Fibrosis Through Immune Modulation and Remodeling Properties in a Rat Remnant Kidney Model. *Stem Cells*, pp.N/A–N/A.

Sheikh, S. et al., 2005. Differing mechanisms of leukocyte recruitment and sensitivity to conditioning by shear stress for endothelial cells treated with tumour necrosis factor-alpha or interleukin-1beta. *British journal of pharmacology*, 145(8), pp.1052–1061.

Shekhani, M.T. et al., 2016. Collagen triple helix repeat containing 1 is a new promigratory marker of arthritic pannus. *Arthritis research & therapy*, 18(1), p.171.

Shields, J.D. et al., 2010. Induction of lymphoidlike stroma and immune escape by tumors that express the chemokine CCL21. *Science*, 328(5979), pp.749–752.

Sibony-Benyamini, H. & Gil-Henn, H., 2012. Invadopodia: the leading force. *European journal of cell biology*, 91(11-12), pp.896–901.

Smith, C.W. et al., 1989. Cooperative interactions of LFA-1 and Mac-1 with intercellular adhesion molecule-1 in facilitating adherence and transendothelial migration of human neutrophils in vitro. *Journal of Clinical Investigation*, 83(6), pp.2008–2017.

Spaeth, E. et al., 2008. Inflammation and tumor microenvironments: defining the migratory itinerary of mesenchymal stem cells. *Gene therapy*, 15(10), pp.730–738.

Spaggiari, G.M. et al., 2008. Mesenchymal stem cells inhibit natural killer-cell proliferation, cytotoxicity, and cytokine production: role of indoleamine 2,3-dioxygenase and prostaglandin E2. *Blood*, 111(3), pp.1327–1333.

Squillaro, T., Peluso, G. & Galderisi, U., 2016. Clinical Trials With Mesenchymal Stem Cells: An Update. *Cell transplantation*, 25(5), pp.829–848.

Stroka, K.M. & Aranda-Espinoza, H., 2011. Endothelial cell substrate stiffness influences neutrophil transmigration via myosin light chain kinase-dependent cell contraction. *Blood*, 118(6), pp.1632–1640.

Suchanski, J. et al., 2017. Podoplanin increases the migration of human fibroblasts and affects the endothelial cell network formation: A possible role for cancer-associated fibroblasts in breast cancer progression. A. Ahmad, ed. *PLoS ONE*, 12(9), p.e0184970.

Sun, L. et al., 2007. Abnormality of bone marrow-derived mesenchymal stem cells in patients with systemic lupus erythematosus. *Lupus*, 16(2), pp.121–128.

Sun, L. et al., 2010. Umbilical cord mesenchymal stem cell transplantation in severe and refractory systemic lupus erythematosus. *Arthritis & Rheumatism*, 62(8), pp.2467–2475.

Sun, W.Y., Pitson, S.M. & Bonder, C.S., 2010. Tumor Necrosis Factor-Induced Neutrophil Adhesion Occurs Via Sphingosine Kinase-1-Dependent Activation of Endothelial $\alpha 5\beta 1$ Integrin. *The American journal of pathology*, 177(1), pp.436–446.

Suraneni, P. et al., 2012. The Arp2/3 complex is required for lamellipodia extension and directional fibroblast cell migration. *The Journal of Cell Biology*, 197(2), pp.239–251.

Suzuki, H. et al., 2008. Induction of podoplanin by transforming growth factor-beta in human fibrosarcoma. *FEBS Letters*, 582(2), pp.341–345.

Suzuki, K. et al., 2011. Mesenchymal stromal cells promote tumor growth through the enhancement of neovascularization. *Molecular medicine (Cambridge, Mass.)*, 17(7-8), pp.579–587.

Suzuki-Inoue, K., 2017. CLEC-2/podoplanin and thromboinflammation. *Blood*, 129(14), pp.1896–1898.

Suzuki-Inoue, K. et al., 2007. Involvement of the snake toxin receptor CLEC-2, in podoplanin-mediated platelet activation, by cancer cells. *The Journal of biological chemistry*, 282(36), pp.25993–26001.

Takagi, S. et al., 2014. Expression of Aggrus/podoplanin in bladder cancer and its role in pulmonary metastasis. *International journal of cancer. Journal international du cancer*, 134(11), pp.2605–2614.

Takaku, M. et al., 1999. An in vitro coculture model of transmigrant monocytes and foam cell formation. *Arteriosclerosis, thrombosis, and vascular biology*, 19(10), pp.2330–2339.

Takemoto, A. et al., 2017. A critical role of platelet TGF-β release in podoplanin-mediated tumour invasion and metastasis. *Scientific Reports*, 7, p.42186.

Takeuchi, S. et al., 2017. Podoplanin promotes progression of malignant pleural mesothelioma by regulating motility and focus formation. *Cancer science*, 108(4), pp.696–703.

Tang, Yi et al., 2009. TGF-β1–induced migration of bone mesenchymal stem cells couples bone resorption with formation. *Nature Medicine*, 15(7), pp.757–765.

Tang, Yu et al., 2013. Activated NF-κB in bone marrow mesenchymal stem cells from systemic lupus erythematosus patients inhibits osteogenic differentiation through downregulating Smad signaling. *Stem cells and development*, 22(4), pp.668–678.

Tejchman, A. et al., 2017. Tumor hypoxia modulates podoplanin/CCL21 interactions in CCR7+ NK cell recruitment and CCR7+ tumor cell mobilization. *Oncotarget*, 8(19), pp.31876–31887.

Teo, G.S.L. et al., 2012. Mesenchymal stem cells transmigrate between and directly through tumor necrosis factor-α-activated endothelial cells via both leukocyte-like and novel mechanisms. *Stem Cells*, 30(11), pp.2472–2486.

Thomas, S.G. et al., 2011. G-protein coupled and ITAM receptor regulation of the formin FHOD1 through Rho Kinase in platelets. *Journal of Thrombosis and Haemostasis*, 9(8), pp.1648–1651.

Trivanović, D. et al., 2013. Immunomodulatory capacity of human mesenchymal stem cells isolated from adipose tissue, dental pulp, peripheral blood and umbilical cord Wharton’s jelly. *Central European Journal of Immunology*, 4, pp.421–429.

Tsimbouri, P.M. et al., 2017. Stimulation of 3D osteogenesis by mesenchymal stem cells using a nanovibrational bioreactor. *Nature Biomedical Engineering*, 1(9), pp.758–770.

Uezumi, A. et al., 2010. Mesenchymal progenitors distinct from satellite cells contribute to ectopic fat cell formation in skeletal muscle. *Nature cell biology*, 12(2), pp.143–152.

van Osch, G.J.V.M., 2012. Effect of arthritic synovial fluids on the expression of immunomodulatory factors by mesenchymal stem cells: an explorative in vitro study. pp.1–7.

Vora, M., Romero, L.I. & Karasek, M.A., 1996. Interleukin-10 induces E-selectin on small and large blood vessel endothelial cells. *The Journal of experimental medicine*, 184(3), pp.821–829.

Wang, W. et al., 2014. Mesenchymal stem cells recruited by active TGFβ contribute to osteogenic vascular calcification. *Stem cells and development*, 23(12), pp.1392–1404.

Wang, Z.-M. et al., 2016. ROCK inhibitor Y-27632 inhibits the growth, migration, and invasion of Tca8113 and CAL-27 cells in tongue squamous cell carcinoma. *Tumour biology : the journal of the International Society for Oncodevelopmental Biology and Medicine*, 37(3), pp.3757–3764.

Waterman, R.S. et al., 2010. A New Mesenchymal Stem Cell (MSC) Paradigm: Polarization into a Pro-Inflammatory MSC1 or an Immunosuppressive MSC2 Phenotype D. Unutmaz, ed. *PLoS ONE*, 5(4), pp.e10088–14.

Watson, C. et al., 1996. IL-6 acts on endothelial cells to preferentially increase their adherence for lymphocytes. *Clinical and Experimental Immunology*, 105(1), pp.112–119.

Wicki, A. & Christofori, G., 2007. The potential role of podoplanin in tumour invasion. *British journal of cancer*, 96(1), pp.1–5.

Wicki, A. et al., 2006. Tumor invasion in the absence of epithelial-mesenchymal transition: podoplanin-mediated remodeling of the actin cytoskeleton. *Cancer cell*, 9(4), pp.261–272.

Wigle, J.T. & Oliver, G., 1999. Prox1 function is required for the development of the murine lymphatic system. *Cell*, 98(6), pp.769–778.

Woodfin, A. et al., 2009. Endothelial cell activation leads to neutrophil transmigration as supported by the sequential roles of ICAM-2, JAM-A, and PECAM-1. *Blood*, 113(24), pp.6246–6257.

Wu, Y. et al., 2007. Mesenchymal Stem Cells Enhance Wound Healing Through Differentiation and Angiogenesis. *Stem Cells*, 25(10), pp.2648–2659.

Wu, Y. et al., 2015. Mesenchymal Stem Cells Suppress Fibroblast Proliferation and Reduce Skin Fibrosis Through a TGF- 3-Dependent Activation. *The International Journal of Lower Extremity Wounds*, 14(1), pp.50–62.

Xiao, Y. et al., 2013. Endothelial indoleamine 2,3-dioxygenase protects against development of pulmonary hypertension. *American journal of respiratory and critical care medicine*, 188(4), pp.482–491.

Yuan, P. et al., 2006. Overexpression of podoplanin in oral cancer and its association with poor clinical outcome. *Cancer*, 107(3), pp.563–569.

Yurugi, Y. et al., 2017. Podoplanin Expression in Cancer-associated Fibroblasts Predicts Poor Prognosis in Patients with Squamous Cell Carcinoma of the Lung.

Anticancer research, 37(1), pp.207–213.

Zhong, D. et al., 2009. Expression of Tiam1 and VEGF-C correlates with lymphangiogenesis in human colorectal carcinoma. *Cancer biology & therapy*, 8(8), pp.689–695.